ROOT WATER UPTAKE AND SOIL WATER DYNAMICS IN A KARST SAVANNA ON THE EDWARDS PLATEAU, TEXAS

A Dissertation

by

IEYASU TOKUMOTO

Submitted to the Office of Graduate Studies of
Texas A&M University
in partial fulfillment of the requirements for the degree of

DOCTOR OF PHILOSOPHY

Approved by:

Chair of Committee,	James L. Heilman
Committee Members,	Kevin J. McInnes
	Cristine L. Morgan
	Clyde L. Munster
Head of Department,	David D. Baltensperger

May 2013

Major Subject: Soil Science

ABSTRACT

Woody plants are encroaching into a karst savanna on the Edwards Plateau in central Texas, but their impact on hydrology is unclear because of high variability in soil depth and uncertainties about shallow and deep root contributions to water uptake, and water dynamics in rocky soil. The overall objectives of this study are to quantify contributions of shallow and deep roots to water uptake, and to quantify the impact of rock on soil hydraulic properties and water storage. A study was conducted in a karst savanna with ~50% woody cover to monitor spatial and temporal variations in soil moisture and root water uptake with neutron probe and time-domain reflectometry measurements. Bulk density was measured using gamma densitometry. Measurements were made to a depth of 1.6 m in a 25 m × 25 m grid (5 m node spacing). The results showed that rock created high spatial variability in water storage. Water storage capacity in the measurement grid ranged from 185 to 401 mm, and coupled with heterogeneous distribution of trees led to high spatial variability in root water uptake. Most of the water uptake came from the upper 1 m of the soil profile, but 10% came from below 1.6 m. This indicated that roots had access to water stored within the bedrock, possibly in soil pockets. Statistical analysis showed that spatial distribution of θ was significantly correlated with rock distribution in the profile. Laboratory evaporation measurements showed that Small volume fractions of rock can increase evaporation from soils by slowing upward movement of water, thereby maintaining capillary connectivity to the surface for a longer period of time. Two simulation models, van Genuchten (VG) and

Durner, were compared with the data from evaporation experiments. Results showed that the Durner model was more appropriate than the VG model for describing water retention and hydraulic conductivity of rocky soils.

DEDICATION

This dissertation is dedicated to my parents and wife, who made all of this possible, for their endless encouragement and love.

ACKNOWLEDGEMENTS

I would like to thank my committee chair, Dr. James L. Heilman, for his time, knowledge, and wisdom. I also thank my committee members, Dr. Kevin J. McInnes, Dr. Cristine L. Morgan, and Dr. Clyde L. Munster, for their guidance and support throughout the course of this research.

I appreciate Mr. Ray H. Kamps for his assistance in establishing my research site. I thank Mr. J. P. Bach, Director of Research at Freeman Ranch, for his assistance in maintaining my research site, and to Texas State University for allowing us to conduct research on the Ranch. I thank Dr. M. Eriksson, professor at Texas A&M University, for excellent help and comments to improve analysis of median polish approach. I also appreciate Dr. B. Mohanty, professor at Texas A&M University, for constructive comments to analyze root water uptake.

The research was supported by a grant from the southeastern region of the National Institute for Climate Change Research (NICCR) through the Office of Biological and Environmental Research, US Dept. of Energy.

Thanks also go to my friends and colleagues and the department faculty and staff for making my time at Texas A&M University a great experience.

Finally, thanks to my family for their encouragement and to my wife, Yoshimi Tokumoto for her patience and love.

TABLE OF CONTENTS

Page

LIST OF FIGURES

LIST OF TABLES

CHAPTER I

INTRODUCTION

Scope of Problem

On the karst Edwards Plateau in central Texas, woody plants, especially Ashe juniper (*Juniperus ashei*) and honey mesquite (*Prosopis glandulosa*) are invading grasslands and savannas. These plants typically have deeper roots than grasses and can potentially exploit more stable sources of water than the grasses. This ability is particularly troubling in contributing and recharge zones of the Edwards aquifer, the main source of drinking water to over 2 million people in the Austin - San Antonio I35 corridor, because increased water uptake, especially from stable sources beyond the reach of grasses, may reduce aquifer recharge. Thus, quantifying the water uptake by tree roots is important when budgeting water in typically dry regions. A complicating factor is that soils are generally shallow and rocky, and rocks create large spatial variability in rooting depth, soil water content, and soil hydraulic properties.

The impact of woody plants on the water budget has been investigated in different environments, but results of their impact on water resources have been conflicting. Some studies showed that juniper negatively impacts water resources by enhancing evapotranspiration, ET (Afinowicz et al., 2005) or reducing recharge by canopy interception (Owens, 2008). Others have shown that juniper root systems are impeded by fractured rocks or bedrock, and can mainly access shallow sources of water (Schwinning, 2008; Heilman et al., 2009). Currently, to help conserve water supplies,

public policies promoting brush management by removing the invading woody plants have been enacted in many areas. Identifying whether or not removing the invading these plants is effective at increasing ground water recharge is critical for establishing an effective brush management program that will increase water availability.

Literature Review

The population of woody species has significantly expanded in grasslands and savannas over the past century (Archer et al, 2001). The effect from these changes in land-cover is complex and certainly not well understood from the hydrological perspective (Wilcox and Thurow, 2006). One possible consequence is the reduction of overall water availability due to the woody plants' ability to increase ET and reduce groundwater recharge. This is especially important all over Central and West Texas where water is suspected to become a scarce commodity because of the invading brush, especially Ashe juniper (*Juniperus ashei*) and honey mesquite (*Prosopis glandulosa*). As a result, millions of dollars are spent each year for brush removal in an attempt to increase water availability (Olenick et al., 2004).

The effectiveness of brush removal policies at improving water yield has been investigated through several field and modeling studies. Wu et al. (2001) simulated that woody encroachment would result in a 35% decrease in water yield. Another simulation showed a relatively negative effect of heavy brush cover on the water recharge based on different brush management scenarios (Afinowicz et al., 2005). Additionally, the woody plants may reduce water recharge by canopy interception (Owen et al., 2006; Lyons et al., 2006; Owens, 2008). Contrary to the previous study, negligible effects of brush

management were observed from the viewpoint of changes in ET and stream flow rate on the Edwards Plateau (Dugas et al., 1998, Wilcox et al., 2010). Different studies have produced positive and negative evidence for woody plants' role in the reduction of groundwater recharge, however, none of these studies address the primary source of water for woody plants.

To develop a better understanding of the impact of woody plants on water resources, it is necessary to understand their primary sources of water. Schenk and Jackson (2002) indicated that shrubs and trees growing on shallow soils over bedrock tend to have deeper root systems than those growing on deeper soils. Jackson et al. (2000) found that water from depths greater than 7 m accounted for 24 % of growing season water use by a juniper whose roots had access to water in a cave. Stable isotope analysis of stem water by McCole and Stern (2007) showed that water use by juniper switched from shallow soil water in winter to deeper epikarst water in summer. However, juniper can take up substantial amounts of shallow soil moisture when it becomes available intermittently in summer (Williams and Ehleringer, 2000).

Recent work by Schwinning (2008) concluded, based on stable isotope evidence, that juniper on the Edwards Plateau does not commonly reduce aquifer recharge by tapping direct into perched water tables, but more likely by reducing water storage in soil and epikarst. Heilman et al. (2009) and Heilman et al. (2012) suggested, based on eddy covariance measurements of ET, that water sources for woody plants on the Plateau are mainly shallow and limited, rather than deep and stable. They found no

evidence that deep roots were extracting significant amounts of water from a perennially stable supply of water.

To determine potential impacts of woody plants on groundwater recharge, it is necessary to know how the plants affect soil water storage (S). Measuring ΔS is challenging in rocky soil, because rock fragments make it difficult to install sensors to observe spatial patterns in θ. Drilling methods have been developed for inserting access tubes for neutron thermalization measurements (Richardson, 1966), and some studies measured θ profiles in rocky soil. For example, Seyfried and Wilcox (2006) reported one dimensional water balances measured by neutron thermalization. They compared two θ profiles before and after shrubs were burned to investigate the effect of brush management on aquifer recharge, and the treatment resulted in potential increases in deep drainage. The presence of rock fragments in soil layers can have a significant impact on water flow (Brakensiek and Rawls, 1994), so the rock density profile is significant in determining whether and how rock fragments affect S.

The vegetation shift on the karst may create high spatial patterns of θ. Accurately understanding temporal and spatial variability in θ is another challenge because root distribution and rock density profile affect θ. A recent study by Estrada-Medina et al. (2012) showed that rocky soil has soil pockets that can store significant quantities of water. The question remains as to how tree roots affect the heterogeneity in θ, and whether the spatial pattern of θ is characterized by rock distribution. Jacques et al. (2001) used a spatial-temporal data analysis approach to quantify θ using an iterative resistant median-polish approach (Cressie, 1993; Jacques et al., 1999), allowing the

investigating of temporal dynamics of vertical and horizontal change in soil water. This approach may work for quantifying the contribution of tree and rock distribution to θ.

Water flow simulation can potentially be used to predict how effective brush management will be at a given location in increasing water availability. The essential factors for water movement are soil hydraulic properties such as the soil water retention curve and hydraulic conductivity that affect water flow in unsaturated soils. The soil hydraulic properties have been widely used by the van Genuchten model (van Genuchten, 1980), which enables the calculation of hydraulic conductivity based on estimated parameters of the water retention curve. Šimůnek et al. (1998) showed that these parameters can be estimated by the evaporation method, which is a laboratory method for monitoring pressure head and water content during the process of evaporation from soil samples. The unsaturated hydraulic properties can be optimized inversely with HYDRUS 1D, a simulation software of water flow developed by Šimůnek (Šimůnek et al., 2005). Recently Peter and Durner (2008) assessed the experimental errors with the Durner model, a modified VG model by Durner (1994). Sakai and Toride (2007a) compared the VG and the Durner models, and highlighted the importance of the hydraulic model selection, depending upon different soil types. Especially, the evaporation method allows us to estimate unsaturated hydraulic conductivities in a wide range of pressure head (h), ranging from approximately -50 cm and -700 cm (Šimůnek et al., 1998). The evaporation method may work for estimating soil hydraulic properties of rocky soil, if hydraulic properties for the soil with and without rock fragments can be compared and evaluated. These results imply that if parameterizations are examined and

evaluated by temporal changes in water content obtained from neutron probe measurements, it may be possible to estimate the intrinsic hydraulic properties for rocky soil.

Objectives

Objectives of this study are; 1) evaluate impact of rock on neutron moisture and gamma density probes in rocky soils; 2) quantify contributions of shallow and deep roots to water uptake; 3) quantify the impact of rock on soil hydraulic properties and water storage; and 4) estimate hydraulic properties for rocky soils to simulate water flow and water uptake in rocky soil. This study will help determine the effect of invading woody plants such as Ashe juniper on ET in rocky soil. The results from this study will be beneficial in deciding the correct policies for ensuring ground water supply in arid regions where woody plants are invading. Employing the proper policy for brush management will maximize the benefit to human populations as well as the ecosystem.

CHAPTER II

SEALING NEUTRON PROBE ACCESS-TUBES IN ROCKY SOILS USING EXPANDABLE POLYURETHANE FOAM*

Introduction

Neutron thermalization is a widely accepted method for repeated non-destructive measurements of soil volumetric water content at a given location (Hignett and Evett, 2002). This method requires insertion of cylindrical access tubes into the soil through which a neutron probe is lowered to measure water content. To prevent preferential water flow of water along the outside of the tube after rain or irrigation, tubes must either have a tight fit with the soil, or the annular space between soil and tube must be backfilled. The backfill may reduce the sensitivity and accuracy of water content measurements, depending on the volume and uniformity of the backfill, and the density and composition of the material (Keller et al., 1990). Creating a uniformly dense backfill is difficult, especially if the access hole is deep. A number of different materials have been used with varying degrees of success, including moistened gravel (Teasdale and Johnson, 1970), kaolinite slurries (Amoozegar, 1989), and bentonite and bentonite/concrete mixes (Keller et al., 1990).

Installation of access tubes in rocky soils can be difficult and often requires large

---

*Reprinted with permission from " Sealing Neutron Probe Access-Tubes in Rocky Soils Using Expandable Polyurethane Foam" by Ieyasu Tokumoto, James L. Heilman, Kevin J. McInnes, and Ray H. Kamps, 2011. Soil Science Society of America Journal, 75, 1922-1925, Copyright 2011 by Soil Science Society of America Journal.

drill rigs to bore through rock. Use of small-diameter screw augers is problematic because of the difficulty for small augers to displace and lift sizeable rock fragments. Larger screw augers can more easily move rock fragments but they create a larger annular space that may reduce the sensitivity of the neutron probe measurements to water content (Amoozegar, 1989). Both small and large augers may create irregularities in the walls when rocks are displaced.

Expandable polyurethane foams have been used for backfilling holes in utility pole installation, where they are poured into the hole as a liquid, and expand and solidify quickly, creating a rigid backfill to support the pole. We tested a commercially available foam for backfilling neutron probe access tube holes, evaluating its ease of application, its impact on the sensitivity of neutron probe measurements of water content, and its ability to create a water-tight seal in rocky soil.

Materials and Methods

Expandable Foam

We used Poly-Set® (Utility Structural Systems, Arlington, TX), which consists of two liquid components. After the components are combined and mixed for 30 s with an impellor attached to a portable drill (as recommended by the manufacturer), the foam expands up to 15 times its pre-mixed volume, and hardens within 10 minutes. Our measurements showed the density of foam to be 0.19 g cm^{-3} after hardening. We immersed foam samples in water for 24 hours and found no increase in foam weight, indicating that the foam was not wettable.

Sensitivity Testing

Tests were done with 5.1 cm o.d. aluminum access tubes in 60 cm diameter × 80 cm tall barrels. Initially, a tube, sealed at the bottom, was placed in the center of a barrel and the barrel was packed homogeneously with dry sand with a bulk density (ρ_b) of 1.73 g cm^{-3}. Count ratios ($CR=N/N_s$), the number of counts in the media (N) relative to counts in a paraffin reference standard (Ns) were measured at depths of 25 to 35 cm with a 503DR moisture probe (CPN International, Inc, Martinez, CA). The probe contains a source of high-energy neutrons (Am-241:Be) and a slow (thermal) neutron detector. A 32-s count interval was used. After measurements were completed, sand samples at the observed depths were collected using 125 cm^3 core samples. Water content (θ) and ρ_b were determined gravimetrically. The sand was then removed from the barrel, placed on a tarpaulin, and a known volume of water was added using a spray bottle. The sand and water were mixed as uniformly as possible. The sand was then repacked in the barrel and a new set of measurements were made. This process was repeated several times to create a range of water contents.

Next, holes of diameter 6.0 cm, 9.0 cm, and 11.5 cm were created in the centers of barrels containing moist sand (θ = 0.16 to 0.20 m^3 m^{-3}). Installation in moist sand was necessary because holes collapsed if the sand was too wet or too dry. Access tubes, sealed at the bottom, were inserted in the centers of the holes, and CR measured with air in the annular spaces. Then the two liquid components of the polyurethane foam were mixed and poured into the annular spaces. Hand-pressure was applied to the top of the tubes to prevent displacement of the tubes as the foam expanded from the bottom

upward. Excess foam that extruded out the top of the holes was removed. After the foam solidified, CR was measured again, and soil samples were collected to determine θ and ρ_b. Measurements with foam surrounding access tubes were repeated with dry sand and saturated sand. Finally, measurements were done with dry gravel (ρ_b = 1.74 g cm^{-3}), saturated gravel, and only water in the barrels, with the same radii of foam used in the sand measurements.

Field Installation

In the summer of 2009, 36 access tubes were installed in a 25 × 25 m grid (5 m node spacing) to a depth of 1.6 m in a Rumple gravelly clay loam (Clayey-skeletal, mixed, active, thermic Typic Argiustolls) in karst terrain on the Freeman Ranch near San Marcos, TX, as part of a study to monitor spatial and temporal variations in water content. The soil profile contains a high percentage of rock as shown in Fig. 2.1. Bore holes were drilled to a depth of 1.6 m using an 8.9 cm diameter screw auger attached to a truck mounted drill rig (CME 75, Central Mine Equipment Co., St. Louis, MO). Drilling time ranged from 10 to 30 min per hole, depending on amount of rock encountered. We mixed the smallest commercially-available volume (1.6 L) of the liquid components, and poured the entire mixture down each hole. Aluminum tubes, sealed at the bottom, were then quickly inserted into the holes and hand-held in the center as the foam expanded. The foam extruded out of the holes within 1 minute. The tubes were held in place for a minute until the foam hardened to touch. The entire process of tube insertion and sealing took less than 2 minutes per hole. Once the foam hardened completely, the extruded portion was removed (Fig. 2.2).

Fig. 2.1 Photograph of the rocky soil profile in which neutron probe access tubes were installed.

Fig. 2.2 Photograph of neutron probe access tube sealed by the polyurethane foam. Also shown is the excess foam above the soil surface that was cut and removed.

Initial calibration was done in an access tube that was installed outside the measurement grid. Count ratios were measured, and soil samples at a depth of 25 to 30 cm were collected using a core sampler for determination of water content. Soil samples were collected within 20 cm of the access tube. Then, a soaker hose was placed in spiral fashion on the soil surface surrounding the tube and 1,500 mm of water applied over a 2-day period. Water ponded on the surface during this process, and some was lost as runoff. Count ratios were measured again after all ponded water infiltrated, and soil samples collected again. The soil samples contained some small stones, so their impact on volumetric water content was included in the calibration curve. Further studies are underway to develop calibration curves as a function of water content and volume fraction of rock.

Results and Discussion

In the neutron thermalization method, fast neutrons from a source in the probe are thermalized (slowed) in soil when they collide with hydrogen nuclei in water, and with other minerals that are fixed in time and space. Slow neutrons returning to the probe are counted by a detector, with the flux of slow neutrons increasing with soil water content. The sphere of influence for the measurements decreases as water content increases.

One possible way for the foam to affect neutron probe measurements is to thermalize fast neutrons and become an additional source of slow neutrons. If this occurs, count ratios should increase with the amount of foam surrounding the access tube. Alternatively, the foam may attenuate the flux of slow neutrons returning to the

detector, resulting in a decrease in CR as foam volume increases. Our measurements in sand, gravel and water showed that CR declined as hole diameter increased (Figs. 2.3 and 2.4). However, when we compared measurements in air-filled and foam-filled holes in moist sand, we found little difference in CR (Table 2.1), indicating that changes in the measurement geometry (zone of influence) rather than the foam were responsible for the reduction in CR with increasing hole diameter. The measurement volume is controlled by the density of hydrogen in the media surrounding the source and detector. As hole diameter increased, a greater fraction of the measurement volume was occupied by the void space between access tube and soil, reducing the sensitivity of the measurements to θ (Amoozegar, 1989). Also, the sphere of influence decreased as θ increased, so that the proportion of that sphere occupied by the void space increased with θ. This resulted in non-linear calibration curves (CR vs. θ) (Fig. 2.3).

To further evaluate the impact of foam, an additional set of measurements was made using a much larger hole (20-cm diameter) in saturated sand (θ = 0.38 m^3 m^{-3}), with air or foam in the annular space between tube and sand (Table 2.1). The hole was lined with a thin-walled aluminum tube to prevent the hole from collapsing. In this case, we found that CR with the foam-filled hole was actually 7.7% higher than CR measured with the air-filled hole, evidence of some thermalization of fast neutrons by the foam. However, at hole diameters that are more typical of field installations, the foam lacked sufficient density to be a major source of thermalized neutrons (Table 2.1).

Analysis of water content profiles in the field showed no evidence of preferential flow through the foam sealant in any of the access tube holes. As an example, Fig. 2.5

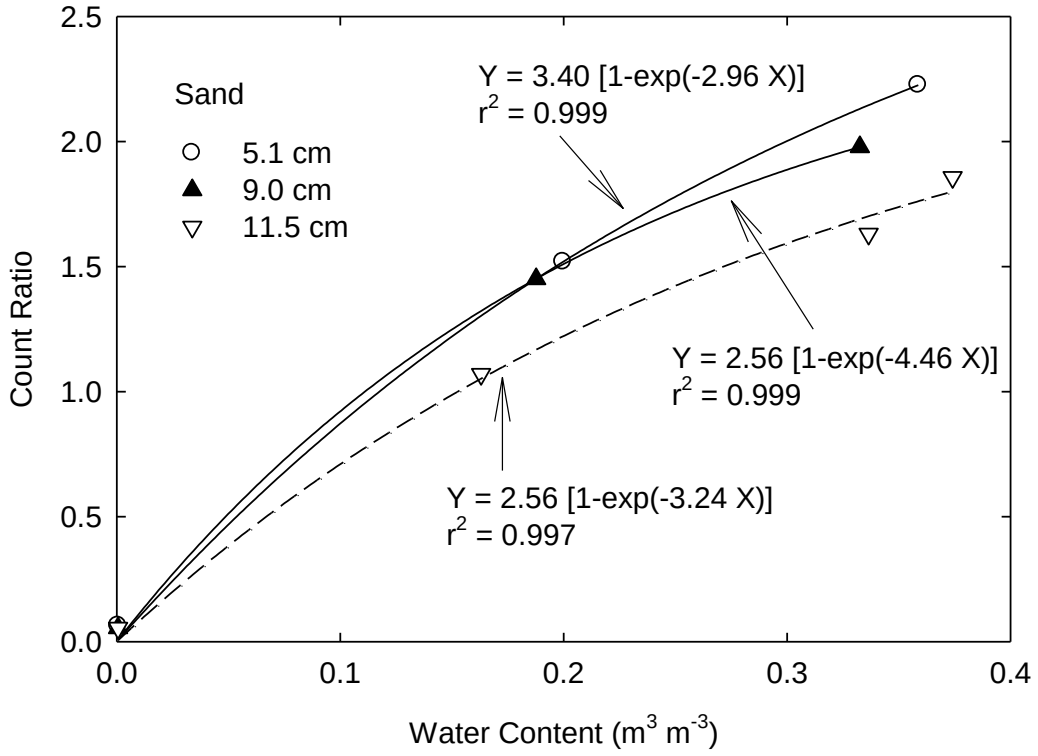

Fig. 2.3 Count ratios as a function of water content and access tube hole diameter. Measurements were done in sand, with the annular space between tube and soil filled with foam sealant.

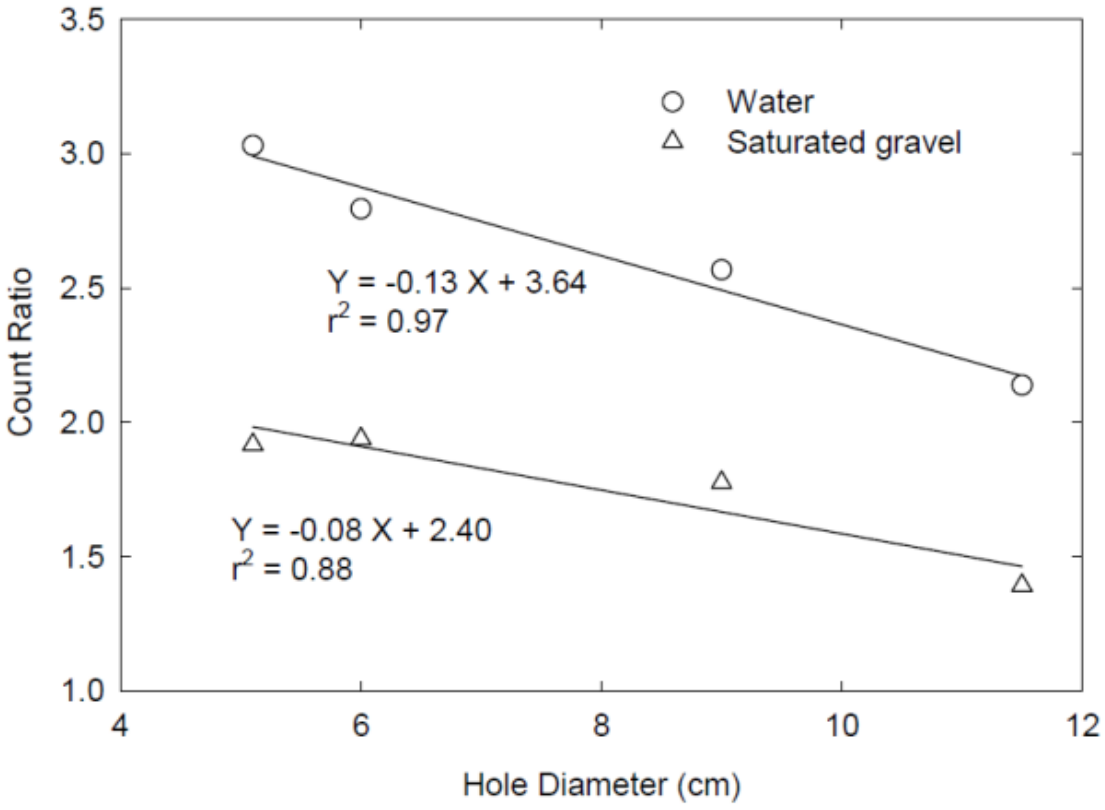

Fig. 2.4 Count ratios in saturated sand and water as a function of foam volume (hole diameter).

Table 2.1 Comparison of count ratios (CR) in air-filled and foam-filled holes of 9, 11.5 and 20-cm diameters. Standard deviations of replicate were <0.01. The sand was saturated (θ = 0.38 m^3 m^{-3}) for the 20-cm hole diameter measurements, but for the 9.0 and 11.5-cm diameter holes, θ was between 0.16 and 0.19 m^3 m^{-3}.

	Count ratio		
Hole diameter (cm)	Air	Foam	% change in *CR*
9.0	1.45	1.47	1.4
11.5	1.07	1.06	-0.9
20.0	0.84	0.91	7.7

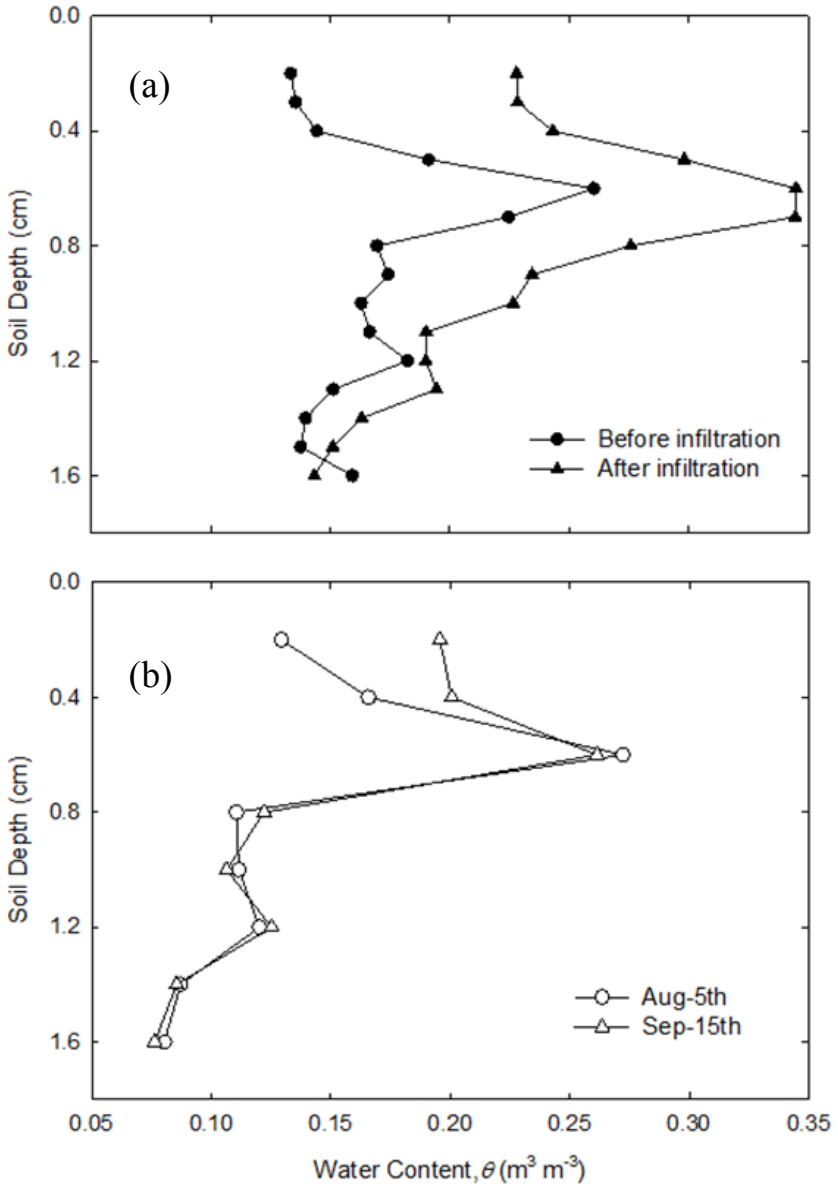

Fig. 2.5 Water content profiles before and after application of 1,500 mm of water (a), and before (August 5, 2009) and after (September 15, 2009) a 50 mm rainfall (b). X-axes of Fig. 2.5a and b have the same scale.

shows water content profiles measured before and after application of 1,500 mm of water during probe calibration, and before and after 50 mm of rainfall. Changes in water content were consistent with normal infiltration, not flow of water in the annular space between tube and hole. To date, we have not observed any cracking of the foam sealant at the soil surface.

Conclusions

We found that expandable polyurethane foam was an acceptable material for sealing neutron probe access tubes. The foam we tested (Poly-Set®), did thermalize fast neutrons, but the foam lacked sufficient density to be a major source of slow neutrons at access tube hole diameters that are typical of field installations. We found that count ratios decreased with increasing hole diameter, but this was due to changes in the zone of influence, not the foam itself. Although some loss of sensitivity occurred at larger hole diameters, sufficient sensitivity was maintained with in situ calibration of the neutron probe to accurately measure water content. Nevertheless, hole diameters should be as small as possible to minimize loss of sensitivity. The foam was easy to use, and allowed access tubes to be quickly inserted and sealed. To date, we have not seen any evidence of preferential flow around access tubes installed in rock soil, indicating that the foam provides a water-tight seal.

CHAPTER III

CALIBRATIONS AND USE OF NEUTRON MOISTURE AND GAMMA DENSITY PROBES IN ROCKY SOILS*

Introduction

Rocky soils are prevalent in many regions of the U.S. and world-wide. Rocks may have a significant impact on soil and plant water relations by reducing volumetric water content, restricting root growth, and impeding and redirecting water flow. In addition, water stored in or beneath layers of rock, and within the rock matrix itself, can be important sources of water that can be extracted by roots (Allen, 2007; Schwinning, 2010). Measuring volumetric water content (θ) in rocky soils is difficult because rocks hinder insertion of probes and sensors. If rocks are avoided during sensor installation to prevent damage to probes such as those used in time domain reflectometry (TDR), measurements of θ will be biased because the impact of rock on θ will be excluded. This is especially true for capacitance and dielectric sensors that have small measurement volumes. Rocks can also alter nuclear scattering/absorption properties of the bulk soil volume important in determining water content with the nuclear methods that have much larger measurement volumes than TDR (Knight and Abad, 1995; Martinez and Byrnes, 2001). Variation of rock content in soil can potentially require a family of calibration

*Reprinted with permission from " Calibration and Use of Neutron Moisture and Gamma Density Probes in Rocky Soils" by Ieyasu Tokumoto, James L. Heilman, Kevin J. McInnes, Cristine L.S. Morgan, and Ray H. Kamps, 2012. Soil Science Society of America Journal, 76, 2136-2142, Copyright 2012 by Soil Science Society of America Journal.

curves and a priori knowledge of rock content to determine water content (Lal, 1979).

Neutron thermalization and gamma ray scattering methods of determining water content and bulk density have advantages over other methods because their measurement volumes are larger, accounting for a larger variation in rock content and rock size. These methods require insertion of cylindrical access tubes into the soil through which radioactive probes are lowered to measure water content and bulk density. Installation of access tubes in rocky soil often requires an auger with rock cutting bits to grind through sizeable rocks. Smaller rocks are often displaced leaving void spaces between the access tube and soil. The void space between tube and soil must be backfilled to prevent infiltration of water along the outside of the tube. However, creating a uniform backfill is difficult if the hole is deep. In a previous study, we investigated expandable polyurethane foam as a sealant for neutron probe access tubes, and found that it was easy to use and created a water-tight seal, but the foam-filled void space between tube and soil created nonlinear calibration curves (Tokumoto et al., 2011).

In this paper, we report on calibration of neutron thermalization and gamma density probes in rocky soil, with the foam sealant around the access tubes, and show some examples of spatial and temporal variability of θ and bulk density profiles in a karst savanna in central Texas. Typically, calibration of neutron and gamma density probes is done in the field, and involves collecting volumetric soil samples for gravimetric determination of water content and bulk density at the time of probe measurements. However, field calibration is difficult because rocks hinder the collection of volumetric samples of an appropriate scale, and information on rock distribution as a

function of depth is generally unknown. We therefore calibrated probes in a drum with known volumes of rock, soil, and water (Gracean et al., 1981). The laboratory calibration allowed us to examine the effect of rock and measurement geometry on the sensitivity of neutron and gamma probe measurements to θ and bulk density.

Theoretical Background

Neutron Thermalization

In the neutron thermalization method, fast neutrons from a source in a probe are thermalized (slowed) in soil when they collide with hydrogen nuclei in water, and with other minerals that are fixed in time and space. Slow neutrons returning to the probe are counted by a detector, with flux of slow neutrons increasing with θ. The effective radius of measurement with neutron thermalization (R_n) decreases with increasing θ, and can be estimated by

$$R_n = 15\theta^{-1/3}, \quad [3.1]$$

where R_n is in cm (Evett, 2003). Evett et al. (2003) reported that the effective axial measurement distance A_n is smaller than R_n, and can be approximated by

$$A_n \text{ (cm)} = 9\theta^{-1/3}. \quad [3.2]$$

Neutron probes generally are calibrated using regression analysis of count ratios ($CR_n=N/N_s$), the number of counts in the media (N) relative to counts in a reference standard (N_s), vs. θ. Calibration curves are typically linear (Hignett and Evett, 2002), but departure from linearity may be induced if the annular space between access tube and soil is filled with material that has scattering properties that differ from the surrounding soil (Tokumoto et al., 2011).

Gamma Radiation Scattering and Absorption

Gamma particles from a source in a probe are absorbed and scattered when passing through a soil-water system. Scattered gamma particles returning to the probe are counted by a detector. A theoretical analysis by Christensen (1974) showed that the effective radius of measurement with gamma scattering (R_d) decreases with increasing bulk density, and can be estimated by

$$R_d = 39\ \rho_{wet}^{-1/3}, \quad [3.3]$$

where R_d is in cm and ρ_{wet} is wet bulk density (g cm^{-3}), the ratio of total soil mass, including water, to its total volume. However, measurements by Morris and Williams (1990) indicated that R_d was smaller than predicted by Eq. [3.3] because of the influence of probe geometry and shielding. They found that the functional relationship between the gamma count ratio (CR_d) and ρ_{wet} could be described by equations of the form

$$CR_d = \rho_{wet}^{\ a} \cdot \exp\left(b + c\cdot\rho_{wet} + d\cdot\rho_{wet}^{\ 2}\right), \quad [3.4]$$

where a, b, c, and d are empirical constants. The maximum count ratio was found to occur at wet bulk densities between 0.5 to 1 g cm^{-3} (Fig. 3.1). Below these densities, scattering is the dominant process and CR_d increases as ρ_{wet} increases. At densities higher than about 1 g cm^{-3}, which is typical of most soils, CR_d decreases as ρ_{wet} increases because absorption dominates (Fig. 3.1).

Materials and Methods

In the summer of 2009, we began a study to monitor spatial and temporal variations in soil water content and root water uptake in a karst savanna with ~50% woody cover (Ashe juniper, honey mesquite) on the Freeman Ranch near San Marcos,

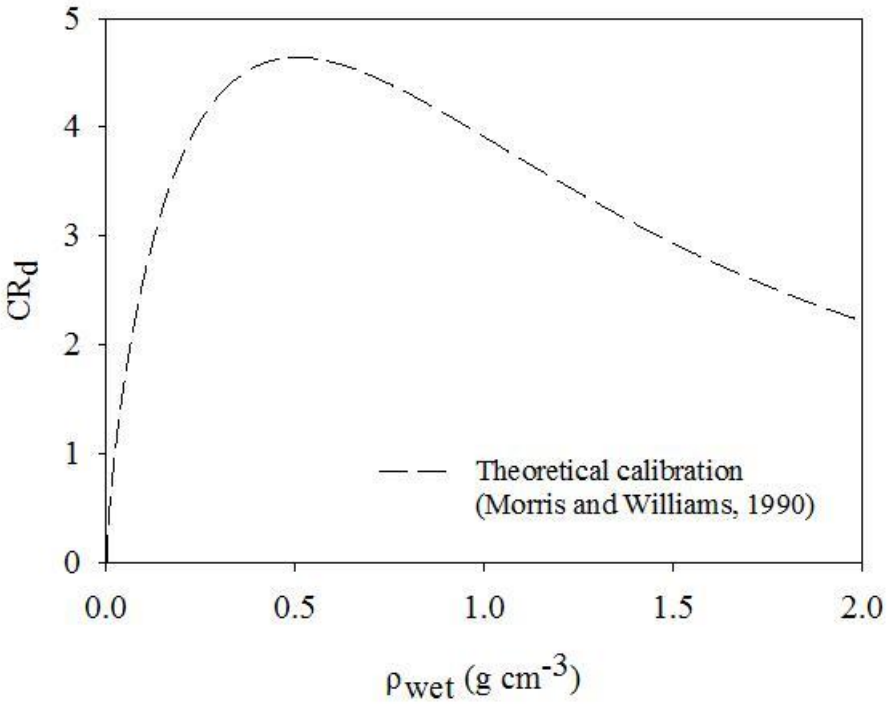

Fig. 3.1 Theoretical calibration curve for CPN 503DR density probe (Morris and Williams, 1990).

Texas. The soil is a Rumple gravelly clay loam (Clayey-skeletal, mixed, active, thermic Typic Argiustolls) with chert fragments occupying ~50% of the soil volume between depths of 0.2 and 1.0 m (Fig. 3.2). From samples excavated at the site, the average volume and density of chert fragments was found to be 52.7 cm^3 and 2.4 g cm^{-3}, respectively. Limestone residuum occurs at depths of 1 to 1.5 m. Because rocks can restrict root growth, and access to water stored beneath rock, locating areas in the soil profile with sizeable rock fragments is an important component of the study.

Thirty six 5.1-cm o.d., thin-walled aluminum access tubes were installed in a 25 × 25 m grid (5 m node spacing) to a depth of 1.6 m (Fig. 3.3) for neutron and gamma probe measurements of water content and bulk density, respectively. Bore holes were drilled using an 8.9-cm diam. screw auger and then access tubes inserted and sealed with expandable polyurethane foam (Poly-Set, Utility Structural Systems, Arlington, TX) as described by Tokumoto et al. (2011). The density of the foam was 0.19 g cm^{-3} after hardening.

Campbell Pacific Nuclear Corp. (CPN) water content and density gauges, models 503DR and 501DR, were calibrated in the laboratory using soil and rocks that were gathered from the field site. The model 503DR moisture probe contained a source of high-energy neutrons (Am-241:Be) and a slow (thermal) neutron detector and the model 501DR density probe contained a Cesium-137 source and a Geiger-Mueller detector. Although the 501DR contained a neutron source and detector as well, we only calibrated the gamma density portion of the probe.

The soil water and density probes were calibrated in a 60-cm diam. by 80-cm tall

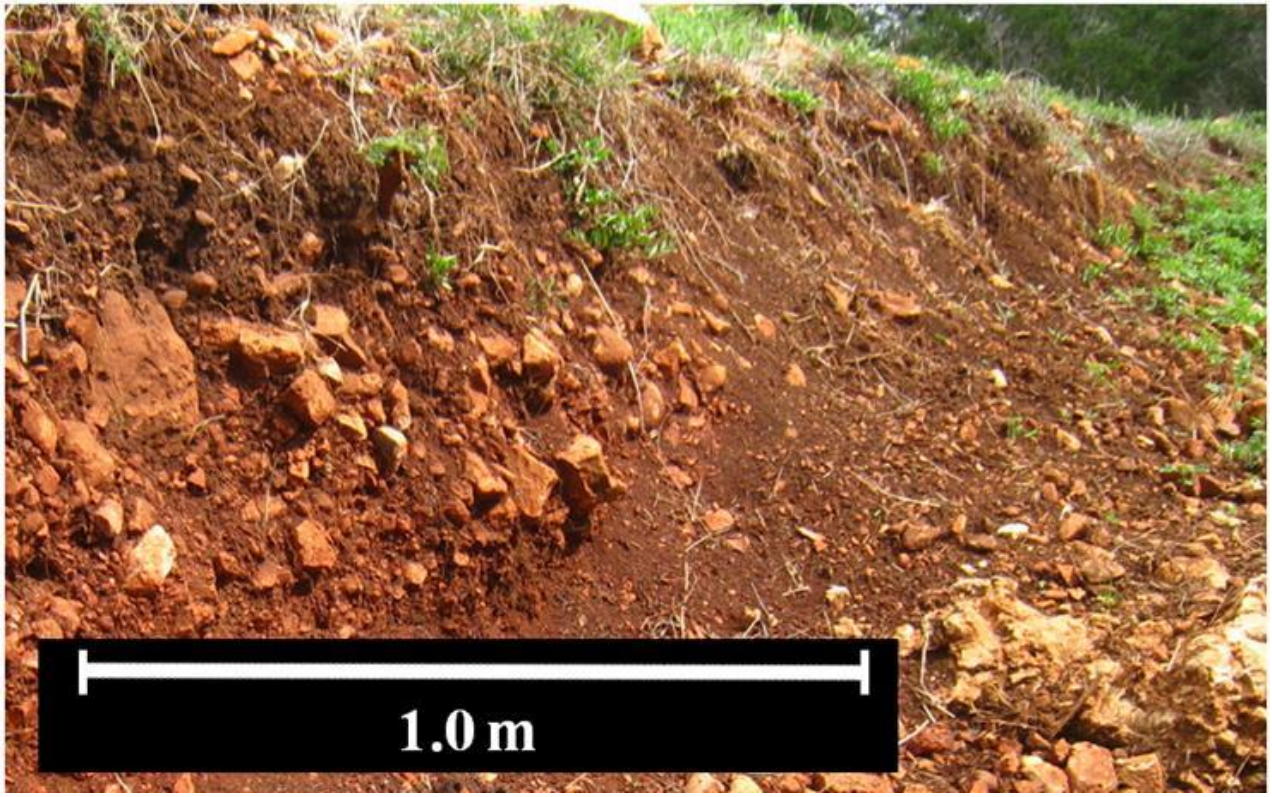

Fig. 3.2 Photograph of a trench excavated near the research site showing chert fragments and limestone slabs in the soil profile.

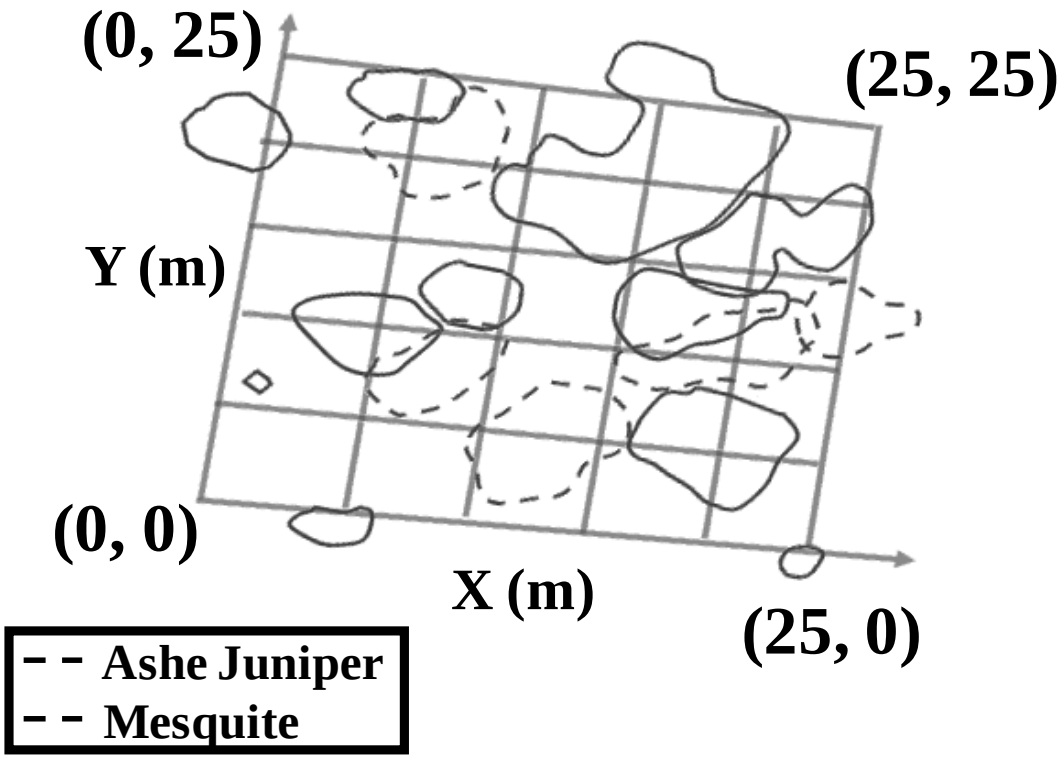

Fig. 3.3 Diagram of experimental site showing the distribution of access tubes and locations of Ashe juniper and honey mesquite in the 25 × 25 m measurement grid.

plastic drum connected at the bottom to a water tank (Fig. 3.4). A 5.1-cm o.d. aluminum access tube was covered with expandable polyurethane foam to create a 9-cm o.d. sealed access tube similar in diameter to those at the Freeman Ranch research site. The drum was filled with 2-mm sieved dry clay loam (particle density of 2.5 g cm^{-3}) above a gravel layer that was at the bottom of the drum, and was packed to a dry bulk density (ρ_b) of 1.15 g cm^{-3}. Water was allowed to infiltrate in a stepwise manner from the bottom at a rate of 1 to 3 cm d^{-1} over a 2-week period to create a range of water contents. Neutron and gamma counts were measured at a depth of 25 cm utilizing a 32-s count interval for the neutron probe, and a 60-s interval for the density probe. Counts in neutron and gamma probe reference standards were measured using 240-s count intervals, and count ratios calculated. Next, measurements were made with 15% and 32% volume of chert fragments distributed in a 42-cm diam. cylindrical volume as shown in Fig. 3.4. A metal tamp was used to pack the soil between rocks to eliminate air-filled voids. Finally, measurements were made with 49% of the volume occupied by pieces of limestone bedrock (density 2.6 g cm^{-3}).

Soil water content was monitored in the drums by time domain reflectometry (TDR100, Campbell Scientific, Logan, UT). Two 30-cm long TDR probes were inserted vertically at a distance of 25 cm from the access tube. We confirmed that there was no influence of TDR probes on neutron and density measurements. Midpoints of each probe were at a depth of 25 cm so that the probes provided a measurement of the average water content in the 10 to 40 cm layer. At the conclusion of the upward infiltration experiment, the difference in θ over the 30-cm distance, measured gravimetrically, was less than 0.05

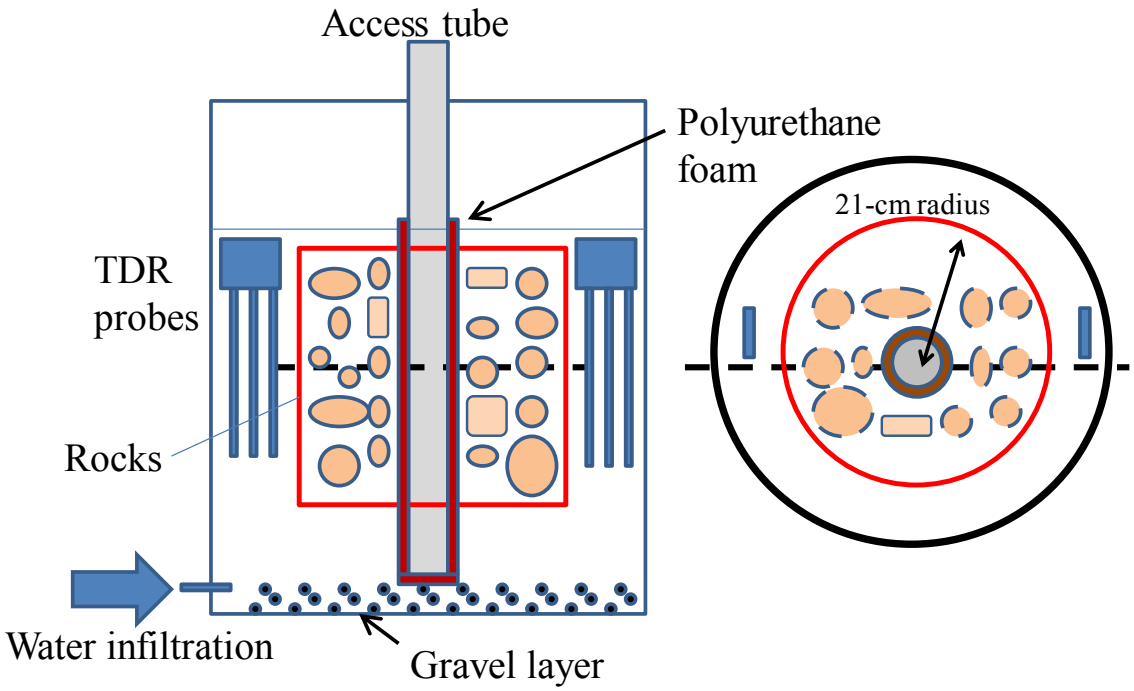

Fig. 3.4 Schematic showing the placement of rock and time domain reflectometry (TDR) probes in the drum used for calibration of neutron and gamma density probes.

m^3 m^{-3}. Prior to the experiment, TDR probes were calibrated using the upward infiltration method proposed by Young et al. (1997). The calibration curve was a third-order polynomial equation of θ vs. dielectric constant. For the calibration, soil samples were collected with a 125 cm^3 soil core sampler to measure θ and ρ_b. The r^2 (n= 6) and the slope of the regression (1:1 line) between θ from TDR and gravimetric sampling were 0.996 and 0.966, respectively.

Calibration of the neutron and gamma density probes required estimates of the water content in the respective measurement volumes of the probes. TDR probes positioned away from the rocks provided an estimate of the volumetric water content of the soil portion (θ_{soil}) of the measurement volume. Water content in the cylindrical volume containing rocks was calculated as

$$\theta_{soil+rock} = (1-f_{rock})\ \theta_{soil} + f_{rock}\ \theta_{rock} \quad [3.5]$$

where f_{rock} is the fraction of the volume occupied by rock, and θ_{rock} is the volumetric water content in rock. Mean θ_{rock} was 0.01 m^3 m^{-3} (n=73), and there was no appreciable change in water content for either chert or limestone during the 2-week period that calibrations were done.

The total measurement volume for neutron probe measurements $V_{t,n}$ was assumed to be an ellipsoid with the x and y dimensions given by Eq. [3.1] and the z dimension by Eq. [3.2], and was calculated as

$$V_{t,n} = \frac{4}{3}\pi \left(15\ \theta_{soil+rock}^{-\frac{1}{3}}\right)^2 \left(9\ \theta_{soil+rock}^{-\frac{1}{3}}\right). \quad [3.6]$$

Volumetric water content in $V_{t,n}$ was estimated by

$$\theta = \frac{\theta_{soil+rock}(V_{t,n}-V_{soil})+\theta_{soil}V_{soil}}{V_{t,n}} \quad [3.7]$$

where V_{soil} is the volume of the portion of the ellipsoid outside the portion containing the soil-rock mixture. In calculating measurement volumes and water contents, we set the radius of the drum as the maximum value for x and y dimensions of the ellipsoid, recognizing that the zone of influence might have extended beyond the drum at low water contents. For the gamma density measurements, the radius of the drum was used as the effective radius for the zone of influence, based on results from Morris and Williams (1990).

Additional measurements were done in sand to evaluate the impact of rock by itself on neutron scattering, and potential leakage of neutrons and gamma radiation from the drum on count ratios. Count ratios were measured in dry sand (θ = 0.02 m^3 m^{-3}) and wet sand (θ = 0.40 m^3 m^{-3}) only, and then in dry sand with rock. The dry sand minimized scattering of neutrons from hydrogen nuclei, and created a worst-case scenario for radiation leakage. Following these measurements, a 95-cm diam. frame was constructed around the drum, filled with saturated sand, and measurements repeated.

Results and Discussion

Neutron Probe Calibration

The relationship between CR_n and θ, obtained with different fractions of rock was nonlinear and nearly identical to that obtained when rock was absent (Fig. 3.5). This indicates that the main effect of rock on neutron thermalization was to reduce water content, and the scattering by hydrogen nuclei. The lesser effect of rock on neutron

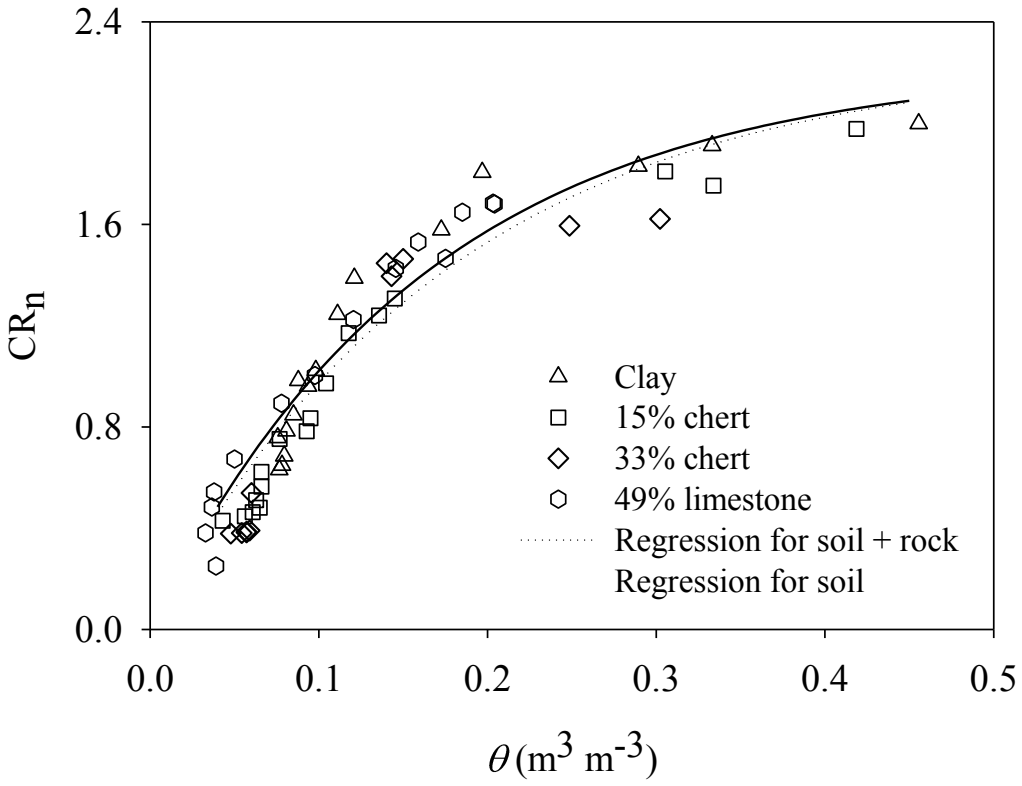

Fig. 3.5 Neutron probe count ratios (CR_n) as a function of volumetric water content (θ). Regressions curves are for soil + rock (solid line) and soil only (dashed line).

Table 3.1 Neutron probe count ratios (CR_n) as a function of water content (θ) and rock volume, measured with and without the drum surrounded by a saturated sand envelope. ΔCR_n is the difference between count ratios measured with the saturated sand envelope and with the drum alone.

		CR_n		
θ ($m^3\ m^{-3}$)	Rock volume (%)	Drum	Drum + saturated envelope	ΔCR_n
0.01	46	0.31	0.47	0.16
0.01	9.6	0.14	0.30	0.16
0.02	0	0.16	0.31	0.15
0.36	9.6	1.64	1.62	-0.02
0.40	0	1.94	2.08	0.14

scattering can be seen in the measurements made in dry sand. Count ratios with 46% rock in the measurement volume averaged 0.31 compared to 0.16 with dry sand only (Table 3.1). This is consistent with findings by Lal (1979) that showed CR_n of gravel-clay mixtures was higher than that of clay. High rock content could potentially reduce measurement sensitivity to θ because the impact of decreased water content could be partially offset by increased scattering by rock. However, we did not find consistent evidence of this in our measurements (Fig. 3.5).

We attribute the nonlinearity to changes in measurement geometry caused by the foam-filled void space (Li et al., 2003). As discussed by Tokumoto et al. (2011), the measurement volume decreases with increasing θ, so an increasingly larger fraction of the measurement volume is occupied by the foam as θ increases. This impact of measurement geometry becomes more pronounced as the diameter augered for the access hole increases.

Our results indicated that a single calibration curve could be used for the conditions at our field site, regardless of the amount of rock in the soil profile. Regression analysis of all measurements, with and without rock, yielded the equation

$$CR_n = 2.29\left(1 - e^{-5.45\,\theta}\right) \quad [3.8]$$

with an r^2 of 0.93. Although the drum method allowed us to create a range of water contents and rock density for more accurate calibration than is achievable in the field, it is possible that leakage of neutrons from the drum affected the calibration. Equation [3.1] implies minimal leakage from the 60-cm diam. drum for $\theta > 0.12$ m^3 m^{-3}, and an increase in leakage as θ decreases. Measurements in sand showed evidence of small

leakage, regardless of water content (Table 3.1). Count ratios with the saturated sand envelope around the drum ranged from 0.14 to 0.16 higher than with the drum alone, except for one set of measurements where CR_n with the saturated envelope was 0.02 lower. These results suggest possible underestimation of θ by Eq. [3.8] in field applications. Because the calibration curve is exponential, the greatest impact of measurement uncertainty occurs at high θ where small changes in CR_n produce the largest changes in estimated water content.

Density Probe Calibration

Morris and Williams (1990) found that the relationship between CR_d and ρ_{wet} for an aluminum access tube of diameter and thickness similar to the tube we used could be described by the equation

$$CR_d = \rho_{wet}^{0.734} \exp(2.82 - 1.65\ \rho_{wet} + 0.191\ \rho_{wet}^{2}). \quad [3.9]$$

However, count ratios we measured were larger than predicted by Eq. [3.9] (Fig. 3.6). We believe the higher values were due to the foam sealant occupying a portion of the measurement volume, thereby reducing the density around the probe and the absorption of gamma radiation. Measurements made with a tight fit between tube and soil (no foam) were similar to what was predicted by Eq. [3.9] (Fig. 3.6). Additional measurements in saturated gravel and water confirmed that CR_d increased with increasing hole diameter surrounding the access tube (Fig. 3.7).

To account for the effect of the foam on CR_d, we applied a multiplier of 1.31, obtained by regression analysis, to Eq. [3.9], yielding the equation

$$CR_d = 1.31\ [\rho_{wet}^{0.734} \exp(2.82 - 1.65\ \rho_{wet} + 0.191\ \rho_{wet}^{2})] \quad [3.10]$$

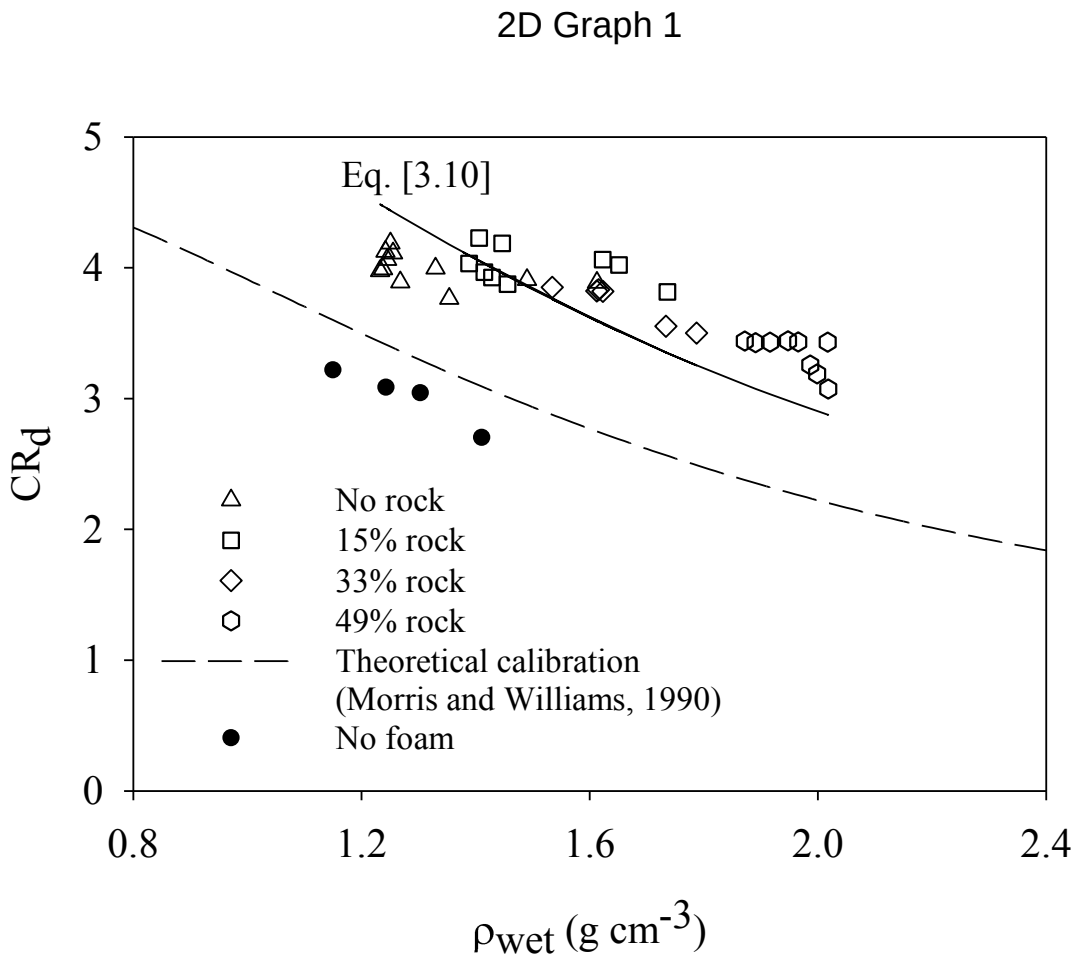

Fig. 3.6 Gamma density probe count ratios (CR_d) as a function of wet bulk density (ρ_{wet}). Open symbols are measurements with the annular space between access tube and soil sealed with polyurethane foam. Solid circles are for measurements in clay with a tight fit between access tube and soil.

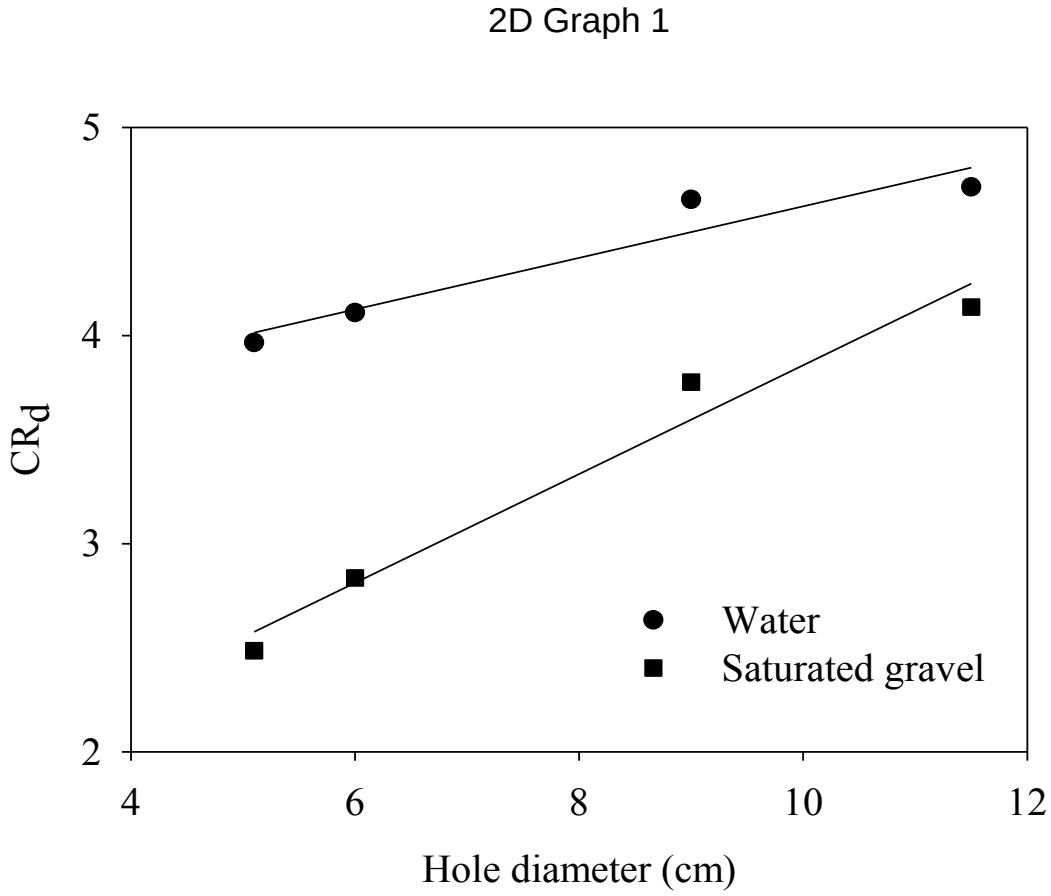

Fig. 3.7 Gamma density probe count ratios (CR_d) in water and saturated sand as a function of access hole diameters. The annular space between access tube and the media soil was filled with the polyurethane foam.

with an r^2 of 0.86 for values of ρ_{wet} in the range of 1.2 to 2.0 g cm^{-3} (Fig. 3.6). While Eqs. [3.9] and [3.10] describe the CR_d-ρ_{wet} relationship over a wide range of densities, iterative procedures are needed to solve for ρ_{wet}. In practice, a linear equation can be used over the higher than measured in the drum alone. Morris and Williams (1990) found leakage errors were <1% errors using the same model probe and a similar size drum. We found no evidence that leakage errors decreased as ρ_{wet} increased.

Field Measurements

Neutron probe and gamma density count ratios at each of the 36 grid points (Fig. 3.3) were measured at 0.20 m intervals from depths of 0.20 to 1.6 m. Figures 3.8 and 3.9 show examples of spatial and temporal variability in θ and ρ_{wet} obtain from application of the calibration Eqs. [3.8] and [3.10]. Measurements are from two days, 4 August and 28 October 2009. The first day was near the end of a 2-year drought, with 45 mm of rain falling in the 30 days prior to the measurement date. The soil profile was dry throughout and areas of very low θ were associated with regions of high ρ_{wet}, suggesting the presence of rock. The second day was during of a period of unusually high autumn rainfall, with 298 mm of rain falling in the previous 30 days. Neutron probe measurements on the second day showed infiltration to depths of 1.0 m. Of interest is the water content at a depth of 0.6 m. Water content was relatively high, except for a region in the upper right-hand quadrant in Fig. 3.8 that was associated with higher ρ_{wet} (Fig. 3.9). At 1.0 m, θ was high in only a small portion of the measurement grid, suggesting preferential flow in that region of the soil profile.

Dry bulk density, estimated by subtracting the density of water in the soil volume

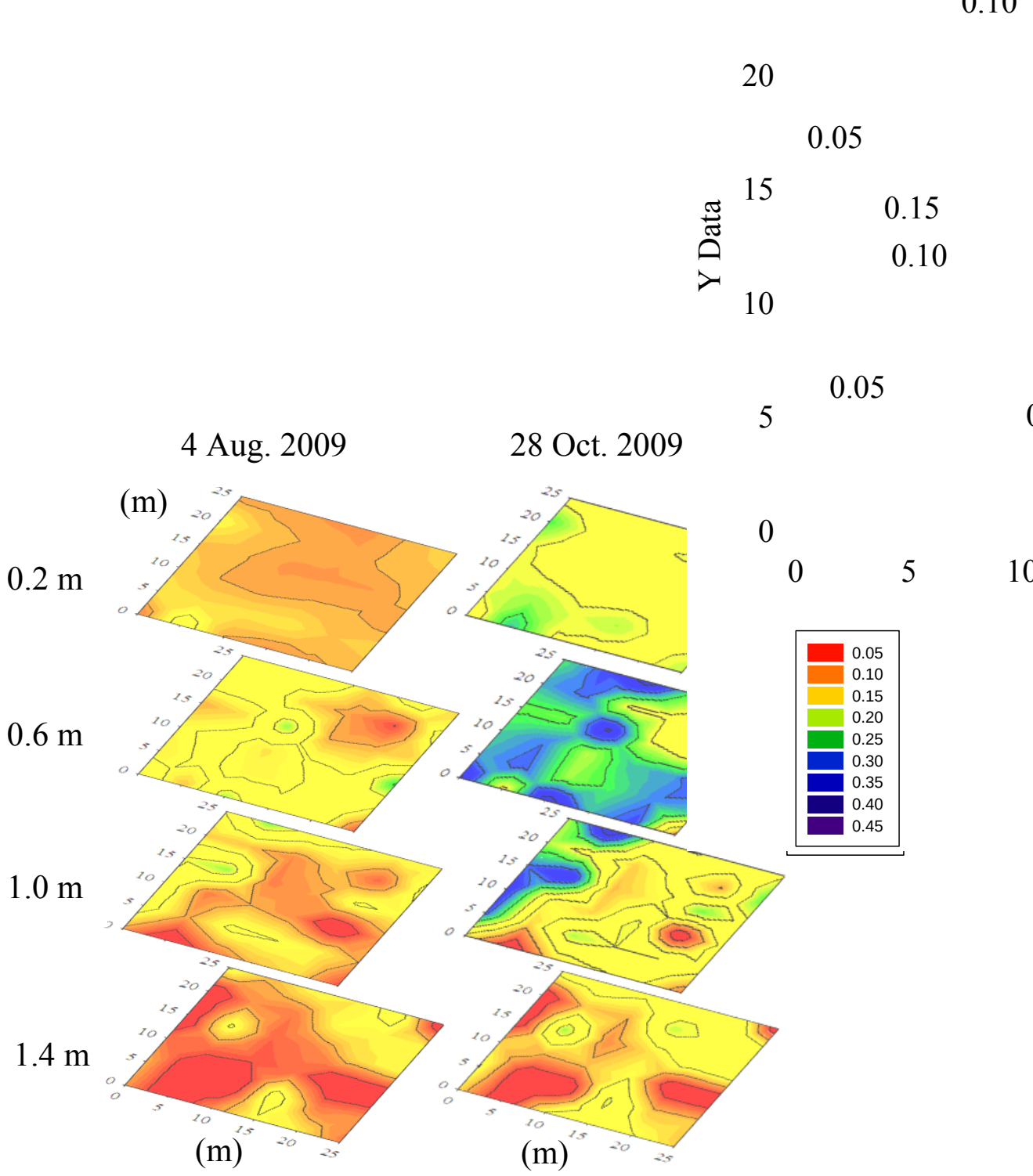

Fig. 3.8 Spatial variability of water content (θ) in the field at four depths on 4 August and 8 October 2009.

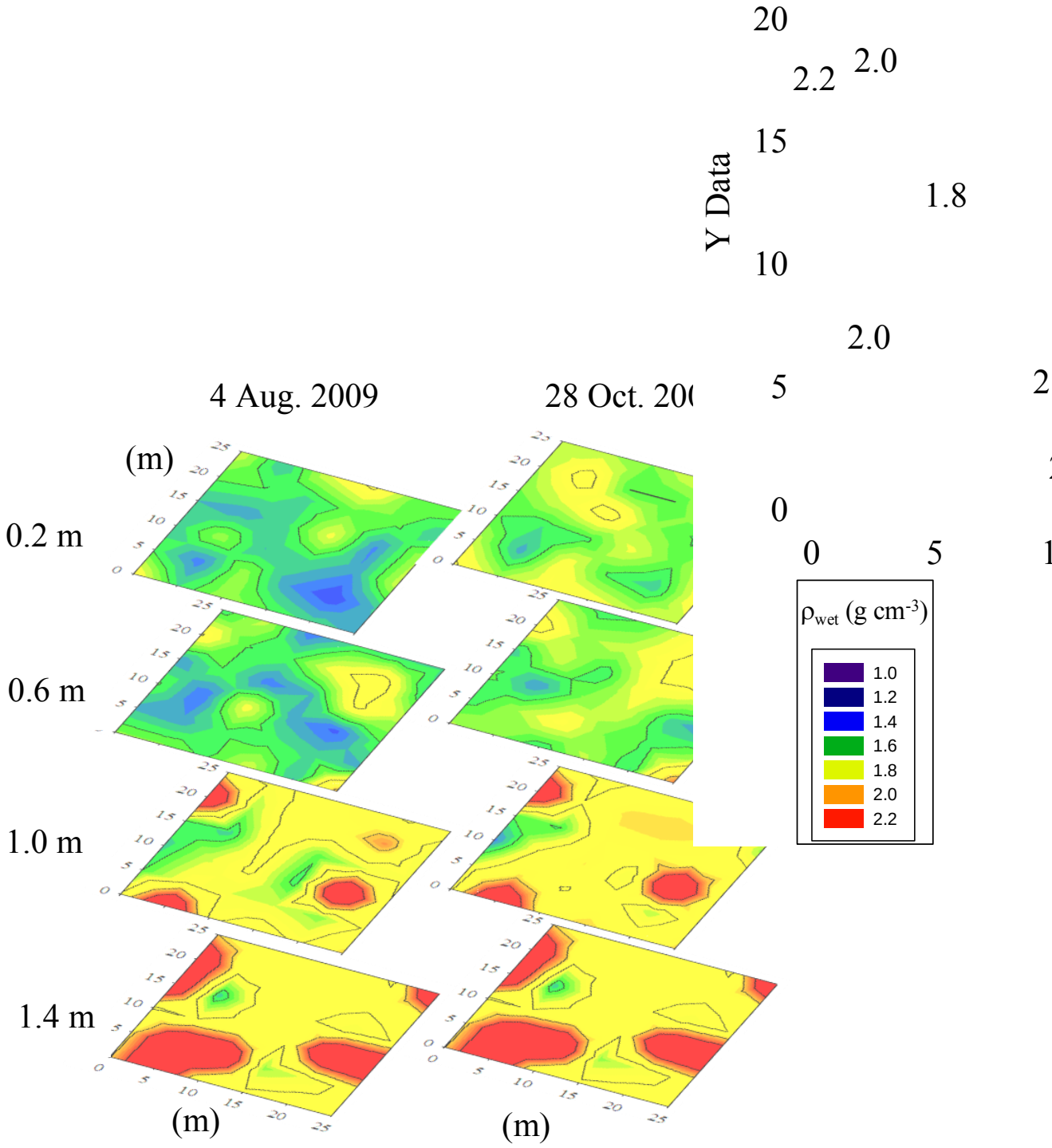

Fig. 3.9 Spatial variability of wet bulk density (ρ_{wet}) in the field at four depths on 4 August and 8 October 2009.

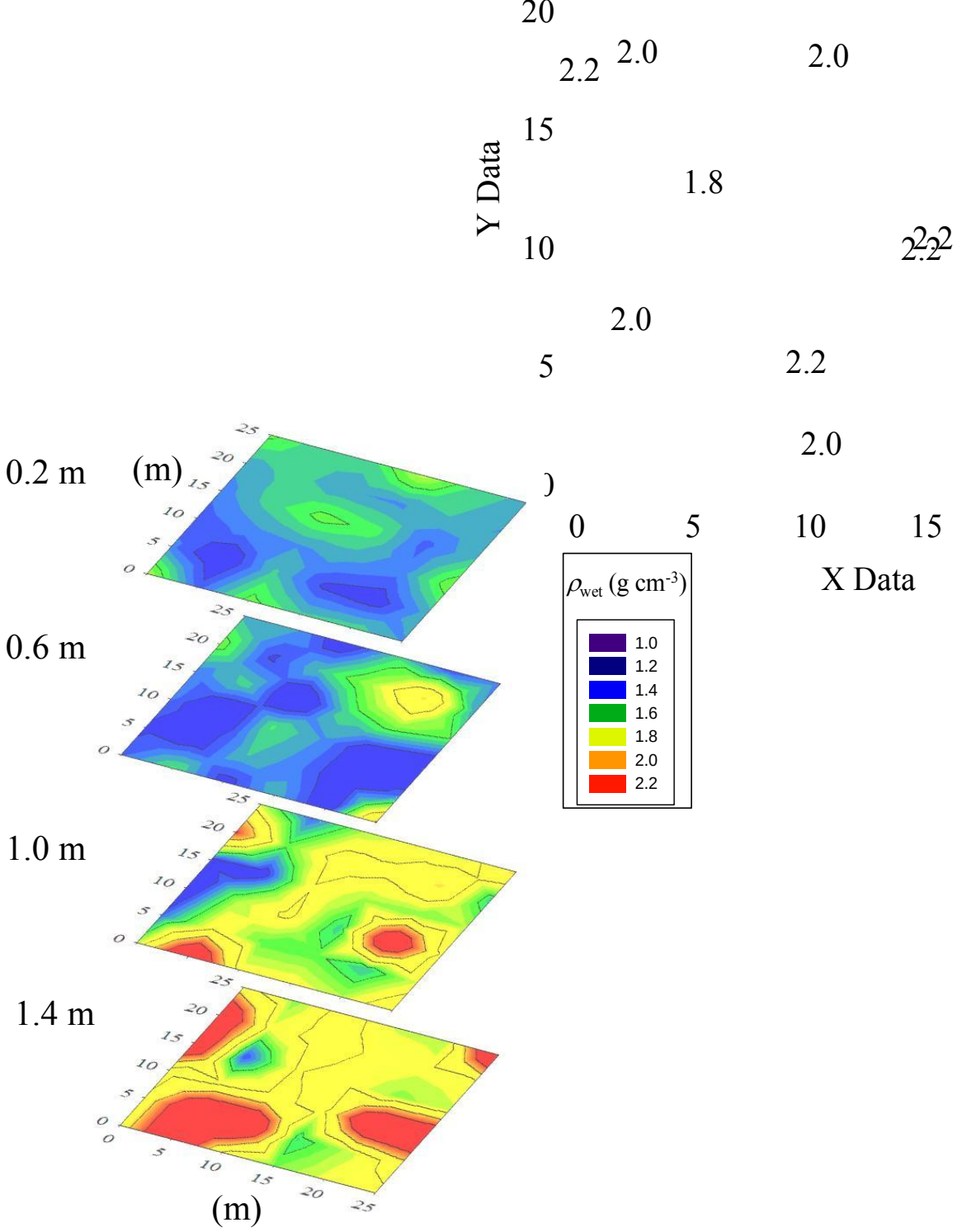

Fig. 3.10 Spatial variability of dry bulk density (ρ_b) at 4 depths in the field. Dry bulk densities were obtained by subtracting density of water from wet bulk density.

from ρ_{wet}, is shown in Fig. 3.10. Densities in Fig. 3.10 are the averages of 5 measurements made between 2009 and 2011. Dry bulk densities ranged from 1.2 to 2.0 g cm^{-3}, higher than for typical clay soils because of rock, and densities were greater in deeper regions of the profile where larger rock fragments were present.

Conclusions

Our study shows that neutron thermalization and gamma densitometry are effective methods of characterizing spatial variability in water content and bulk density in rocky soils. Although rock does scatter neutrons, it mainly affects neutron thermalization through its impact on water content in the measurement volume. The rock that we used in probe calibration was dry, so rock reduced water content. However rock such as limestone and weathered granite, can have water storage capacities that are comparable to coarse-textured soils (Zil'berbord et al., 1979; Graham et al., 1997). Neutrons are thermalized by rock-bound water, so the neutron method can be used to account for water stored in rock (Zil'berbord et al., 1979). For neutron thermalization, a single calibration curve can be used over a wide range of rock densities, eliminating the need for a family of curves and a priori knowledge of rock distribution in the soil profile to obtain accurate measurements of water content. Combined use of neutron thermalization and gamma densitometry allows dry bulk density to be determined so that regions of high rock density can be located.

A complicating factor in use of neutron and gamma densitometry probes in rocky soil is that bore holes will generally have larger diameters than the access tubes, so the material used to backfill the holes will affect the measurements. In our case, we used low

density polyurethane foam as a sealant which caused some loss of sensitivity of neutron probe measurements at high water contents. The foam decreased absorption and increased scattering of gamma particles, resulting in greater count ratios than are obtained with a tight fit between access tube and soil. However, it did not result in loss of sensitivity of the gamma method to bulk density.

CHAPTER IV

WATER STORAGE AND UPTAKE IN A KARST SAVANNA ON THE EDWARDS PLATEAU, TEXAS

Introduction

Woody plants are encroaching into arid and semi-arid grasslands and savannas across the globe, with potentially serious consequences for local and regional hydrology. This is especially concerning in karst landscapes because karst aquifers provide 25% of freshwater for human consumption worldwide, and 40% in the U.S. (White et al., 1995). Karsts are formed from dissolution of soluble rock, generally limestone or dolomite, resulting in well-developed underground drainage and strong interactions between surface water and groundwater. Soils on karst are generally shallow, and rock occupies a significant fraction of the soil volume. This limits water retention (Fiés et al., 2002) and creates high spatial variability in water storage capacity. The shallow bedrock restricts vertical root growth but roots can penetrate weathered rock through cracks and solution-enhanced fissures (Grigg et al., 2010; Katsura et al., 2009). Weathered limestone products such as marl, and soil pockets that may occur between layers of rock can also store significant quantities of water (Querejeta et al., 2006; Estrada-Medina, 2012), but preferential flow through fissures and channels can rapidly remove water from the root zone (Dasgupta et al., 2006; Arbel et al., 2010; Canton et al., 2010).

Trees growing on karst differ in the their rooting patterns and responses to water deficits (Estrada-Medina et al., 2012; Jackson et al., 1999; Schwinning, 2008), and some

species may undergo seasonal shifts in water consumption from predominantly shallow to predominantly deep sources (McCole and Stern, 2007). Jackson et al. (2000) found that an Ashe juniper (*Juniperus ashei*) growing on the karst Edwards Plateau, Texas, with root access to water in a cave obtained 24% of its water from depths greater than 7 m. Pockman et al. (2008) reported that deep roots of juniper on the Plateau provided 60% of daily water use during a prolonged drought. Estrada-Medina et al. (2012) in a study in northern Yucatán, found that roots were strongly associated with soil-filled dissolution cavities within the limestone matrix. These soil pockets accumulated water from rainfall and had higher water contents than the topsoil. This water was available to plants longer than water in topsoil and allowed trees to survive during drought. In contrast, studies by Schwinning (2008), Heilman et al. (2009), and Heilman et al. (2012) on the Edwards Plateau found little evidence that deep roots extracted significant amounts of water from stable sources at depth. They found that trees on the Plateau used water stored in rock, but these sources were quickly depleted like the topsoil above. Kukowski et al. (2012) examined water use of three coexisting species (cedar elm – *Ulmus crassifola*; live oak – *Quercus fusiformis*; Ashe juniper) growing on shallow soil above bedrock on the Plateau, and found they used nearly identical sources of water with no evidence of a shift to deeper sources of water when shallow sources were depleted. Instead, the species partitioned water differently by time with live oak showing the greatest rate of decline in sap flow during drought, and juniper the slowest rate.

Identifying and quantifying sources of water used by woody plants is key to evaluating the impact of woody encroachment on karst hydrology. The focus of our

study is a savanna with ~50% woody cover in the Texas Hill Country, a karst ecoregion on the eastern edge of the Edwards Plateau in south and west central Texas. This region includes the Edwards-Trinity aquifer which provides drinking water to over 2 million people. Suppression of wildfires and overgrazing have permitted woody species like Ashe juniper (*Juniperus ashei*) and honey mesquite (*Prosopis glandulosa*) to encroach into grasslands and savannas, producing large areas dominated by dense thickets of woody plants. Brush removal has become widely-accepted as a means of increasing water yield (Tennesen, 2008), despite a lack of quantitative information on how water use is affected by local geology, plant species composition, and rainfall.

In an earlier study, Heilman et al. (2012) compared 5 years of water and energy fluxes from the savanna with that from a nearby woodland. They found that ET from the savanna was higher than the woodland by an average of 24 mm y^{-1} in spite of less energy available for evaporation, and concluded that greater water storage in the savanna due to deeper soil was responsible for higher ET. Yet, ET at both sites became water-limited within days after rainfall ended which indicated that water uptake was predominantly from shallow roots. This apparent contradiction between higher ET and rapid depletion suggests that roots in the savanna had access to sources of water in fractured rock that were slow to deplete, allowing higher transpiration to be maintained over the long term when shallower sources of water were exhausted. In this paper, we examine spatial and seasonal variability in water storage at the savanna, and examine root water uptake as a function of depth to estimate proportional contributions of shallow and deep roots to ET.

Materials and Methods

Site Description

The research site (29°56.5'N, 97°59.4'W) is a savanna on the Freeman Ranch, a 1700 ha research area near San Marcos, Texas, USA (Fig. 4.1). The savanna contains clusters of Ashe juniper and mesquite (*Prosopis glandulosa* Torr.) interspersed among grassland dominated by King Ranch bluestem (*Bothriochloa ischaemum* (L.) Keng) and Texas wintergrass (*Nassella leucotricha* (Trin. & Rupr.) Pohl), a C_3 species. Tree densities are 336 juniper ha^{-1} and 304 mesquite ha^{-1}. Seasonal maximum leaf area indices were 1.81 for juniper and 0.65 for mesquite (Elkington et al., 2012). The soil is a Rumple gravelly clay loam (Clayey-skeletal, mixed, active, thermic Typic Argiustolls, 1% slope) with chert fragments occupying ~50% of the soil volume between depths of 0.2 and 1.0 m. The average volume and density of chert fragments (n= 73) are 52.7 cm^3 and 2.4 g cm^{-3}, respectively. Limestone residuum (density = 2.6 g cm^{-3}) occurs at depths of 1 to 1.5 m.

Water Content Measurements

In the summer of 2009, 36 aluminum access tubes (5.1-cm diam.) were installed in a 25 × 25 m grid (5 m node spacing) for neutron probe measurements of volumetric soil water content θ (Fig. 4.2). Bore holes were drilled to a maximum depth of 1.6 m using a 8.9-cm diam. screw auger attached to a truck-mounted drill rig (CME 75, Central Mine Equipment Co., St. Louis, MO), and access tubes inserted and sealed with expandable polyurethane foam (Poly-Set, Utility Structural Systems, Arlington, TX) as described by Tokumoto et al., (2011). At 8 locations, the drill encountered impenetrable

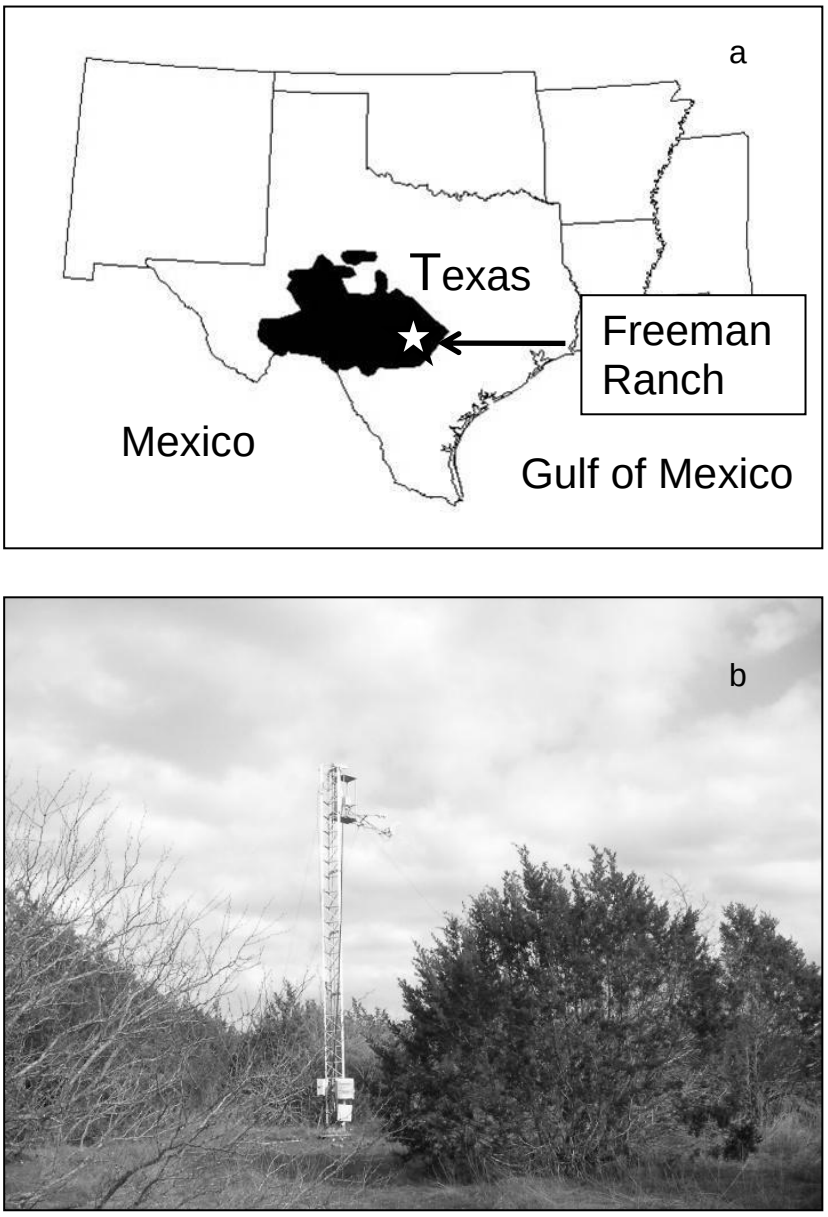

Fig. 4.1 Location of the Edwards Plateau (shaded) and view of the Freeman Ranch.

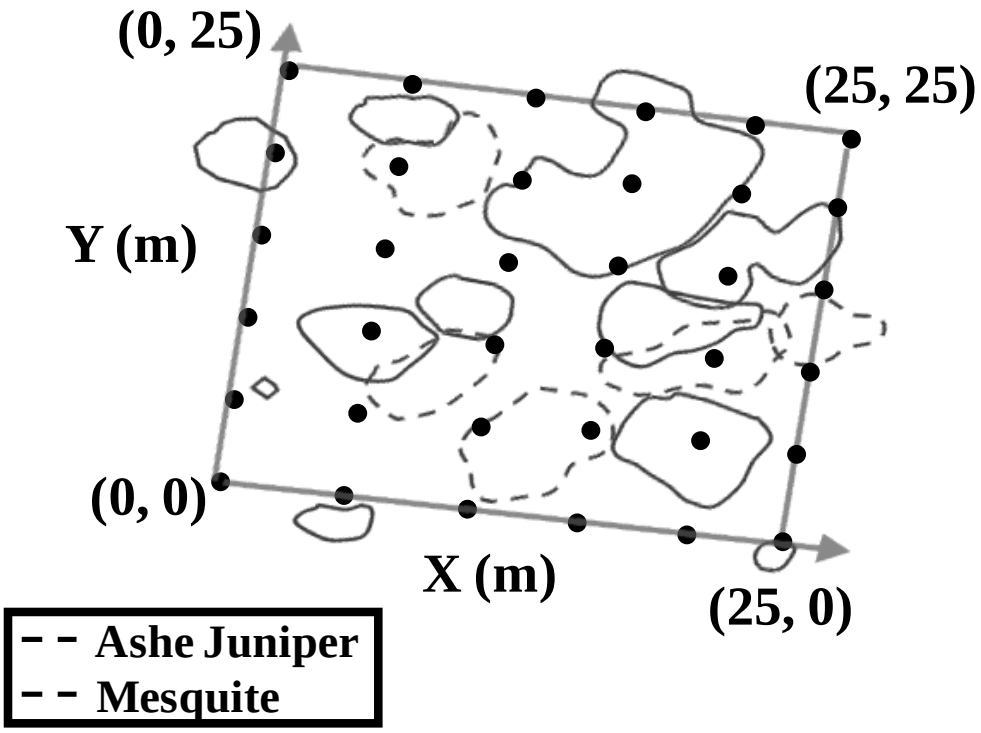

Fig. 4.2 Diagram of experimental site showing the distribution of access tubes and locations of Ashe juniper and honey mesquite in the 25 × 25 m measurement grid.

rock at depths ranging from 0.8 to 1.2 m, which restricted insertion of probes to those depths. Water content profiles were measured at 0.2 m depth intervals, beginning at 0.2 m below the soil surface, using a CPN Model 503DR neutron moisture gauge (Campbell Pacific Nuclear Corp., Concord, CA). Water content in the upper 0.15m was measured by time domain reflectometry (TDR) with probes installed near the access tubes. Wet bulk density (ρ_{wet}) profiles were measured in each access tube using a model CPN 501DR density probe (Campbell Pacific Nuclear Corp.). Neutron and density probes were calibrated in a 189 L drum with known volumes of soil, rock, and water (Tokumoto et al., 2012). Dry bulk density (ρ_b) was estimated by subtracting density of water from ρ_{wet}. TDR measurements were recorded every 6 hr by a model CR1000 datalogger (Campbell Scientific, Logan, UT). Neutron probe measurement intervals ranged from days to weeks depending on amount and frequency of rainfall.

Evapotranspiration Measurements

Evapotranspiration (ET) was determined by eddy covariance using the equation

$$\mathrm{ET} = \overline{w'\rho_v'} \qquad [4.1]$$

where w (m s^{-1}) is vertical wind speed, ρ_v (g m^{-3}) is water vapor density, $'$ denotes fluctuation about a mean value, and the overbar is a temporal average (30-min in our case). Vertical wind speed and vapor density were measured by a sonic anemometer (CSAT3, Campbell Scientific) and open-path gas analyzer (LI-6262, Li-COR, Lincoln, NE), respectively, mounted at a height of 10 m above the surface on a tower that was 66 m downwind of the soil water content measurement grid. Processing of eddy covariance measurements included spike removal, 'natural wind' coordinate rotation (Lee et al.,

2004), adjustments for variations in air density due to water vapor (Webb et al., 1980), corrections for frequency response (Massman, 2000), and corrections for energy balance closure (Twine et al., 2000). Data collected during low turbulence (friction velocity < 0.15 m s^{-1}) were rejected. Data gaps created by low turbulence and instrument malfunctions were filled using the on-line tools of Reichstein (http://www.bgc-jena.mpg.de/~MDIwork/eddyproc/upload.php).

Water Balance

We used a water balance analysis to examine dynamics of soil water storage and root water uptake. The change in water storage in each layer of thickness Δz, at depth d, over time interval was Δt calculated as

$$\Delta S_d = (\theta_{i,t} - \theta_{i,t+\Delta t})\,\Delta z_i \qquad [4.2]$$

where θ is volumetric water content in layer i of thickness Δz_i (0.2 m in our case for neutron probe measurements, 0.15 m for TDR), and t is time. Changes in storage at each depth interval were calculated for every grid point, and then averaged to obtain a spatial mean ($\overline{\Delta S_d}$). At the locations where insertion of access tubes was restricted by rock, we assumed that the remainder of the profile beneath the depth of insertion was occupied by rock. The relative amount of ET originating from root water uptake at depth d ($\frac{ET_d}{ET}$) during periods without rainfall was estimated by the equation

$$\frac{ET_d}{ET} = \frac{\overline{\Delta S_d}}{ET_{ec}} \qquad [4.3]$$

where ET_{ec} is the sum obtained by eddy covariance over time interval Δt. Equation [4.3]

assumes negligible drainage between layers. The fraction of total water uptake originating from below the maximum measurement depth was estimated as 1 - $\frac{ET_d}{ET}$. We estimated drainage below the maximum depth of our measurements using the equation

$$\sum_{t}^{t+\Delta t} D = \sum_{t}^{t+\Delta t} R - \sum_{i}^{n} \overline{\Delta S_d} - \sum_{t}^{t+\Delta t} ET_{ec} \qquad [4.4]$$

where R is rainfall and n is the number of soil layers.

Results and Discussion

Environmental Conditions

Microclimatic conditions at the savanna site from 1 July 2009 (Day 182), the day measurements began, through December 2010 are shown in Fig. 4.3. Solar radiation during the summer was similar in both years, but summertime air temperature and vapor pressure deficits (VPD) were higher in 2009 than in 2010, reflective of the dry conditions at the beginning of the study. July and August 2009 were the final months of a 2-year drought, and total rainfall during these months was only 31 mm. Rainfall during the remainder of the year was 490 mm, 144 mm above the 30-y mean for those months. Total rainfall in 2010 was 796 mm, below the annual mean of 858 mm. There were several pronounced drying cycles during the study during which little or no rainfall occurred (Fig. 4.3). Summertime ET was higher in 2010 than in 2009, and seasonal variations mirrored changes in θ and solar radiation (Fig. 4.3). Total ET over the 17-month study was 1024 mm, 81% of total rainfall.

Soil Water Storage and Uptake

There was high spatial and temporal variability in water storage in the

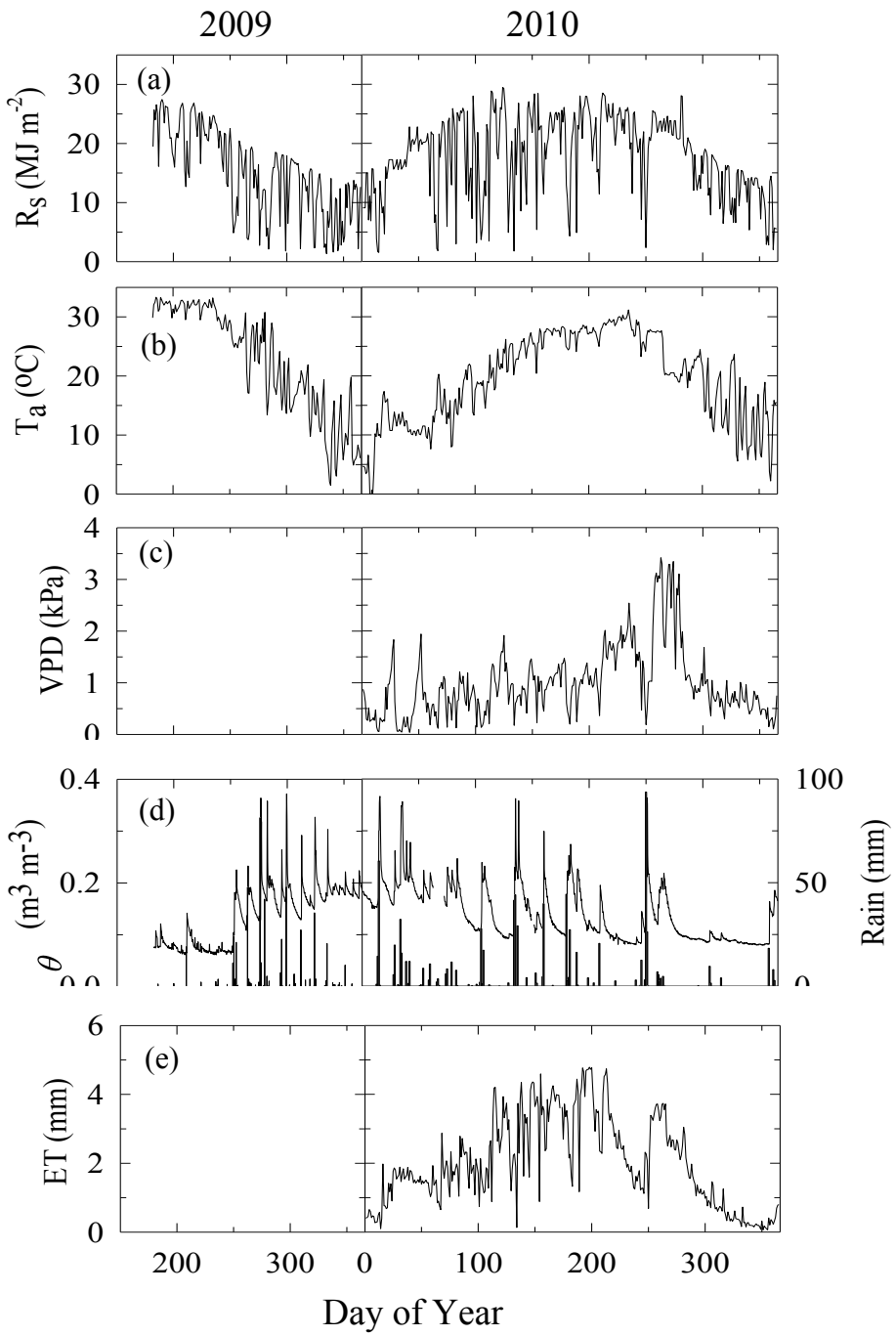

Fig. 4.3 Seasonal variation of (a) solar radiation (R_s), (b) air temperature (T_a), (c) vapor pressure deficit (VPD), (d) rainfall and mean volumetric water content (θ) from 0 to 15 cm deep, and (e) evapotranspiration (ET) from the experimental grid on the Edwards Plateau.

measurement grid as illustrated by Fig. 4.4 which shows water storage before-and-after rainfall in the middle of September, 2009. The amount of rain and cumulative ET during the period were 194 mm and 48 mm, respectively. Water storage capacity, estimated from water content measurements in early February 2010 after heavy autumn and winter rainfall, ranged from 185 to 401 mm (Fig. 4.5). Seasonal changes in water storage, averaged over the entire measurement grid, are shown in Fig. 4.6. Total water storage at the beginning of the study was low, < 200 mm in early August, but after the heavy autumn rains, it rose to 320 mm, of which 63% of the water was in the top half of the profile (Fig. 4.6). Cumulative drainage below 1.6 m for Sept.– Dec. as calculated by Eq. [4.4] was 100 mm, so there was considerable movement of water through lower parts of the profile. However, less water was retained in the lower part of the profile because of higher volume of rock which reduced storage capacity. In 2010, storage ranged from a maximum of 320 mm to a minimum of 207 mm. Cumulative drainage was calculated at 147 mm. Over the course of the 17-month study, an estimated 19% of rainfall drained below the 1.6 m profile. Rock created high spatial variability in θ and ρ_b (Fig. 4.7). Bulk densities were higher than what is typical for clay soil due to rock, and densities were higher in deeper regions of the profile because larger rock fragments were present. Measurements on three days in 2010 (26 Feb., 8 May, 12 Aug.) illustrate this variability. Water content on the first day (26 February) was relatively high due to heavy autumn and winter rainfall. There were areas of low θ that were associated with high bulk density, indicating high rock content. The greatest changes in θ as the soil dried occurred at depths above 1 m. There was evidence of water loss at deeper depths as well,

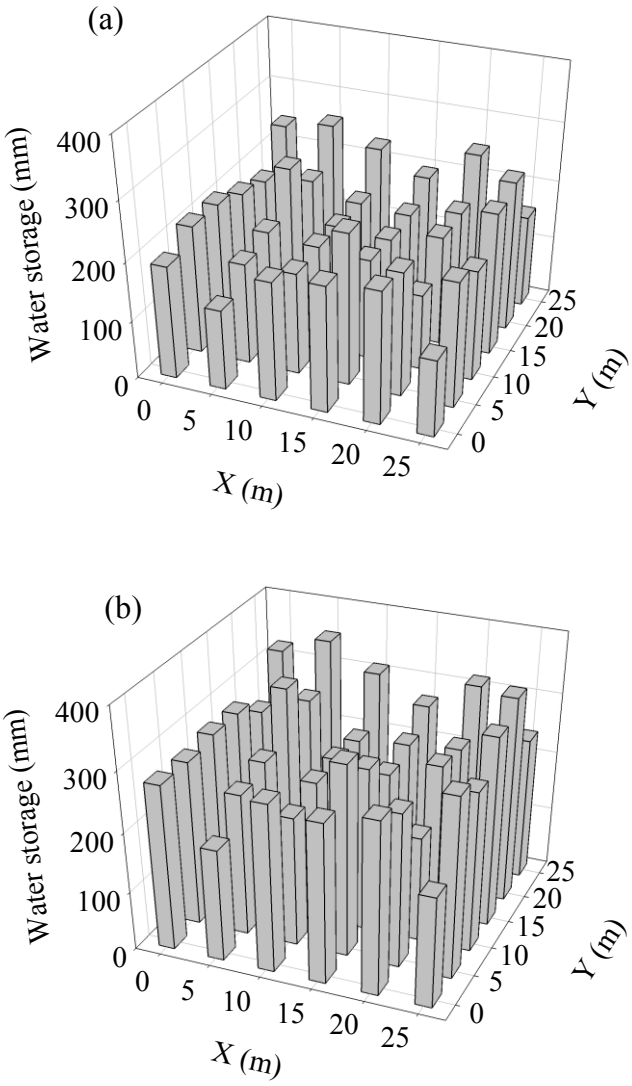

Fig. 4.4 Temp ırements on 15 September (before rainfall) (a) and 7 October (after rainfall) (b) in 2009. The amount of rainfall during the period was 194 mm.

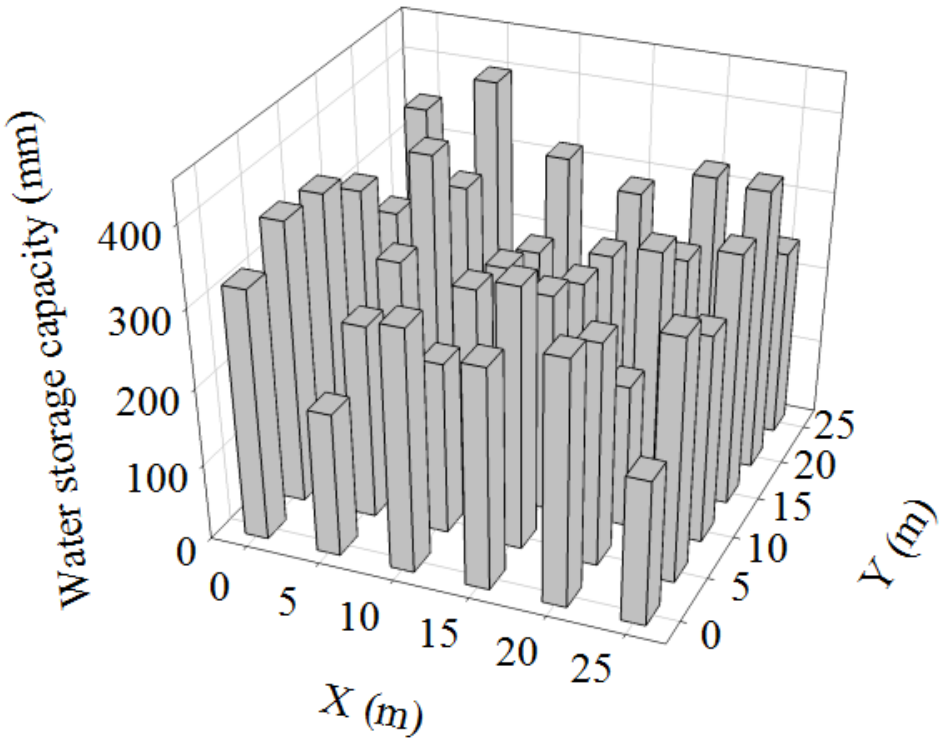

Fig. 4.5 Spatial variability in water storage capacity estimated from water content measurements in February 2010.

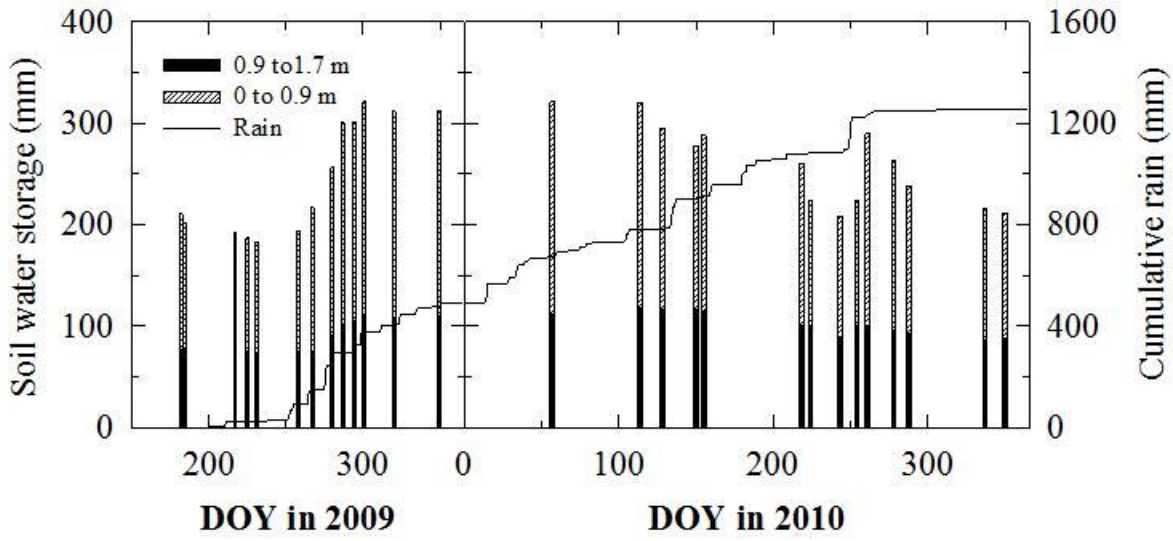

Fig. 4.6 Temporal changes in water storage in the upper 1.6 m of the root zone, along with cumulative rainfall during the study. Values of water storage on each date are the mean of 36 profiles.

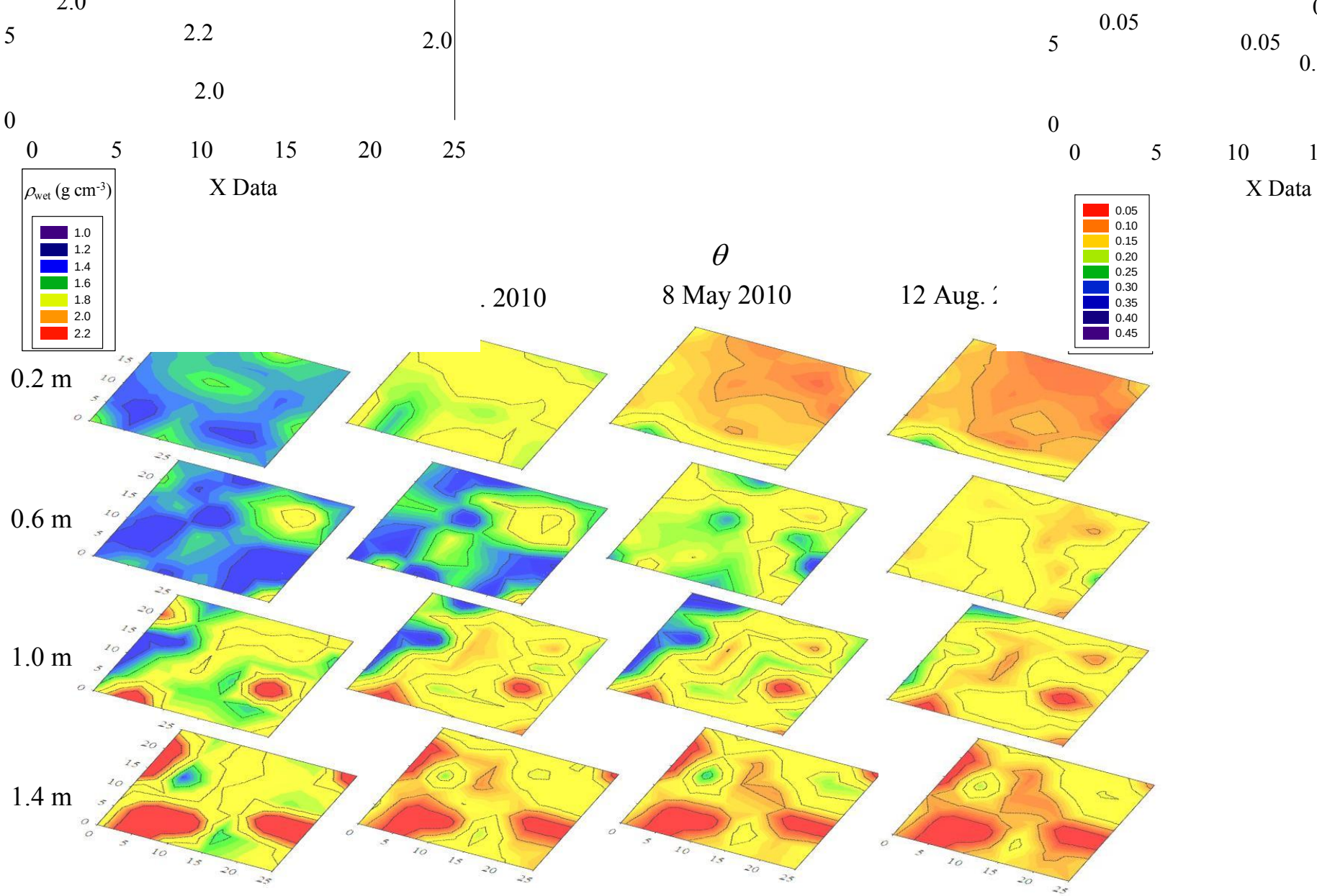

Fig. 4.7 Spatial variability of water content (θ) and dry bulk density (ρ_b) at four depths on 4 August 2009, 28 October 2009, 26 February 2010, 8 May 2010, and 12 August 2010.

most notably near the center of the measurement grid (e.g. grid coordinates 15,15 at the 1.4 m depth in Fig. 4.7), suggesting water uptake at those locations. There were also deeper pockets of stored water (e.g. grid coordinates 5,15 at the 1.4 m depth in Fig. 4.7), similar to the findings of Estrada-Medina at al. (2012), but θ changed very little with time, indicating minimal root uptake at those locations.

Figure 4.8 shows water content profiles beneath a mesquite-juniper cluster, a juniper alone, and in a location where trees were absent for the same days shown in Fig. 4.7. At the mesquite-juniper location, there was high rock density at depths between 0.6 and 1.0 m which resulted in low θ (Fig. 4.8a). Although rock density was high, water moved through or around this layer and was retained at deeper depths, as indicated by the profile on 26 Feb. The largest temporal decreases in θ occurred near the surface and immediately below the rock layer, suggesting substantial root water uptake in those regions of the profile. Temporal changes in θ at the bottom of the profile were minimal. Water content beneath the juniper (Fig. 4.8b) was highest at depths of 0.6 and 0.8 m. The largest temporal changes occurred in the upper 1 m, but there was evidence of water extraction at deeper depths as well. There was less rock in the profile at this location which resulted in greater water retention than beneath the mesquite. Again, there was minimal change in θ at the bottom of the profile. The no-tree location (Fig. 4.8c) had the highest water contents in the upper part of the profile of any location in the measurement grid. It is likely that infiltration at that location was higher because there was no interception of rainfall by tree canopies. There was little change in θ below 1 m, suggesting the absence of significant root water uptake below this depth.

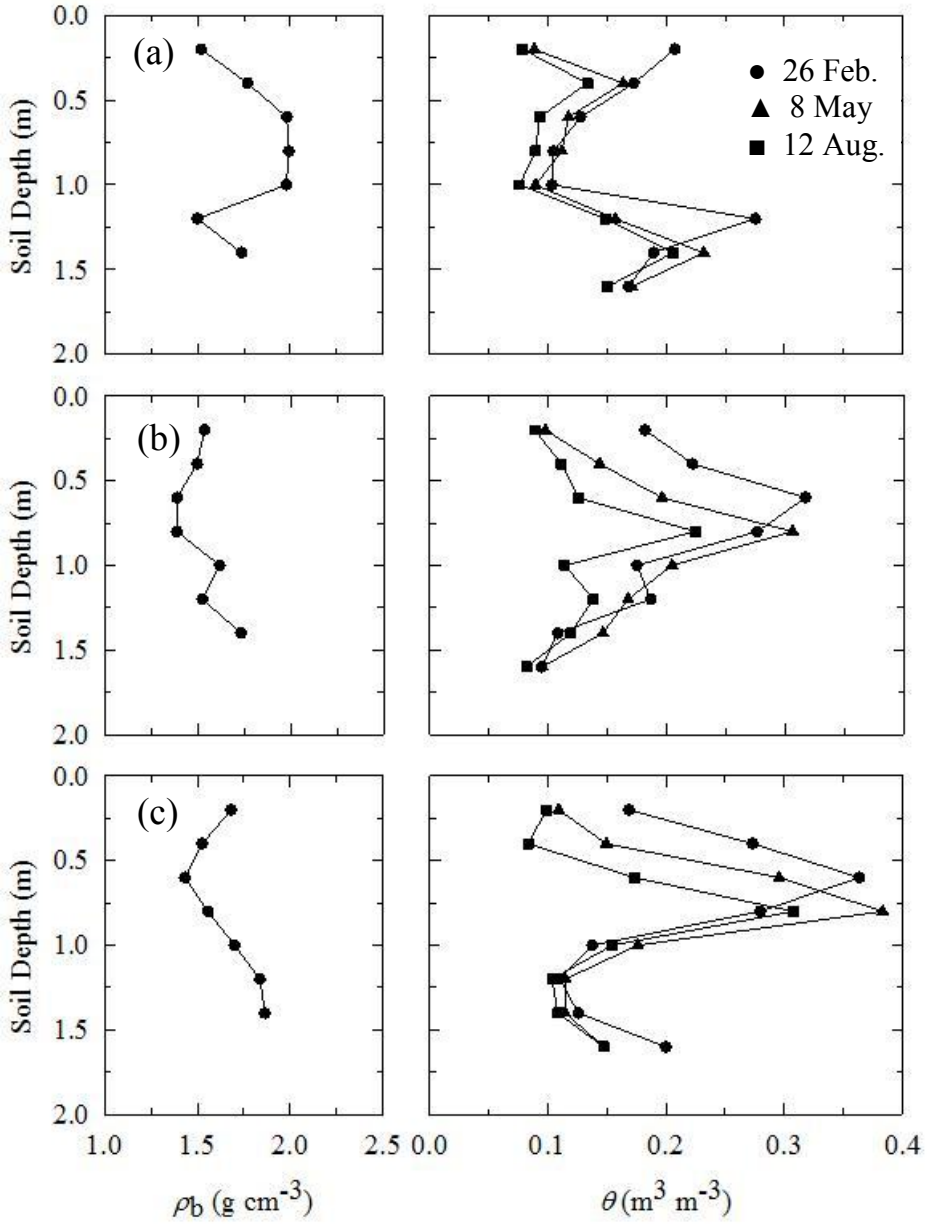

Fig. 4.8 Profiles of bulk density (ρ_b) and water content (θ) beneath a mesquite-juniper cluster (a), juniper (b), and a location where trees were absent (c). Grid coordinates for the three locations are (5,20), (20,20), and (15,0), respectively.

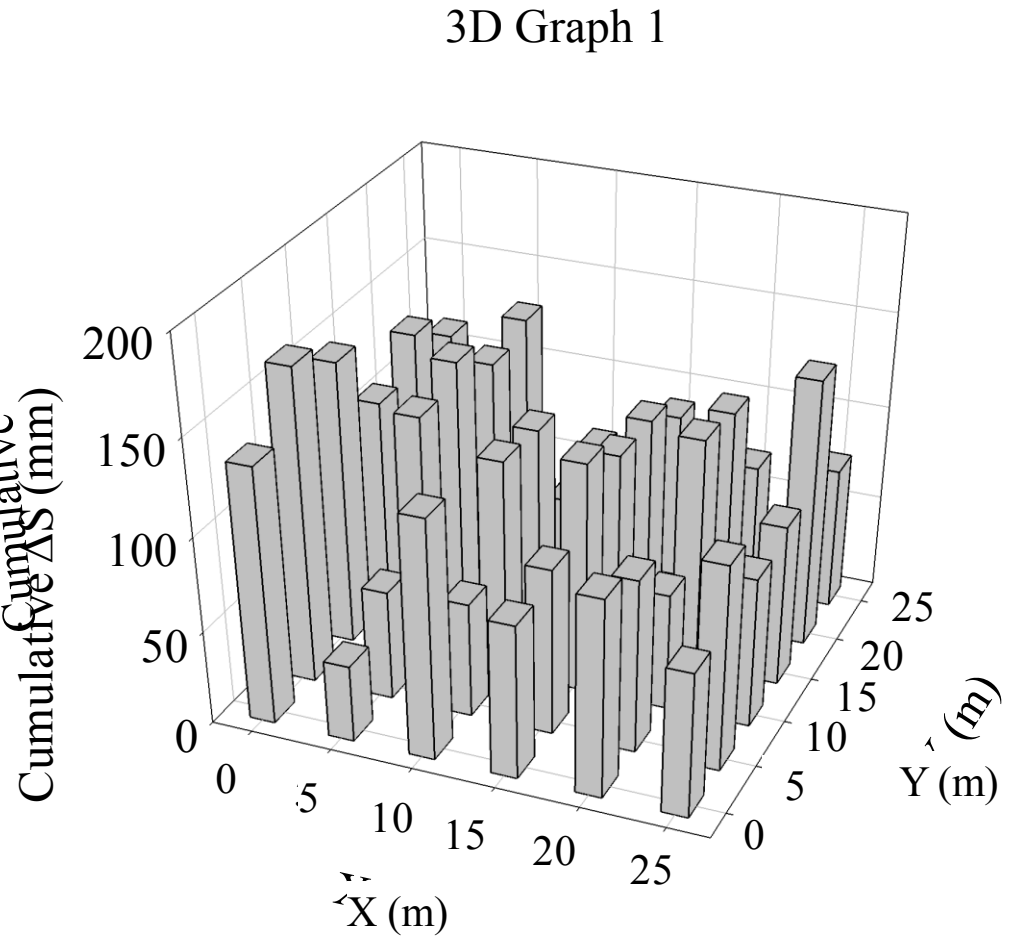

Fig. 4.9 Cumulative changes in water storage (ΔS) between 4 August 2009 and 12 August 2010 in the upper 1.6 m of the soil profile.

The high spatial variability in θ and in distribution of trees let to large spatial differences in water depletion (Fig. 4.9). In the period between 5 August 2009 and 12 August 2010 there was a 125 mm difference between maximum and minimum cumulative ΔS measured at the 36 grid points. The highest water loss occurred at no-tree locations (grid coordinates 0,5 and 0,10 in Fig. 4.9) where rock densities were among the lowest in the grid and water contents among the highest (Fig. 4.7). The least water loss occurred beneath a juniper at grid coordinate 5,0, a location with high rock density (Fig. 4.7). Changes in storage were larger beneath trees that at no-tree locations (Fig. 4.10), indicating greater water extraction by trees than grass.

The highest proportion of the water used in ET, estimated by Eq. [4.3] for periods with no rainfall, came from the upper 1 m of the profile as shown by the three examples in Fig. 4.11. Also shown in Fig. 4.11 are water content profiles during the measurement periods, averaged over the entire grid, along with maximum water contents measured during the study. Maximum θ occurred in early February 2010, following heavy autumn and winter rains, and is an approximation of field capacity. In the first example between 30 May and 4 June 2010 (Fig. 4.11a), 87% of the estimated water uptake came from the upper 1 m, with 54% coming from the 0.4 to 0.8 m depths. Uptake was maximal at 0.4 m. An estimated 4% came from depths between 1.2 and 1.6 m, and 9% from depths below 1.6 m. At the start of this measurement period, θ in the upper 0.6 m was less than field capacity, but there was little departure from field capacity at the remaining depths. ET during this period averaged 3.1 mm d^{-1}, and 120 mm of rain fell in the 30 days prior to the measurement period.

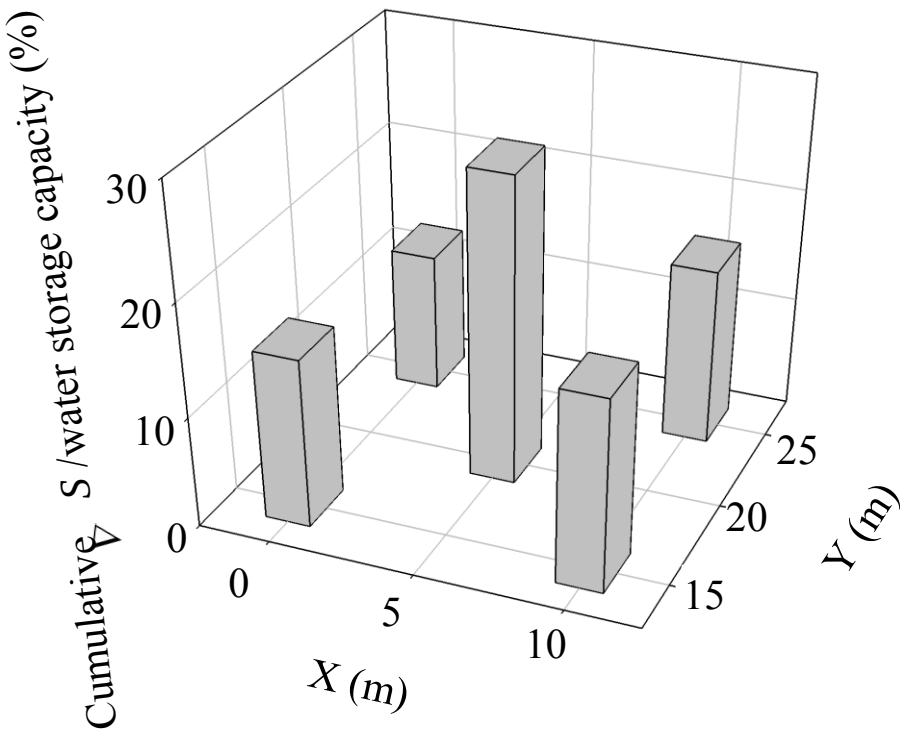

Fig. 4.10 Ratio of cumulative change in water storage (ΔS) between 11 September and 15 October 2010 in the upper 1.6 m, to total water storage capacity beneath a mesquite-juniper cluster located at grid coordinate 5, 20 and at no-tree locations (grid coordinates 0,15, 0,25, 10,15 and 10,25).

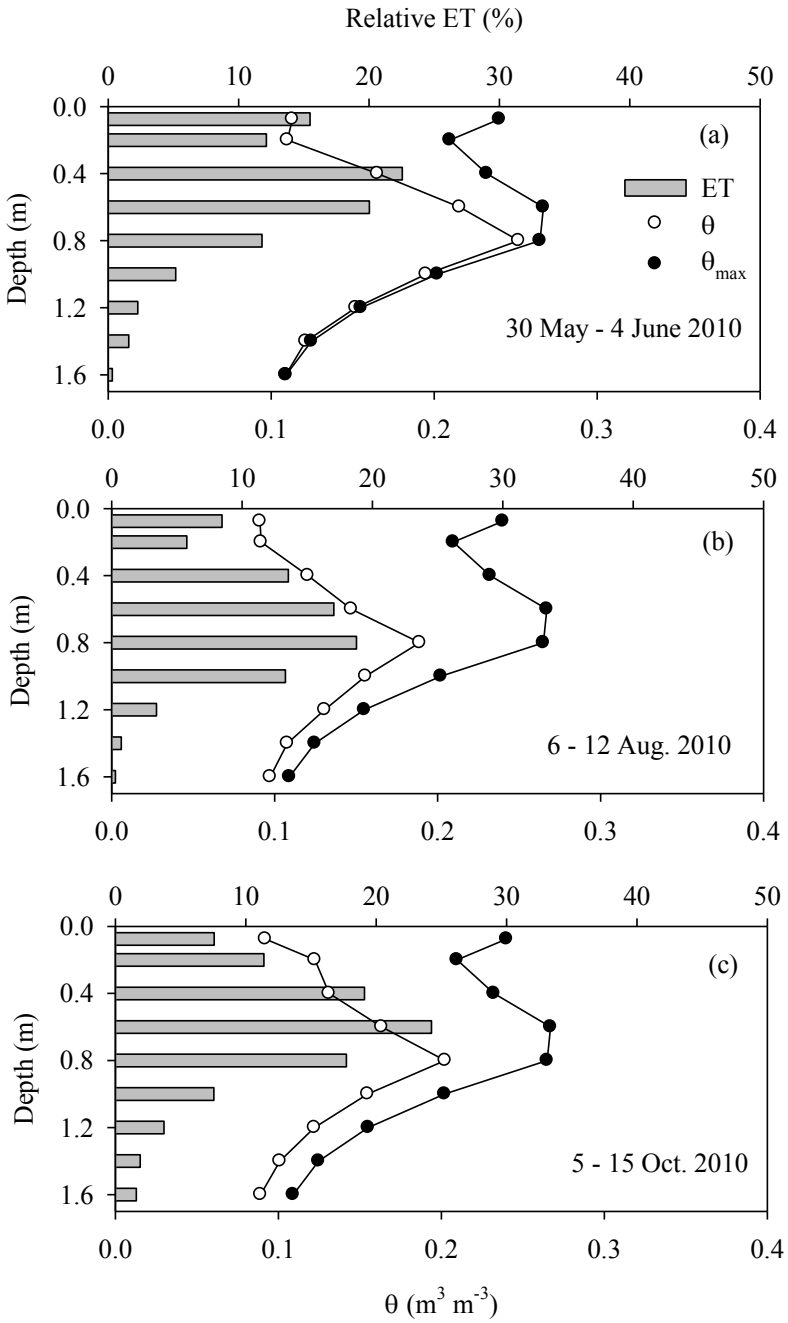

Fig. 4.11 Percentage of evapotranspiration (ET) as a function of soil depth during three periods in 2010. Also shown are water content (θ) profiles during these periods, along with maximum water content (θ_{max}) measured during the study.

In the second example between 6 and 12 August 2010 (Fig. 4.11b), 77% of the ET came from water in the upper 1 m, with 63% from depths of 0.4 to 1.0 m. Maximum uptake occurred at 0.8 m, deeper than the previous example. Four percent of the water came from depths of 1.2 to 1.6 m, with an estimated 19% coming from below 1.6 m. The soil was drier than the previous example, apparently resulting in a shift to deeper sources of water, consistent with results of McCole and Stern (2007). ET averaged 2.1 mm d^{-1} during this period, but only 44 mm of rainfall occurred in the previous 30 days.

In the final example, between 5 and 15 October 2010, 88% of the uptake came from the upper 1 m, with the maximum occurring at 0.6 m (Fig. 4.11c). Seven percent of the uptake came from depths between 1.2 and 1.6 m, and an estimated 5% from below 1.6 m. ET averaged 2.0 mm d^{-1}, and 148 mm of rainfall occurred in the prior 30 days.

A prominent feature of water content profiles was the consistently higher θ at depths of 0.6 to 0.8 m. A plausible explanation is that high rock content at depths of 1 m and greater restricted downward water flow, allowing water to accumulate above the rock.

The profiles of water uptake were in general agreement with root distributions mapped in 2006 at a location 80 m north of the measurement grid. The mapping was done in a 5.4-m long, 2-m deep trench that was excavated over a width of 2 m (Fig. 4.12). All roots of diameters ≥ 3mm were counted in 10 × 10 × 10 cm soil volume increments. The mapping showed that 90% of juniper roots were in the upper 0.7 m of the root zone, while 90% of mesquite roots were above 1 m. Highest root densities occurred at a depth of 0.4 m for both species. Roots of both species were observed

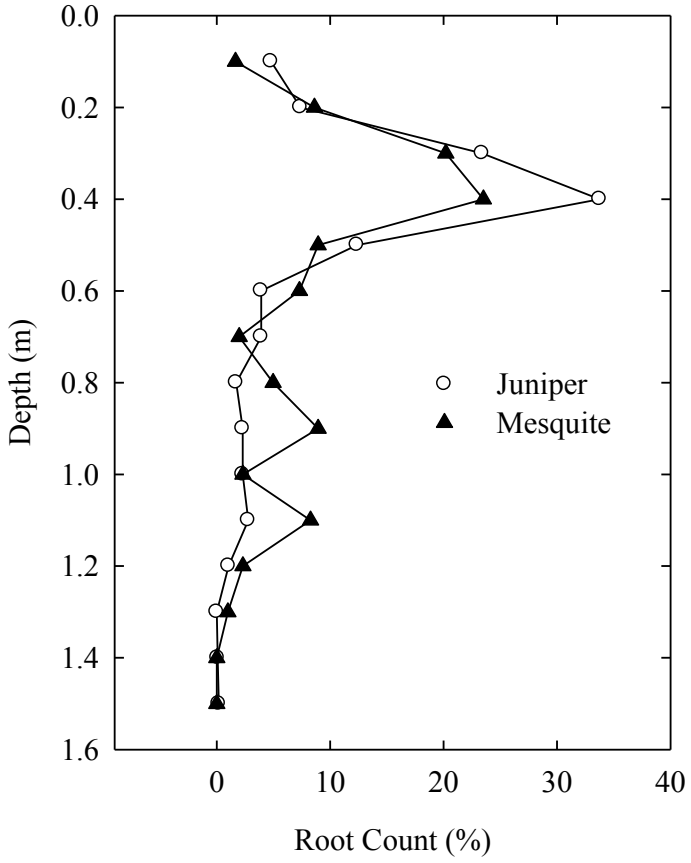

Fig. 4.12 Root count profiles for a juniper and a mesquite mapped in a trench excavated near the water content measurement grid.

disappearing into the bedrock below 1.5 m, consistent with our observations of uptake from below the depth of our water content measurements.

We restricted our evaluation of root water uptake to periods with no rainfall so that drainage between layers would be minimized in application of Eq. [4.3]. There were frequent rainfall events during the study which limited to 6 the number of rain-free periods of sufficient duration and high enough ET to create measurable differences in θ. For those 6 periods, water uptake from the upper 1 m accounted for, on average, 81% of ET, while uptake from below the depth of our measurements averaged 10% of ET.

Our results were similar in some respects to those of Estrada-Medina et al. (2012) who found that that roots in the karst Yucatán were concentrated in the shallow topsoil (<30 cm deep), and in soil pockets within the rock. Fluctuations in water content at their sites were rapid and large, but there was sufficient water stored in rock to allow trees to withstand the dry season. The topsoil at our site was deeper, but high volume of rock reduced significantly the soil water storage capacity, especially deeper in the soil profile. As a result, roots were concentrated in shallow layers, and ET quickly became water-limited during drying cycles between rainfall events (Heilman et al., 2012). However, there also was uptake from sources in the bedrock, either from soil pockets within the rock matrix or with the rock itself, that was sufficient to sustain transpiration when shallow sources of available water was depleted.

Estrada-Medina (2012) found high concentration of roots in soil pockets within the rock matrix. This may be due to vigorous root growth above rock which enhances exploration of cracks in the rock (Poot and Lambers, 2008; Schwinning, 2013). In their

case, high root concentration resulted in rapid depletion of water from these pockets. We also found evidence of water storage in soil pockets, but depletion was slow, indicating a low concentration of roots. In some cases, there was no apparent access by roots to these sources of water, most notably beneath grass in locations where trees were absent.

Conclusions

We examined water storage and uptake in a karst savanna with ~50% woody cover on the Edwards Plateau, TX. Rock created high spatial variability in water storage, and coupled with heterogeneous distribution of trees led to high spatial variability in root water uptake. Most of the water uptake came from the upper 1 m of the soil profile, indicating that roots were concentrated in predominantly shallow layers. Although water storage and presumably root growth below 1 m were restricted by rock, there was water uptake from below this depth, though it was much less than from shallower depths. Water extracted from below 1.6 m, the maximum depth of our measurements, accounted for approximately 10% of ET, indicating that roots had access to water stored within the bedrock, possibly in soil pockets.

Water stored in rock may have played a significant role in survival of trees during the Texas drought of 2011. The drought was classified as exceptional, and killed an estimated 6% of the trees in the state, including some of the most drought-tolerant species. All regions of the state were affected, and there were areas where local mortality approached 100%, including on the Edwards Plateau. However, no trees died at the savanna site, and mortality on the Freeman Ranch as a whole was limited to isolated trees.

Our study illustrates the difficulty of measuring water content profiles in karst terrain. Because spatial and temporal variability in water storage and retention are high, a large number of measurements are required to quantify water dynamics in the root zone. Hydrologic and vegetation models must account for this variability, and need to include the impact of water storage within the rock matrix if they are to provide realistic simulations of ET and water dynamics (Schwinning, 2013).

CHAPTER V

SPATIOTEMPORAL PATTERNS OF SOIL MOISTURE IN A KARST SAVANNA ON THE EDWARDS PLATEAU, TX

Introduction

Woody plant encroachment into grasslands and savannas has been occurring over the past 100–200 years (Archer et al., 2001; Wilcox et al., 2008). On karst terrain, the combination of shifts in vegetation and soils that are shallow and rocky may create high spatial variability in soil water content. A recent study by Estrada-Medina et al. (2012) highlighted the variability in water storage in karst landscapes. On the karst Edwards Plateau in central Texas, woody plants, especially Ashe juniper (*Juniperus ashei*) and honey mesquite (*Prosopis glandulosa*) are encroaching into semi-arid grasslands and savannas. Schwinning (2008) and Heilman et al. (2009) suggested that water sources for woody plants on the Plateau are mainly shallow and limited. Results from Chapter IV of this dissertation showed that water uptake from the upper 1 m accounted for, on average, 81% of evapotranspiration in the karst savanna. The question remains as to relative contributions of root water uptake and rock distribution to heterogeneity in soil water content (θ). Spatial pattern analysis of θ is a key to the assessment of temporal changes in soil water storage in response to local ecosystem shifts in plant species composition.

Knowledge of the spatial variability of θ is very important to understanding the pedological and hydrological processes in karst regions (Schume et al., 2003). Spatial variability can be described by spatial autocorrelation functions such as Moran's I

(Moran, 1950). Zhao and Shao (2011) found spatial autocorrelation between θ along transects using Moran's I on the Loess Plateau in China, and spatiotemporal variability of θ in shrub- and grass-land was analyzed with other variables such as hydraulic conductivity and bulk density (Hu et al., 2008; Hu et al., 2011). While it is difficult to identify root water uptake and preferential flow based on θ profiles, temporal changes in Moran's I of θ could quantify the effect of root water uptake and preferential flow on θ to spatially find localized interconnected networks of flow pathways.

Understanding the spatial pattern of θ is fundamental to expanding the relation between measured θ at a point scale and estimated θ at a remote sensing footprint scale. When a point-scale θ is investigated with direct *in-situ* methods, e.g., gravimetric sampling, time domain reflectometry (TDR), or neutron measurements, observation number (n) is a critical factor to accurately characterize the spatial pattern. The larger the scale, the more spatial samplings are required to evaluate the temporal stability of the spatial structure of θ and the scale of temporal stability (e.g., Kachanoski and de Jong, 1998; Mohanty et al., 2000; Joshi et al., 2011). However, investigating spatial soil moisture patterns with a large number of samples is labor intensive in the Edwards Plateau and difficult because of rock. Most soil moisture studies using direct *in-situ* methods have been conducted with low spatial and/or temporal sampling frequency (Farmiglietti et al., 1998).

Jacques et al. (2001) used a spatial-temporal data analysis approach to quantify the contribution of two factors, depth and location, to the observed variance of field-measured θ along an 8-m long transect with low spatial samplings (n= 60). In their

study, they adopted an additive model presented by Mohanty and Kanwer (1994) to investigate the spatial and temporal variability of soil water. This model empirically evaluates the contribution of soil depth and horizontal space to soil moisture variability using the following equation,

$$\theta_t(x,z) = \mu_t + \alpha_t(z) + \beta_t(x) + \varepsilon_t(x,z) \quad [5.1]$$

where x and z are the horizontal and vertical coordinates respectively, subscript *t* is time, θ is the water content ($m^3\ m^{-3}$), μ_t is the overall mean water content for all θ measurements at time t, $\alpha_t(z)$ is the depth trend at time t, $\beta_t(x)$ is the location trend in the horizontal plane at the time t, and ε_t represents experimental error and microheterogeneity. The different terms in Eq. [5.1] are estimated using an iterative resistant median-polish approach (Cressie, 1993; Jacques et al., 1999). The median polish approach allows the investigation of temporal dynamics of soil water by location and depth, which can help identify the scale-specific relationship between its components: θ, dry bulk density (ρ_b), and root water uptake.

The objective of this study was to quantify spatial patterns of θ in shallow and rocky soils using two approaches: (i) Moran's I test to find spatial autocorrelation between θ and ρ_b profiles during soil dry and wet periods, and (ii) an additive model to quantify the micro-heterogeneity of θ using the median polish approach to determine how tree roots and rock distribution affect the heterogeneity in θ.

Materials and Methods

Experimental Design and Measurements

In 2009, we investigated the spatial patterns of θ and ρ_b profiles on the Freeman Ranch, a 1,700 ha research area near San Marcos, TX (Fig. 5.1). The soil is a Rumple gravelly clay loam (Clayey-skeletal, mixed, active, thermic Typic Argiustolls) with chert fragments occupying ~50% of the soil volume between depths of 0.2 and 1.0 m (Figs. 5.1a and 5.1b). The average volume and density of chert fragments were 52.7 cm^3 and 2.4 g cm^{-3}, respectively. Limestone residuum (density = 2.6 g cm^{-3}) occurs at depths of 1 to 1.5 m. Water content was measured with neutron probe measurements in a 25 × 25 m grid (5-m node spacing) along six east-west transects (Fig. 5.2). The vegetation is savanna with ~50% woody cover (Ashe juniper and honey mesquite). Thirty six 5.1-cm o.d. aluminum access tubes were installed in the sampling grid to a depth of 1.6 m. Bore holes were drilled using an 8.9-cm diam. screw auger, and access tubes were inserted and sealed with expandable polyurethane foam (Poly-Set, Utility Structural Systems, Arlington, TX) as described by Tokumoto et al. (2011). Water content profiles were measured at 0.2 m depth intervals, beginning at 0.2 m below the surface, using CPN Model 503DR moisture gauge (Campbell Pacific Nuclear Corp, CA). Soil moisture measurements were made to a depth of 1.6 m. Bulk density profiles were determined in each access tube using a CPN Model 501DR density probe (Campbell Pacific Nuclear Corp, CA) following procedures described by Tokumoto et al., (2012). Neutron and density probes were calibrated in a 189 L drum with known volume of soil, rock, and water (Tokumoto et al., 2012).

(a)

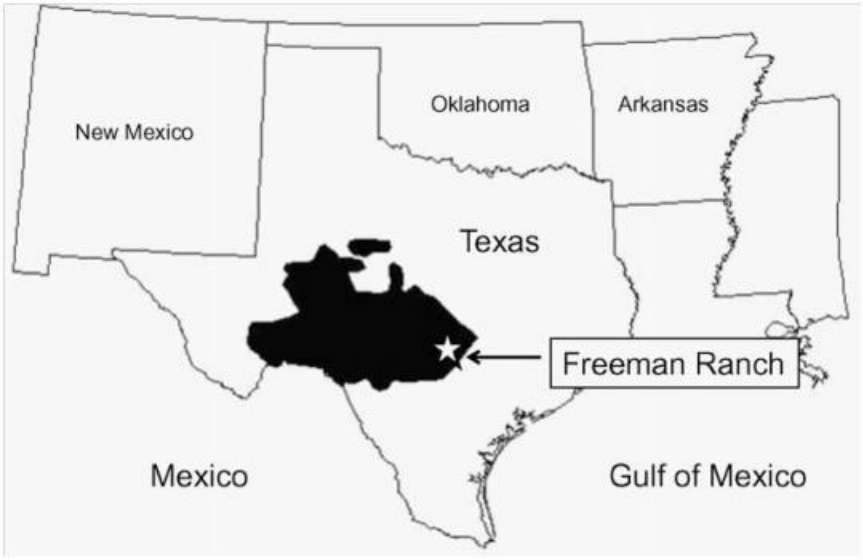

(b)

(c)

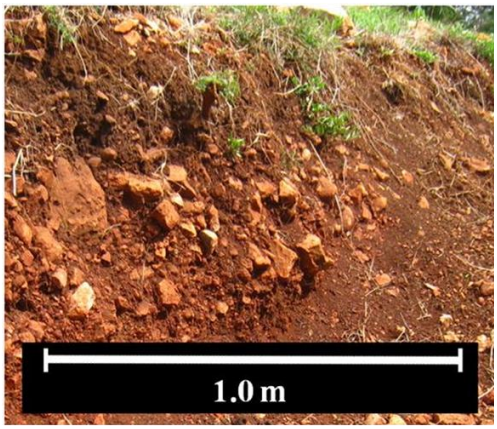

Fig. 5.1 Location of the Edwards Plateau and the Freeman Ranch in Texas, USA (a) along with photographs showing the distribution of the trees (b) and the soil profile (c).

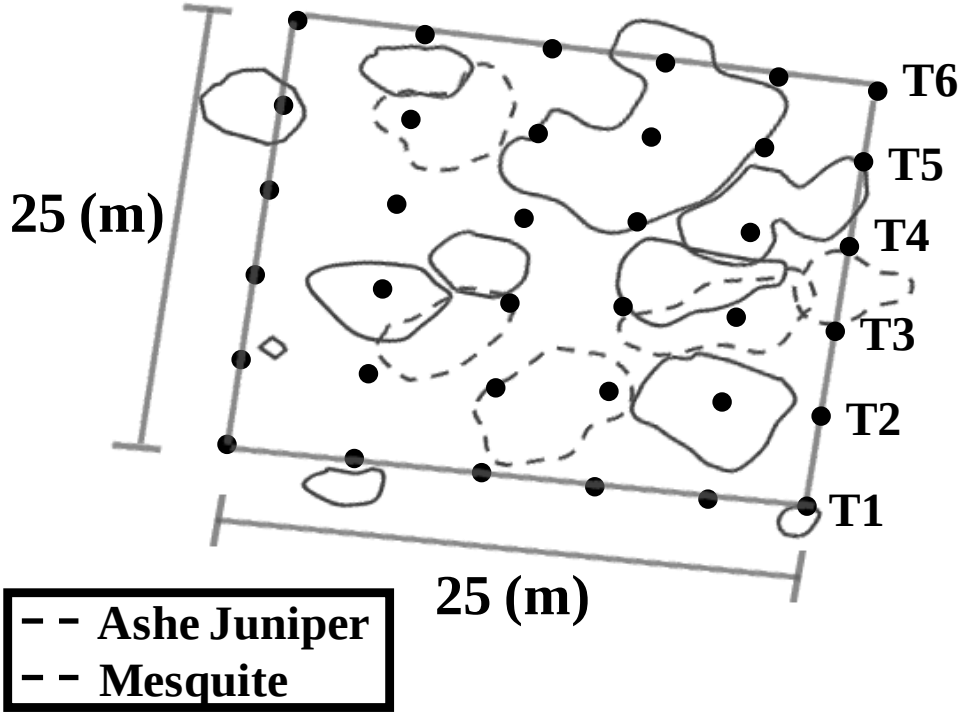

Fig. 5.2 Schematic diagram showing tree cover in a 25 m × 25 m plot with six transects (T1 to T6).

The θ and ρ_b were measured between July and December of 2009. Neutron probe measurement intervals ranged from days to weeks depending on the amount and frequency of rainfall. The ρ_b profiles were determined as averages of density probe measurements take on 4 dates. During this time, microclimate conditions were also measured to compare with temporal changes in θ and ρ_b profiles. Evapotranspiration (ET) was monitored with eddy covariance, described by Heilman et al. (2009), at a flux tower 66 m downwind of the soil water content measurement grid.

Moran's I Test

Moran's I was used to find the spatial autocorrelation between θ measurements at the same depth on the experimental grid where

$$I = \frac{n}{\sum_i^n \sum_j^n W_{ij}} \frac{\sum_i \sum_j W_{ij}(X_i - \bar{X})(X_j - \bar{X})}{\sum_i W_i (X_i - \bar{X})^2}, \quad [5.2]$$

In Eq. [5.2], n is the number of locations, W_{ij} is the measure of the physical proximity of locations *i* and *j*, with X_i and X_j being the observed θ at locations *i* and *j*. The term W_{ij} is the element in the *i*th row and *j*th column of the summary matrix W. Moran's I test with Monte-Carlo simulation was carried out using statistical software R, developed by R Development Core Team (2010). Prior to the Monte-Carlo simulation, histograms of θ and quantile-quantile (QQ) plots were used to check the normality of θ. Spatial autocorrelation of horizontal ρ_b were examined as well as θ using 6 × 6 matrices at depths of 0.2 to 1.4 m. We used "rook's definition" for a physical proximity to compare θ distribution in a 3 × 3 lattice of *W*, where 9 neighbors are located as shown in Table 5.1. According to rook's definition, 4 neighbors can be compared with θ in the center

Table 5.1 Definition of neighbors for location e rectangular 3 × 3 lattices.

Definition of proximity					
Locations			W_{ij}		
a	b	c	0	1	0
d	e	f	1	×	1
h	i	j	0	1	0

(W_{ij} = 1), excluding the 4 corners (W_{ij} = 0). Moran's I is a measure of autocorrelation similar in interpretation to the Pearson's correlation statistic, and both statistics range from 1.0 (strong positive autocorrelation) to 0 (random pattern) to -1.0 strong negative spatial autocorrelation) (Iqbal et al., 2005). In our 6 × 6 matrices at different depths, Moran's I for no autocorrelation would be - 0.029 (= -n/(1-n)), and Moran's I statistic of 0.3 or greater presents evidence of spatial correlation between neighbors (Strock et al., 2001). We analyzed temporal changes in Moran's I of θ especially during dry and wet conditions in terms of understanding the effect of root water uptake and preferential flow on the spatial variability in θ. Next, Moran's I was calculated along six transects of θ and ρ_b profiles to investigate how the θ profiles were affected by rock distributions as a function of depth. Additionally, we estimated the Pearson's correlation between θ and ρ_b profiles.

Median Polish Approach

Median polish is used for trend removal in geostatistics (Cressie and Read, 1989; Cressie, 1993). Given the specific two-dimensional sampling layout used in the experiment and the nature of the median-polishing estimation technique (see Cressie, 1993, for details about the algorithm), the median of θ at a specific depth i and location j can be calculated (Fig. 5.3). If the observed θ is located on a m × n lattice [$\theta_{ij}\{i$ = 1... m, j = 1... n}], θ_{ij} can be expressed as

$$\theta(i,j|t) = M(\mathrm{t}) + D(i|t) + L(j|t) + r(i,j|t) \qquad [5.3]$$

where $M(t)$, $D(i|t)$, $L(i|t)$, and $r(i,j|t)$ are the ultimate overall mean water content for all observed θ ($m^3\ m^{-3}$), the depth trend ($m^3\ m^{-3}$), the location trend ($m^3\ m^{-3}$), and residuals

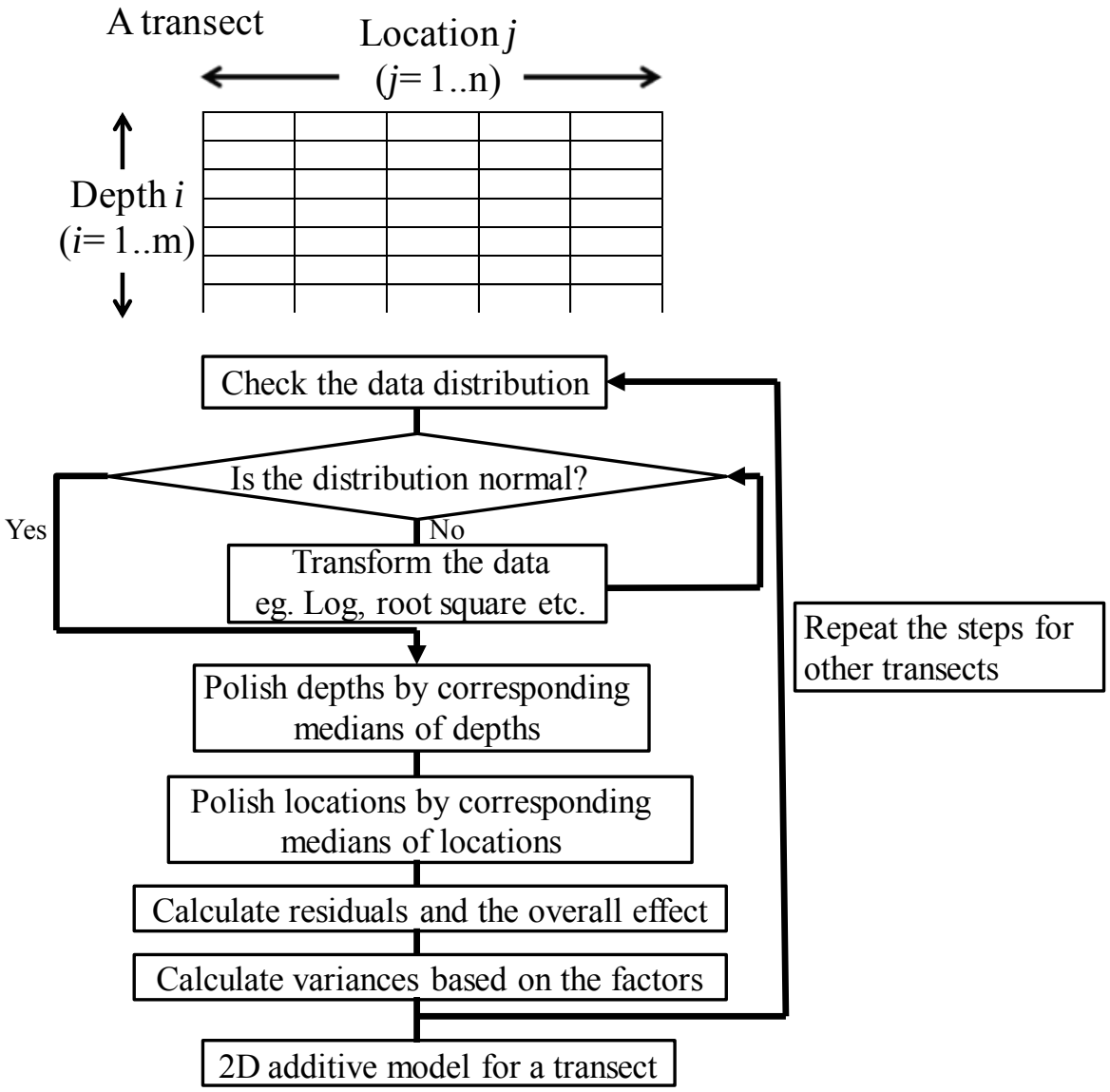

Fig. 5.3 Schematic flow chart for the two-dimensional median-polish scheme.

(m^3 m^{-3}) at a given time, respectively. The two vectors $D(i|t)$ and $L(i|t)$ are non-parametric measurements of a depth and a location trend. Here, we hypothesized that the depth trend and the location trend represent rock distribution and tree location, respectively because results in Chapter IV showed that rock density increased with depth, and there was no apparent access by roots to soil water pockets, most notably beneath grass in locations where trees were absent.

When the profile θ data along a transect were normalized by the transformation of root square (≈ 0.95), the median θ at each soil depth was subtracted from individual observations of θ at the corresponding soil depth to leave the residuals in the matrix. The median of row θ was recalculated as $D(i|t)$ at each depth. Next, medians of column θ were calculated using the remaining values in the matrix and the results again subtracted from the matrix, leaving a new set of residuals. The median of column θ was stored as the $L(i|t)$ at each location. This procedure iterates to obtain the *i*th depth trend, the *j*th location trend, and the overall mean at a given time *t* in Eq. [5.3]. The variance of θ is defined using the equation.

$$s^2 = \frac{1}{N-1}\sum_i \sum_j \big(\theta(i,j|t) - M(t)\big)^2. \quad [5.4]$$

To evaluate spatial patterns of the depth and location trends, the variance of the summation of the depth and the location trends was calculated as

$$s^2{}_{DL} = \frac{1}{N-1}\sum_i \sum_j \big(D(i|t) + L(j|t)\big)^2 \quad [5.5]$$

and compared with the variances of individual depth or the location trends calculated using the equations

$$s^2{}_{-D} = \frac{1}{N-1}\sum_i \sum_j \left(\theta(i,j|t) - M(t) - D(i|t)\right)^2 \quad [5.6]$$

and,

$$s^2{}_{-L} = \frac{1}{N-1}\sum_i \sum_j \left(\theta(i,j|t) - M(t) - L(j|t)\right)^2 . \quad [5.7]$$

Results and Discussion

Environmental Conditions

Microclimatic conditions at the savanna site from 1 July (Day 182) through December 2009 are shown in Fig. 5.4. July and August 2009 were the final months of a 2-year drought, and total rainfall during these months was only 31 mm. Rainfall during the remainder of the year was 490 mm, 144 mm above the 30-y mean for those months (Fig. 5.4a).

Bulk Density and Soil Moisture

Figure 5.5 shows examples of spatial and temporal variability in θ and ρ_b. Linear interpolation was used for the 3D map. Bulk densities for the bulk soil were higher than that for the clay soil matrix soil (ρ_b= 1.15 g cm^{-3}), and ρ_b increased gradually from the soil surface to the deeper layers because of larger rock fragments and more soil/rock heterogeneity. Soil moisture measurements in Fig. 5.5 are from 1 July, 4 August, 15 September, and 15 December 2009. The θ profiles were measured near the end of a 2-year drought. During this period, the areas of lowest θ were correlated with regions of high ρ_b, suggesting the presence and effect of rock on total soil moisture storage. The September measurement was the beginning period of heavy autumn rainfall, with 62 mm of rain falling in the previous 7 days. The December measurement occurred after 328

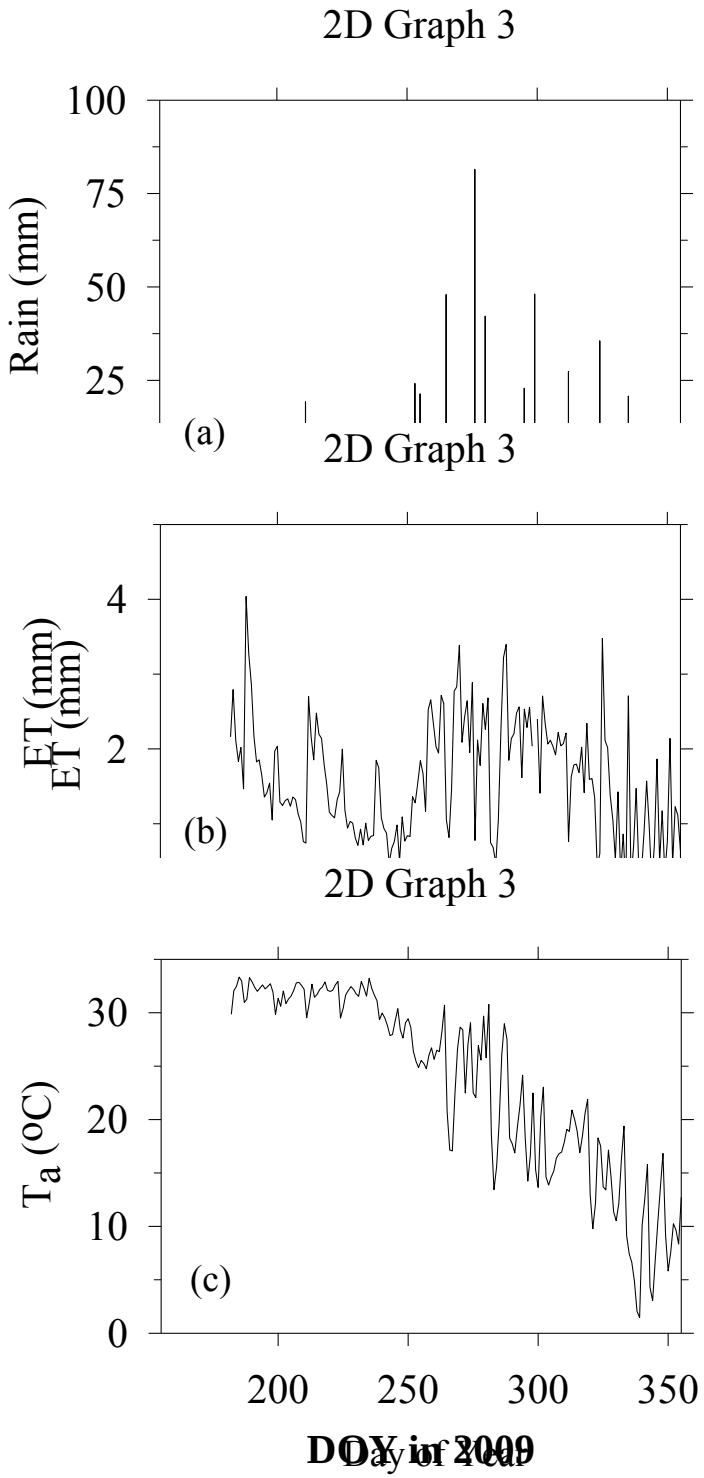

Fig. 5.4 Temporal change in (a) rainfall, (b) evapotranspiration (ET), and (c) daily air temperature (T_a) in 2009.

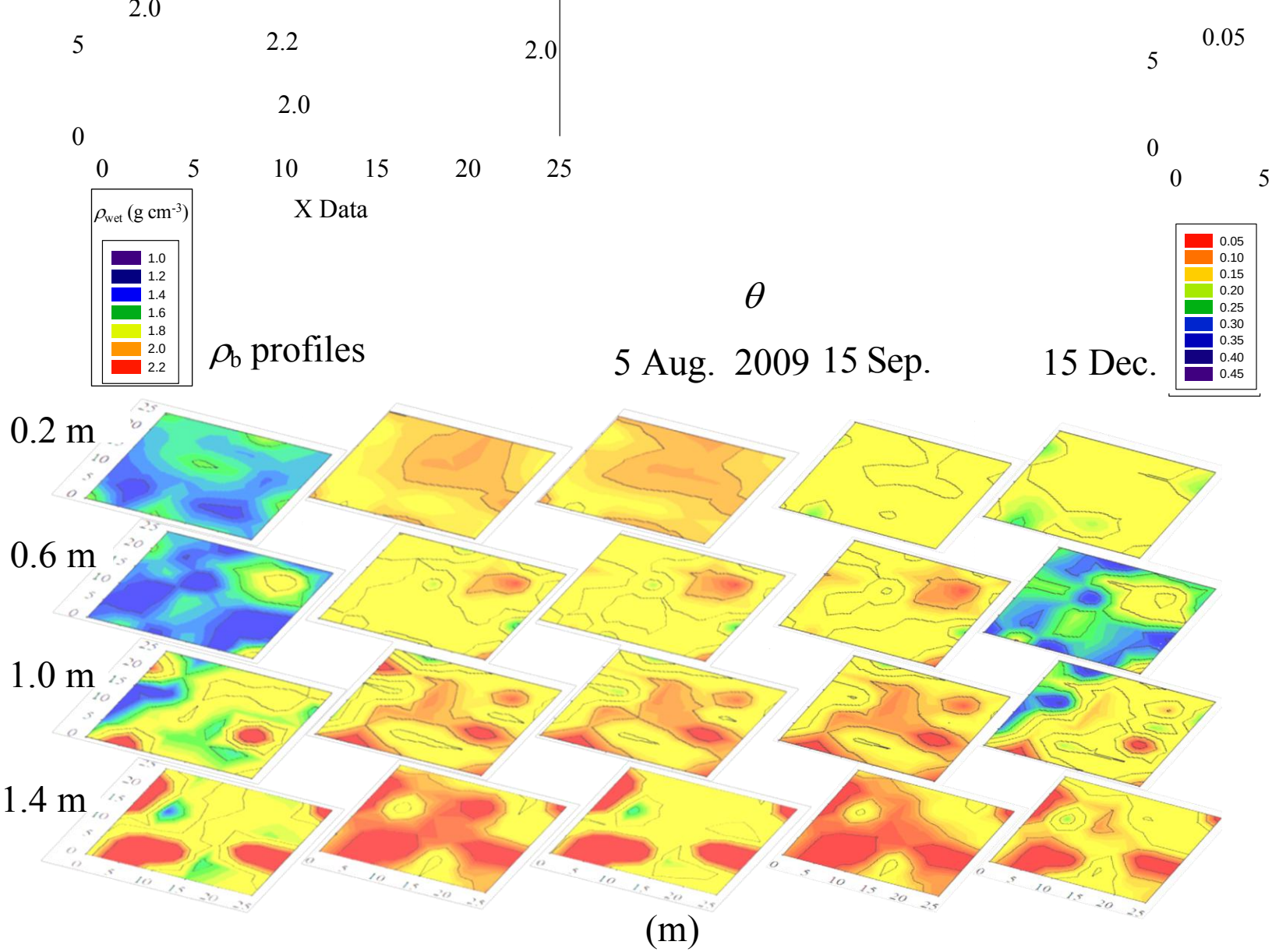

Fig. 5.5 Horizontal 3D map of ρ_b and θ distribution from 0.2 m to 1.4 m deep on 1 July, 5 August, 15 September, and 15 December 2009.

mm of rain in the previous two months, and θ profiles indicated infiltration of rainfall to depths of 1.6 m. This resulted in an increase in θ heterogeneity. The soil water content was relatively high, except for a region in the northeast quadrant that was associated with high ρ_b indicating high rock volume. At 1.0 m, θ was high in only a small portion of the measurement grid.

Figure 5.6 shows temporal changes in the means of θ and coefficients of variation (CV) of θ at depths of 0.2, 0.60, 1.0, and 1.4 m. Mean θ slightly decreased at depths of 0.2 and 0.6 m until September (Figs. 5.6a and 5.6b), although mean θ in deeper layers remained constant (Figs. 5.6c and 5.6d). After heavy rainfall events, mean θ increased gradually from the soil surface to the deeper layers. Maximum and minimum θ were also plotted in Fig. 5.6 to show changes in soil water storage as a function of soil depth. Minimum θ (θ = 0.01 m^3 m^{-3}) at depths of 1.0 m and 1.4 m reflects volumetric water content of rock. Infiltration due to the heavy rainfall widened differences between maximum and minimum θ, especially in the deeper layers. Although infiltration did not create significant differences in CV of θ (Figs. 5.6e, 5.6f, 5.6g, and 5.6h), the CV increased clearly with soil depth. Thus, the volumetric water content of rock fragments strongly influenced the CV of θ.

Spatial Autocorrelation

Table 5.2 shows results of average Moran's I test for horizontal θ and ρ_b profiles in 2009. All Moran I of horizontal θ profiles were lower than 0.3 and not significantly different from zero, indicating no spatial autocorrelation in θ (p-value > 0.05). Standard

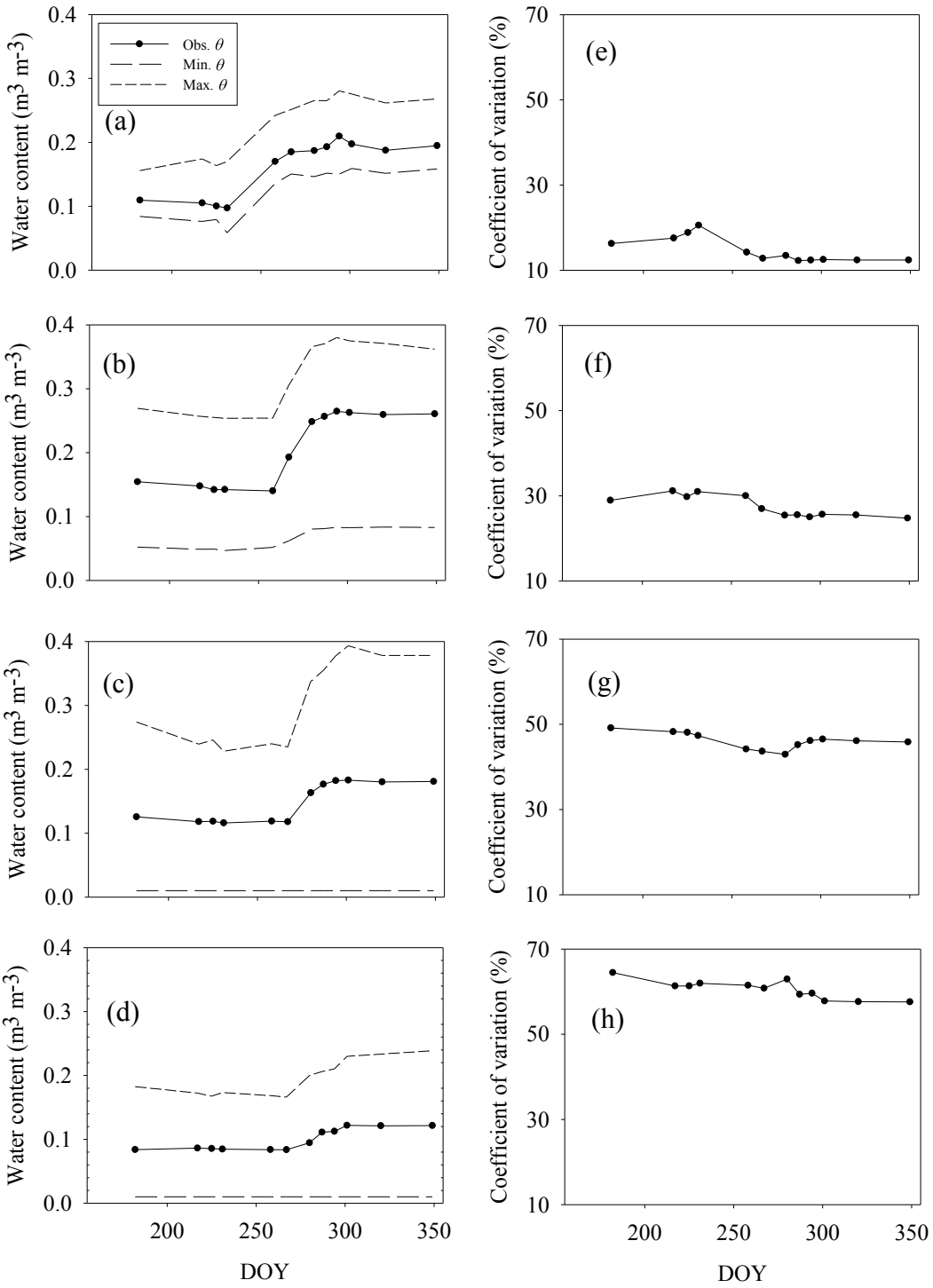

Fig. 5.6 Temporal changes in mean θ at depths of (a) 0.2, (b) 0.60, (c) 1.0, and (d) 1.4 m, and coefficient of variation of θ at depths of (e) 0.2, (f) 0.60, (g) 1.0, and (h) 1.4 m.

Table 5.2 Moran's I test and standard deviation (S.D.) for θ and ρ_b profiles at different soil depths in 2009, along with Pearson's coefficients between θ and ρ_b profiles.

	θ profiles		ρ_b profiles		Pearson's coefficient (%)
Soil depth (m)	Moran's I (S.D.)	p-value (S.D.)	Moran's I	p-value	
0.2	0.164 (0.043)	0.063 (0.062)	0.089	0.156	-0.543
0.4	0.023 (0.046)	0.334 (0.134)	-0.036	0.538	-0.581
0.6	-0.052 (0.034)	0.576 (0.105)	0.035	0.287	-0.782
0.8	0.108 (0.061)	0.154 (0.112)	0.105	0.152	-0.741
1	0.124 (0.035)	0.115 (0.058)	-0.023	0.489	-0.757
1.2	0.034 (0.016)	0.307 (0.045)	-0.042	0.513	-0.827
1.4	0.152 (0.039)	0.076 (0.045)	0.111	0.142	-0.827

deviations (S.D.) of Moran's I and p-values were small. Moran's I values for horizontal ρ_b profiles were not significantly different from zero , indicating that rock fragments were located randomly at the scale measured, although Pearson's coefficient for horizontal θ and ρ_b had negative values, ranging from -0.54 to -0.83. Additionally, two seasonal changes in Moran's I values during the dry period (Jul.-Aug.) and the wet period (Sep.-Dec.) were examined (Table 5.3). Both seasonal changes in Moran's I values showed no autocorrelation in θ. Although the highest root densities occurred at a depth of 0.4 m for the juniper and mesquite (Chapter IV), this result suggested that clustered tree distribution did not cause autocorrelation in θ even in the shallow soil layer. In the 5-m sampling design for θ, the effect of soil water pockets with rock, reported in Chapter IV on spatial variability of θ was not detected as well.

Moran's I of vertical θ and ρ_b profiles along six transects were examined (Table 5.4). As required by Moran's I test, normal distribution of the θ profiles was confirmed by a histogram and QQ plot (data not shown). Likewise, the ρ_b profiles were normally distributed. Moran's I values of the vertical θ and ρ_b profiles were higher than 0.3 (excluding that of ρ_b profile at TS 4), and significant at a p-value of 0.001. As a result, there were some spatial patterns of θ, which is likely because of rock distribution within the soil profile.

Spatiotemporal Data Analysis

As mentioned above, spatial variability in θ along six transects was found, so that time series of $M(t)$ and s^2 in Eqs. [5.3] and [5.4] were estimated by the median polish

Table 5.3 Seasonal changes in Moran's I test and standard deviation of θ profiles at different soil depths during a dry period (July-August) and wet period (September-December).

	Jul.-Aug.		Sep.- Dec.	
Soil depth (m)	Moran's I (S.D.)	p-value (S.D.)	Moran's I (S.D.)	p-value (S.D.)
0.2	0.146 (0.073)	0.097 (0.107)	0.173 (0.018)	0.045 (0.014)
0.4	0.017(0.058)	0.370 (0.178)	0.025 (0.043)	0.315 (0.116)
0.6	-0.091 (0.014)	0.694 (0.045)	-0.033 (0.021)	0.517 (0.067)
0.8	0.059 (0.035)	0.233 (0.076)	0.132 (0.056)	0.115 (0.109)
1	0.078 (0.009)	0.189 (0.028)	0.146 (0.014)	0.078 (0.017)
1.2	0.035 (0.017)	0.309 (0.060)	0.034 (0.016)	0.305 (0.040)
1.4	0.142 (0.028)	0.082 (0.038)	0.158 (0.044)	0.073 (0.051)

Table 5.4 Moran's I test for θ and ρ_b profiles along 6 transects in 2009.

	θ profiles		ρ_b profiles	
Transect	Moran's I (S.D.)	p-value	Moran's I	p-value
1	0.489 (0.100)	0.001	0.478	0.001
2	0.531 (0.080)	0.001	0.473	0.001
3	0.635 (0.052)	0.001	0.576	0.001
4	0.315 (0.080)	0.001	0.042	0.001
5	0.381 (0.101)	0.001	0.391	0.001
6	0.439 (0.059)	0.001	0.475	0.001

approach (Fig. 5.7). The M(t) and s^2 had a similar trend, increasing with rainfall between 13 September (DOY 257) and 21 October (DOY 294). The s^2 varied from 0.001 to 0.01 $m^3\ m^{-3}$. Transect 3 had the largest s^2 (Fig. 5.7b), likely because large rock at the 1.0 m created a high CV of ρ_b (Fig. 5.5). Water content difference between soil and rocks increased with heavy rainfall events, so the s^2 was correlated with M(t). In contrast, Jacques et al. (2001) reported that s^2 was negatively associated with the general patterns of M(t) in soil without rock. This suggests that s^2 between the near-surface and deeper-soil θ becomes smaller after heavy rainfall as the near-surface θ increases. However, our finding of micro-heterogeneity of θ in rocky soils was that s^2 responded to the antecedent θ and the amount of rain. Volumetric water content of chert and limestone was 0.01 ($m^3\ m^{-3}$) and stable, but θ of the soil alone without rock fragments can vary from 0.08 to 0.55 ($m^3\ m^{-3}$) (Chapter VI). As a result, for rocky soils the s^2 can increase with θ, because the effect of rock distribution on s^2 is significant.

Variation in θ as a result of location and depth trends was calculated by Eqs. [5.5], [5.6], and [5.7]. Figure 5.8 shows temporal changes in the variance of θ from depth and location trends. The summation of both depth and location trends (s^2_{DL}) had a similar pattern to the time series of s^2 (Fig. 5.8a). The variance of θ without mean θ and the depth trends (s^2_{-D}), was fairly constant in September and then started to increase in October, so there seemed to be a time delay when comparing with s^2_{-L} (Fig. 5.8c). This indicates that lateral water flow or horizontal θ redistribution occurred more slowly than vertical water infiltration. A recent study with a rainfall simulator, reported by Gregory et al. (2009), found approximately 2.5 m hr^{-1} of preferential flow rate in a cave located

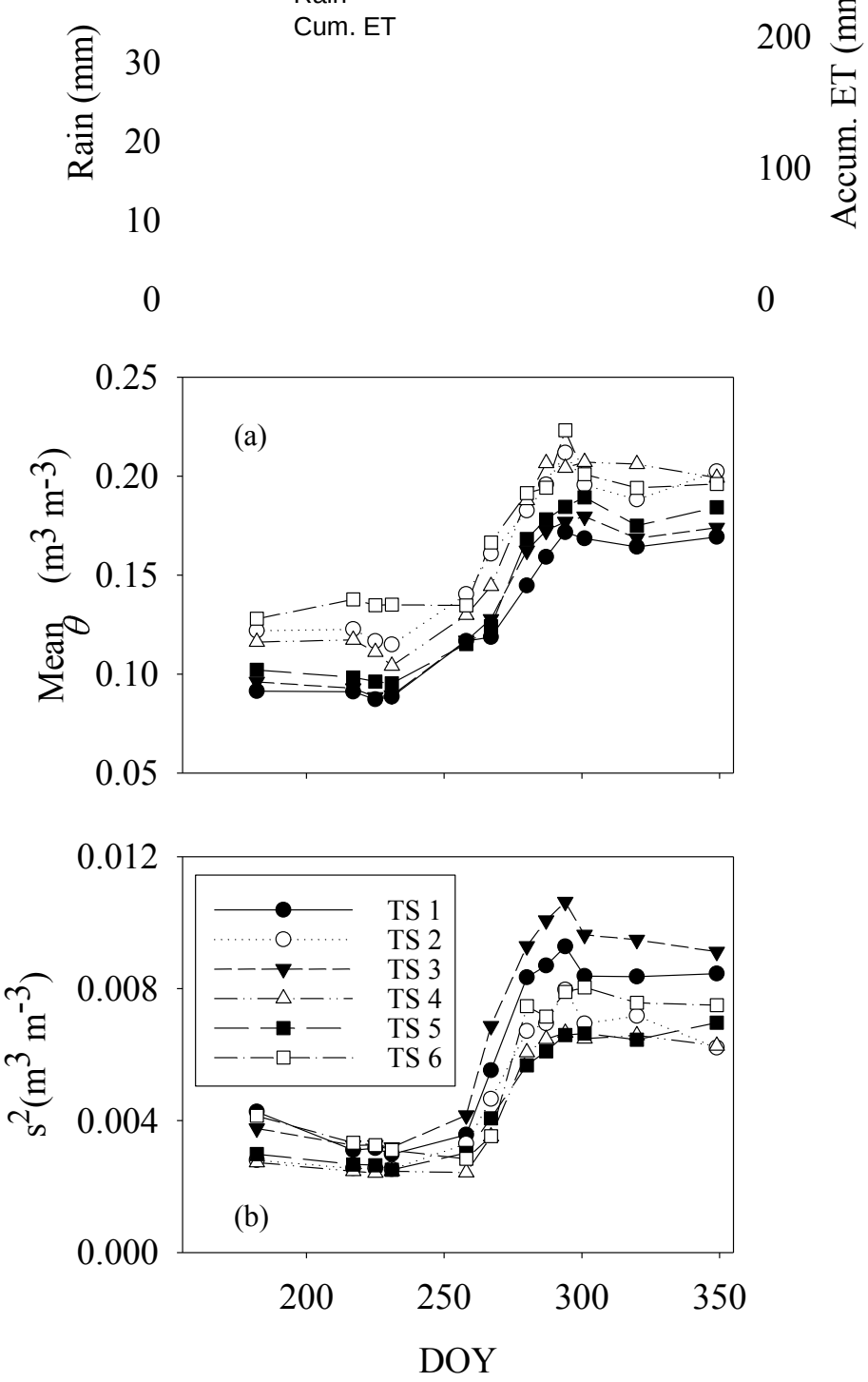

Fig. 5.7 Time series of overall mean θ (a) and total variance of θ (s^2) (b), defined by Eq. [5.4].

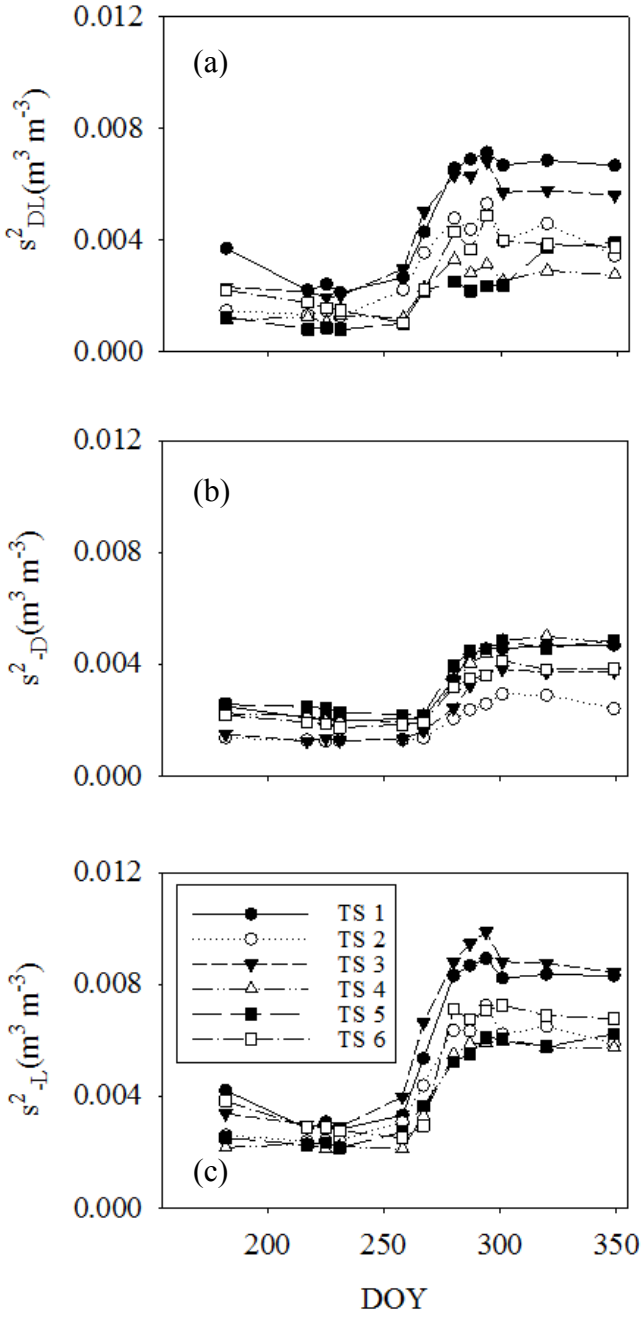

Fig. 5.8 Time series of the summation of the depth and location effects, $s^2_{DL,}$ (a) (the variance of θ without the depth effect and mean θ (s^2_{-D}) (b), and the variance of θ without the location effect and mean θ (s^2_{-L}) (c) along six transects (TS) in the experimental grid.

5 m below the soil surface on the karst Edwards Plateau, TX. This suggested that vertical water flow may be dominated by preferential flow when heavy rain occurs. According to Chapter IV, 63% of total water storage in the profile after the heavy autumn rains was in the upper 0.8 m, but there was considerable movement of water through lower parts of the profile. Thus, the depth trend, which is related to vertical flow, can express the temporal change in θ more accurately than the location trend.

Additionally, we found that s^2 -$_D$ was lower than s^2 -$_L$, further suggesting that the depth trend was larger than the location trend (Figs. 5.8b and 5.8c). This result was also consistent with results of Moran's I for θ, which showed that spatial variability of vertical θ was much higher than horizontal θ. As a consequence, spatial patterns of θ were affected by the depth trend rather than the location trend because of the rock distribution.

Conclusions

The spatial and temporal variability of θ was investigated using Moran's I test and an additive model with the median polish approach. The research site was designed to measure θ and ρ_b down to a 1.6 m depth that contains shallow and rocky soils in a 25 m × 25 m grid. Moran's I test resulted in non-autocorrelation between horizontal θ and ρ_b profiles in the rocky soil, but spatial autocorrelation of vertical θ profiles along six transects (1.6 m deep × 25 m long grids) was found. These results suggested that influence of rock on spatial variability of θ was significant.

The additive model was created with 4 components (i.e. median θ, the depth trend, the location trend, and residuals) to quantify the spatial variability of θ at different depths and locations along the six transects. Spatial variation of θ responded to the antecedent θ and the amount of rain, and was affected by the depth trend rather than the location trend because of the rock distribution. With regard to the impact of rock distribution on spatiotemporal change in θ, the depth trend was more significant than the location trend, suggesting that a reduced model except for the location trend may be applied to the small grid.

CHAPTER VI

ESTIMATING UNSATURATED HYDRAULIC PROPERTIES OF ROCKY SOILS USING THE EVAPORATION METHOD

Introduction

Hydraulic properties of rocky soils, especially the water retention curve (WRC), play an important role in assessing regional hydrology in karst ecosystems. Karst areas are located widely across the U.S. (Veni, 2002), and soils on karst are generally shallow and rock occupies a significant fraction of the soil volume. This limits water retention and creates a high spatial variability in water storage capacity, indicating that rock fragments are critical for quantifying water content more accurately (Chapter IV). Some studies based on field measurements have shown the effects of rock fragments on infiltration (Valentin and Casenave, 1992; Valentin, 1994), saturated hydraulic conductivity (Dunn and Mehuys, 1984), and water content (Cousin et al., 2003). A complicating factor is that the sampling of undisturbed soil cores containing rock fragments remains difficult (Mehuys et al., 1975). Katsura et al. (2005) measured WRC and hydraulic conductivities of weathered granitic bedrock using the pressure plate method, but little is known about the effect of volume fraction of rock on unsaturated hydraulic properties of the entire volume of soil plus rock.

Definition of volumetric water content (θ) for rocky soil is critical because rock reduces θ (Ravina and Magier, 1984; Poeesen and Lavee, 1994; Tokumoto et al., 2012). Fiés et al. (2002), using glass-soil mixtures, showed that WRCs changed with volume of

glass. This supports the idea that volume fraction of rock needs to be included in defining WRC for rocky soils. Ma et al. (2009) and Ma et al. (2010) applied the Brooks-Coney hydraulic parameter model (Brooks and Corey, 1964) to the estimation of hydraulic conductivity and WRC for rocky soils using a one-dimensional absorption experiment based on infiltration into dry soil. This analytical method assumes that the cumulative infiltration rate is proportional to the square root of time (Philips, 1957), but there remains some uncertainties on the mechanism of water flow in rocky soil to validate the assumption without observations of changes in pressure head and θ. While the Brooks-Coney model is one of the most widely known hydraulic models, the van Genuchten model (van Genuchten, 1980) is much better adapted for S-shaped retention curves characteristic of relatively fine-textured soils (Sakai and Toride, 2007a). Durner (1994) proposed a modified VG model to predict more accurately WRC even in a low range of pressure head (h). The VG and the Durner models have a pore connectivity parameter, l, which can represent the tortuosity factor for better estimating unsaturated hydraulic conductivity based on the statistical pore-size distribution model of Mualem (1976).

The evaporation method involving monitoring pressure head and water content during the process of evaporation from soil samples has been commonly used to estimate both WRC and unsaturated hydraulic conductivity. Wind (1968) estimated WRC from average θ and h readings at several depths in a soil column, and determined hydraulic conductivity from measured h profiles and changes in θ distribution using the evaporation method. With the evaporation method, unsaturated hydraulic conductivities

can be particularly determined for h ranging from approximately -50 cm to -700 cm (Šimůnek et al., 1998). Sakai and Toride (2007b) and Šimůnek et al. (1998) evaluated optimum conditions for predicting hydraulic parameters for the van Genuchten (VG) model using the evaporation method. Studies have assessed the significance of the hydraulic model selection, depending on soil types. Peter and Durner (2008) examined the Durner model to evaluate the errors of the evaporation experiment using coarse-textured and fine-textured soils. Sakai and Toride (2007a) compared the VG and the Durner models, and suggested that the Durner model can express unsaturated hydraulic conductivity at h lower than -700 cm with appropriate model parameters. Their results highlighted the importance of proper estimation of l. Mualem (1976) assumed $l = 0.5$ based on empirical studies. However l may be different in rocky soils because tortuosity increases with rock content (Sauer and Logsdon, 2002).

The objective of this study was to observe the effect of volume fraction of rock on hydraulic properties and to estimate the unsaturated hydraulic properties for rocky soil using the evaporation method. We examined the validity of the VG and the Durner models to express unsaturated hydraulic properties for clay loam containing rock fragments. Using the experimental data, hydraulic model parameters of the VG and the Durner models were inversely optimized over a wide range of h. We also investigated the relationship between l and rock volume fraction. The effect of rock fragments on unsaturated hydraulic properties was evaluated by comparison of measured and predicted h and θ.

Theory

Water Flow Model for Rocky Soils

The equilibrium single porosity model, proposed by Ma et al. (2008), is a simplified model for water flow in rocky soils when the transfer rate of water between soil and rock fragments is very small and water content of rock fragments is ignored. The governing equation for multi-dimensional, isothermal Darcian flow in rocky soils is given by the Richards equation:

$$\frac{\partial \theta}{\partial t} = \nabla \cdot [\nabla \cdot K\, h] \qquad [6.1]$$

where θ is the volumetric water content ($cm^3\ cm^{-3}$), h is the soil-water pressure head (cm), K is the hydraulic conductivity ($cm\ d^{-1}$), and t is time (d). Volumetric water content includes the impact of rock, and is estimated as

$$\theta = (1 - R_V)\theta_{soil} \qquad [6.2]$$

where R_V is the volumetric fraction of rock ($cm^3\ cm^{-3}$), and θ_{soil} is volumetric water content of the soil ($cm^3\ cm^{-3}$). The single-porosity flow model requires functions for the water retention curve and hydraulic conductivity. Determination of proper hydraulic functions and estimation of the function parameters for rocky soils is important for the single-porosity model. In this paper, we used the evaporation method (Šimůnek et al., 1998) to examine the van Genuchten (van Genuchten, 1980) and the Durner (Durner, 1994) models for obtaining the water retention curve and hydraulic conductivity. Initial and boundary conditions applicable to the evaporation experiment were as follows:

$$h\,(z,0) = h_i\,(z), \qquad [6.3]$$

$$K\,(\nabla \cdot h) = q_{evap}\,(L,t), \qquad [6.4]$$

and

$$q(0,t) = 0 \quad [6.5]$$

where h_i is the initial soil-water pressure head due to hydrostatic linear pressure head from the bottom, L is a coordinate of the soil length, $q_{evap}(L,t)$ is evaporation flux from the soil surface (cm d^{-1}), and $q(0,t)$ is water flux from the bottom. The $q_{evap}(L,t)$ is the time-variable evaporation flux that decreases with time and the bottom is a no flow condition. To solve Eq. [6.1] numerically, we used Hydrus 1D, a simulation model for analysis of saturated-unsaturated water flow, developed by Šimůnek et al. (2005).

Water Retention Curve Models

van Genuchten Model

The van Genuchten (1980) model describes water content and hydraulic conductivity in unsaturated soil using the equations

$$S_e = \frac{\theta-\theta_r}{\theta_s-\theta_r} = [1+\alpha h^n]^{-m} \quad [6.6]$$

and

$$K\,(S_e) = K_s\, Se^l\, [1-(1-Se^{1/m})^m] \quad [6.7]$$

where S_e is the effective water content, K_s is the saturated hydraulic conductivity (cm d^{-1}), θ_r and θ_s are residual and saturated water contents (cm^3 cm^{-3}), respectively, n, m (1-1/n) and α (cm^{-1}) are empirical parameters, and l is a pore connectivity parameter related to pore tortuosity. We assumed that θ_s and θ_r, calculated by Eq. [6.2], decreased as R_v increased. The van Genuchten (VG) model uses a predictive $K(S_e)$ model based on the statistical pore-size distribution model of Mualem (1976) in conjunction with Eq. [6.6] (Šimůnek et al., 1998). The pore connectivity, l in the hydraulic conductivity function, is

considered as 0.5 for many soils (Mualem, 1976). However, *l* can vary and be used to optimize the other model parameters with the evaporation method (Sakai and Toride, 2007b). For rocky soils, *l* could be affected by the volumetric fraction of rock and rock size.

Durner Model

For conductivity estimation in heterogeneous pore systems, Durner (1994) modified the water retention curve of the VG model as

$$S_e = \frac{\theta-\theta_r}{\theta_s-\theta_r} = \sum_{i=1}^{k} w_i[1 + (\alpha_i|h|^{n_i})]^{-m_i} \quad [6.8]$$

where w_i is a weighting factor for the water retention curves, subject to $0 < w_i < 1$ and $\Sigma w_i = 1$, and α_i, n_i, and m_i are curve-shape parameters. The Durner model can define a water retention function for bimodal pore-size distributions ($i \leq 2$) in soils containing inter- and intra-aggregated pores. Figure 6.1 shows a hypothetical S_e water retention curve based on the Durner model in which the stepwise shape of the curve indicates intra-aggregate pores are depleted of water at high *h* (0 to -100 cm in this example) and inter-aggregate pores at lower *h*. Thus, S_e is expressed as the sum of intra-aggregate moisture (first curve) and inter-aggregate moisture (second curve) (Sakai and Toride, 2007a). Although the Durner model is typically used for aggregated soils, we applied it to water retention curves for rocky soil. When the relative hydraulic conductivity is coupled to Eq. [6.8] by the predictive $K(S_e)$ model of Mualem (1976), it gives the unsaturated hydraulic conductivity for aggregated soils ($i \leq 2$) (Priesack and Durner, 2006) as

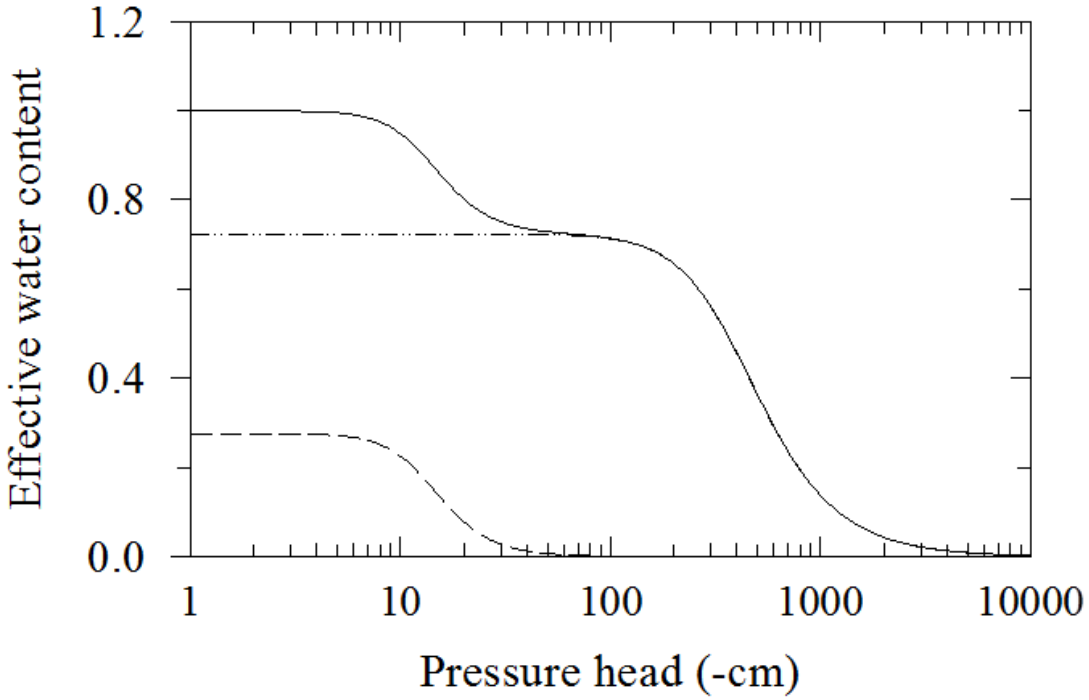

Fig.6.1 A bimodal porosity curve of the Durner model (Eq. [6.8]). Dashed and dash-dot lines indicate the first and second terms of the right-hand side of the equation, respectively, and solid line shows the sum of the two terms.

$$K\,(S_e) = K_s\,[\sum_{i=1}^{k} w_i[1+(\alpha_i|h|^{n_i})]^{-m_i}]^{l} \times \frac{\left(\sum_{i=1}^{k} w_i\alpha_i\left[1-(1-S_{e_i}^{\frac{1}{m_i}})^{m_i}\right]\right)^2}{(\sum_{i=1}^{k} w_i\alpha_i)^2}. \quad [6.9]$$

In rocky soils, the proportion of soil pores < 2 mm is reduced by rocks. Hypothetically, the air entry value should be equal to that of the soil because the largest soil pore size should be preserved when voids between rocks are filled with soil. Thus, the air entry value can be expressed by the first curve of the Durner model. The second curve is more flexible to show the water retention curve in the lower range of *h*. We assumed that changes in tortuosity with increasing R_v correspond to the parameter *l*.

Materials and Methods

Evaporation Experiments

Rumple gravelly clay loam (Clayey-skeletal, mixed, active, thermic Typic Argiustolls) with chert fragments added was used for the experiment. The soil was screened by a 2 mm sieve. The particle density of the clay loam and the density of chert were 2.5 Mg m^{-3} and 2.4 Mg m^{-3}, respectively. The shape of chert fragments in this study was blocky, and the longest length was less than 7 cm. The average volumetric water content of chert (n=72) was 0.01 m^3 m^{-3}. Additionally, spherical-shaped gravel (diameter < 1 cm and density = 2.6 Mg m^{-3}) was used to compare with the effect of different rock sizes on hydraulic properties.

The evaporation method was carried out with two different size columns: a 7.9-cm i.d. × 15-cm long cylindrical soil column for non-rocky soil, gravel, and small chert (longest length < 4 cm and thickness < 2 cm), and a 10-cm i.d. × 30-cm long soil column for large chert (longest length < 7 cm and thickness < 4 cm). Initially, the evaporation

method used clay loam without chert. The air-dried soil sample was packed uniformly to a bulk density of 1.15 g cm^{-3} in the 15-cm soil column. The soil water pressure head was monitored with 5 mm diam. and 10 mm long tensiometers inserted horizontally at depths of 3, 8, and 13 cm in the smaller soil column (Fig. 6.2). In the larger column, tensiometers were inserted horizontally at depths of 5 cm and 10 cm. The tensiometers were connected to pressure transducers, and soil samples were saturated using a mariotte bottle that provided water from the bottom of the column for 3 days. Saturated hydraulic conductivity K_s of the clay loam was measured with a constant hydraulic pressure head at the top of the soil column. Then, the bottom inlet was closed and the soil surface on the top of column was exposed to air for to allow evaporation. A small fan circulated air over the soil surface. The soil column was placed on a digital scale, and the water loss was measured to calculate the average evaporation flux for a given time interval. After the experiment was completed, average volumetric water content in the entire soil column, θ_{ave} and bulk density, ρ_b were obtained gravimetrically.

Evaporation experiments were then done with 0.20 m^3 m^{-3} volume fraction of gravel 0.12 m^3 m^{-3} of rock provided by 6 small rocks, and 0.24 m^3 m^{-3} provided by 24 larger rocks. The air-dried gravels were packed uniformly in the columns with the air-dried soil sample (ρ_b = 1.15 g cm^{-3}). Two small rocks were placed at depths of 2.5, 7.5, and 12.5 cm in the small soil column. Six large rocks were at depths of 3, 7, 12, 17, 23, and 28 cm in the larger soil column. Plastic tamps were used to pack the soil between rocks. Saturated hydraulic conductivity for the three different values of R_v was measured, and then the evaporation experiments were conducted (Fig. 6.2). At the end of

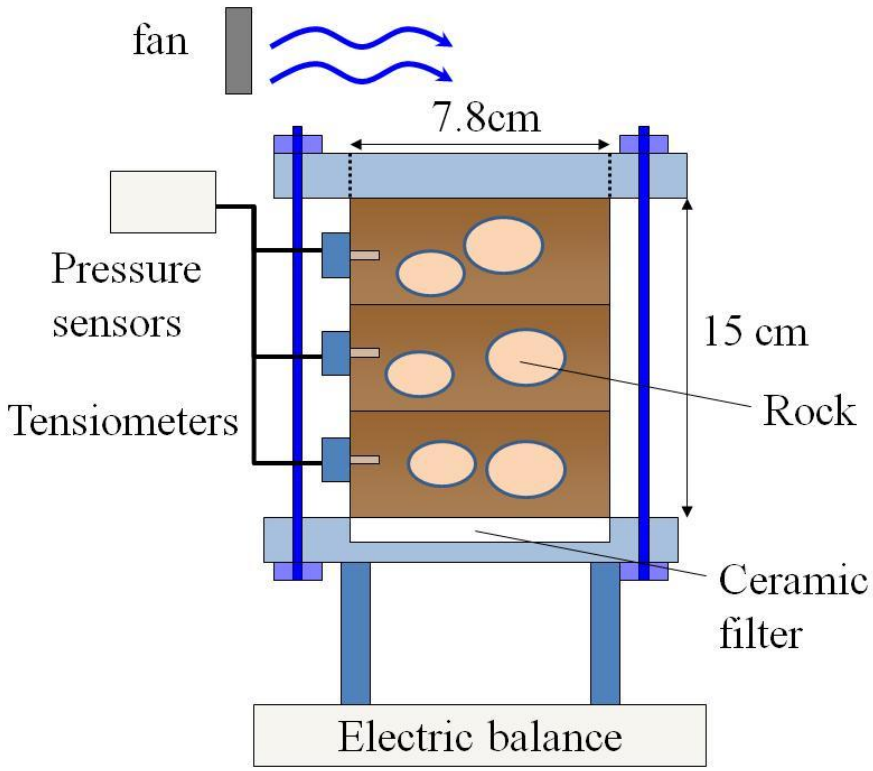

Fig. 6.2 Schematic figure of the evaporation experiment for rocky soils. Rock fragments were distributed as uniform as possible.

the experiments, θ_{ave} and ρ_b were determined gravimetrically.

Parameter Estimation

Initial Estimate of Model Parameters

We used inverse analysis to estimate model parameters. Because parameter optimization is affected by initial estimates of the parameters (Šimůnek et al., 1998), it was important that our initial values were reasonable. We used parameters obtained from the water retention curve for the soil without rocks as the basis for estimating parameters for rocky soil. The water retention curve for the soil alone was measured using the hanging water column method ($0 < h < -100$ cm) and soil psychrometry ($h < -410$ cm). The VG model parameters for the measured retention curves were determined with a computer program for fitting a water retention curve, RETC, developed by van Genuchten et al. (1991). Figure 6.3 shows the fitted water retention curve for the VG model with parameters $\theta_r = 0.079$ m^3 m^{-3}, $\theta_s = 0.53$ m^3 m^{-3}, $\alpha = 0.086$ cm^{-1}, and $n = 1.23$. The estimated air entry value based on the fitted curve was ≈ -10 cm.

Initial θ_s and θ_r for rocky soil were a function of R_v (Eq. [6.2]), consistent with a study by Fiés et al. (2002) that showed addition of glass fragments to soil decreased θ in proportion to the amount of glass added. Using the initial θ_s, θ_r, and the measured θ(h) shown in Fig. 6.2, we determined initial α and n for the VG model. Saturated hydraulic conductivities with different R_v were measured, but based on measured θ_s and porosity, the soil column was only at 92% of saturation due to entrapped air. Thus, we used an optimized value for K_s based on parameter estimation, rather than the measured value. The initial estimate of the parameter l for hydraulic conductivity was 0.5, as

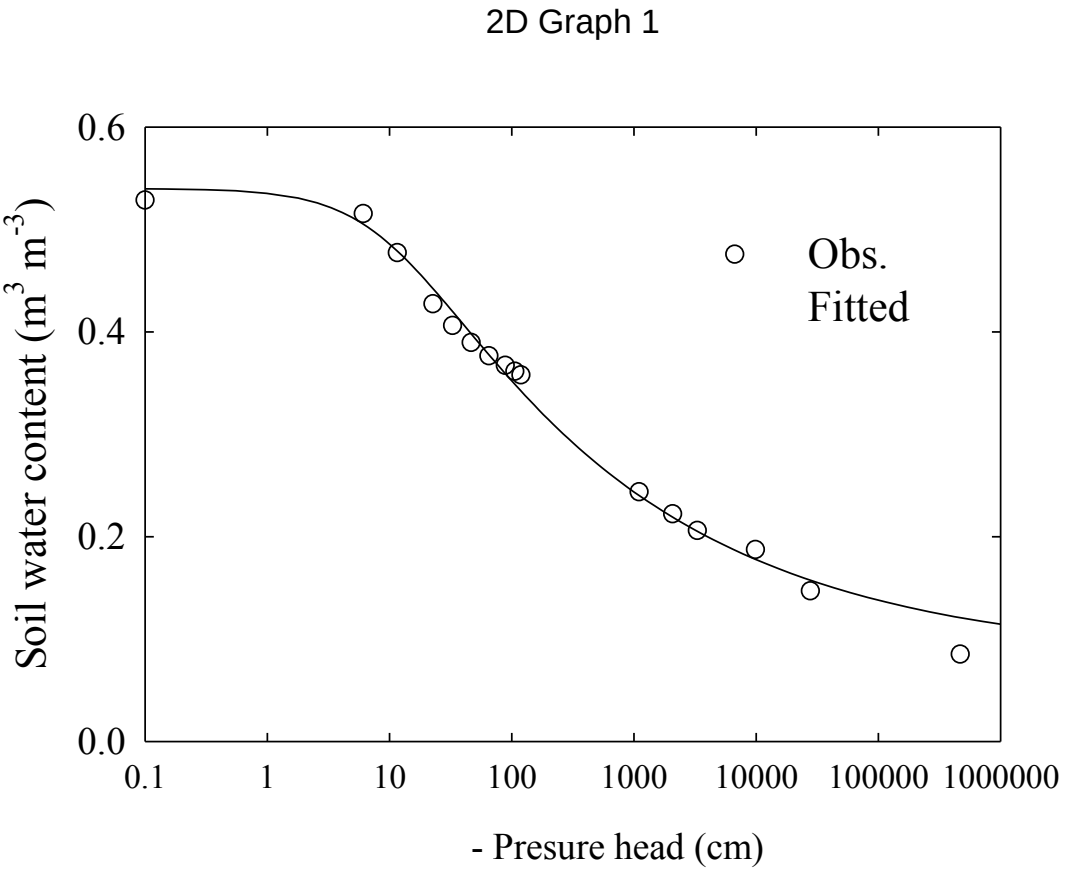

Fig. 6.3 Observed and fitted water retention curve for clay loam without rock fragments. The fitted curve is the VG model.

recommended by Mualem (1976). The Durner bimodal porosity model makes it more complicated to estimate initial parameters. To facilitate convergence of the parameters, initial θ_s and θ_r were calculated based on R_v for the Durner model as well as the VG model. The other initial parameters α_1, n_1, α_2, n_2 and w_2 for the first and second step-curves were determined by fitting the measured $\theta(h)$ after the initial θ_s and θ_r were calculated by Eq. [6.2]. In the fitting process, we assumed that α_1, representing the air entry value of the rocky soil, was the same as that of the clay loam because the pore size distribution of Mualem (1976) would be preserved in rocky soil. The other initial estimates for parameters n_1, α_2 and n_2 based on w_2 (≥ 0.5) were obtained iteratively using the measured water retention curve for the clay loam.

Optimization of Parameters

Optimization of parameters involved iteration to minimize an objective function Φ as outlined by Šimůnek et al. (2005). The function Φ, is defined using changes in pressure head, observed water retention curve for soil excluding rocks, $\theta(h)$ (< initial θ_s), and θ_{ave} as

$$\Phi = \sum_{j=1}^{m} v_{h,j} \sum_{i=1}^{n_j} w_h \left[h_j^*(t_i) - h_j(t_i)\right]^2$$
$$+ v_{\theta(h)} \sum_{i=1}^{n_\theta} w_{\theta(h)} [\theta(h)^* - \theta(h)]^2$$
$$+ w_\theta [\theta_{ave}^* - \theta_{ave}]^2 \qquad [6.10]$$

where m represents the different sets of measurements (pressure head, measured water retention curve, and average water content), n is the number of measurements in a particular measurement set, superscript * is observed measurement, $h_j(t_i)$ is pressure

head at depth j at time t_i, and w_h, $w_{\theta(h)}$, and w_θ are weighting coefficients for pressure head, observed water retention curve, and average water content, respectively. Measured θ and h are required to optimize parameters for the θ–h relationship in the inverse analysis method to minimize the differences between observed and estimated θ and h. The measured θ–h relationship for soil without rock enhanced convergence of numerical solutions for rocky soils. In this study, we assumed that $w_{\theta(h)}$ was equal to 1; however, w_h and w_θ were set to 10 to evaluate water balance more accurately (Sakai and Toride, 2007a). Weighting coefficients v were calculated by

$$v = \frac{1}{n\sigma^2} \quad [6.11]$$

where σ^2 is the measurement variance for different measurements. Weighting coefficients are required to compare data among the different measurements, which have different data numbers and measurement ranges. For example, h ranged from 0 to - 700 cm compared with θ which ranged from 0 to 0.55 $m^3\ m^{-3}$. The Levenberg-Marquardt method (Marquardt, 1963) was used to minimize Φ for the VG and the Durner models. The parameter adjustment was repeated until the inverse analysis simulations of the parameters converged.

Results and Discussion

Observed Evaporation and Pressure Head

Figure 6.4 shows temporal changes in observed cumulative evaporation and pressure head of soil, gravel (R_v = 0.20 $m^3\ m^{-3}$), small rock (R_v = 0.12 $m^3\ m^{-3}$), and large rock (R_v = 0.24 $m^3\ m^{-3}$). Initially, evaporation was highest for the soil alone and soil with

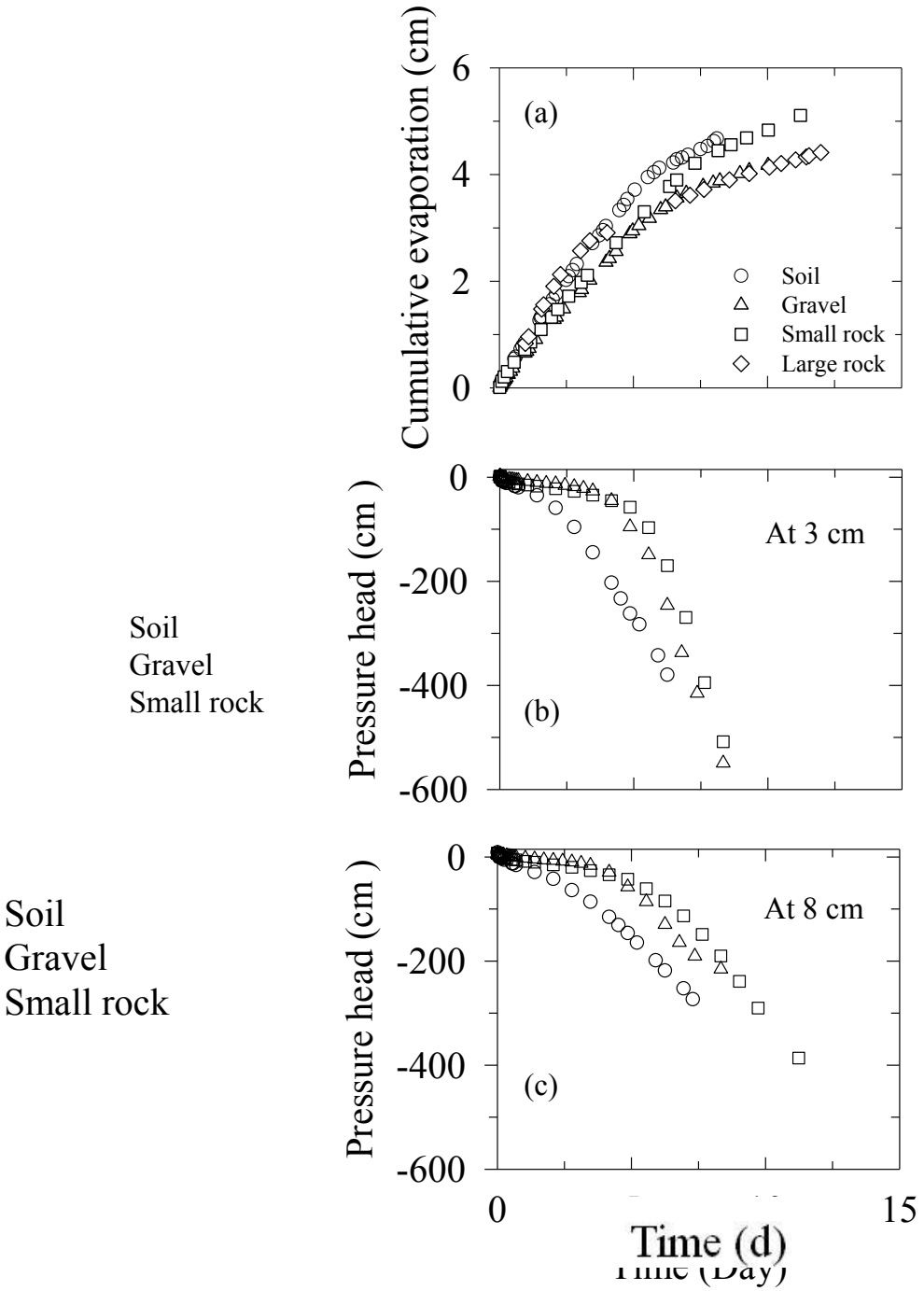

Fig. 6.4 Comparison of observed cumulative evaporation (a), pressure heads at a depth of 3 cm (b), and 8 cm (c) between soil, soil + gravel (R_v = 0.20 m^3 m^{-3}), soil + small rock (R_v = 0.12 m^3 m^{-3}), and soil + large rock (R_v = 0.24 m^3 m^{-3}).

gravel, but over time, cumulative evaporation with soil and small rocks reached values similar to the other two cases (Fig. 6.4a). Evaporation was lowest for soil with the larger rock. Saturated hydraulic conductivity was estimated at 20 cm d^{-1} for soil was higher K_s = 13 cm d^{-1} for gravel and K_s = 14 cm d^{-1} for soil with small rock. Gravel and small rock maintained a higher h than soil alone (Fig. 6.4b). These results suggest that gravel and small rocks slowed upward movement of water, thereby maintaining flow of liquid water to the surface for a longer period of time.

Additional experiments were done with the same R_v using shorter columns (3-cm long or 5-cm long column) than the 15-cm long column to observe the effect of rock on cumulative evaporation (Fig. 6.5). The experiments were carried out for 3 days when average relative humidity was 41.5%. Maximum rates of evaporation for soil, the gravel, the small rock, and large rock were 2.4, 2.4, 2.1, and 1.3 cm d^{-1}, respectively. Cumulative evaporation was highest for soil with small rock, and with gravel (Fig. 6.5a), consistent with the data in Fig. 6.4a. van Wesemael et al. (1996) found that evaporation can increase with soil-gravel mixtures in dry soil conditions. Our results and those of van Wesemael et al. (1996) imply that capillary flow can be maintained with small rocks, but may be disrupted by with large rocks. Calculated θ_s was 0.581, 0.572, 0.566, and 0.479 m^3 m^{-3} for soil, gravel, small rock, and large rock, respectively. Measured values of θ_s were 0.584, 0.49, 0.543, and 0.465 m^3 m^{-3}, which were similar to values obtained θ_s by Eq. [6.2].

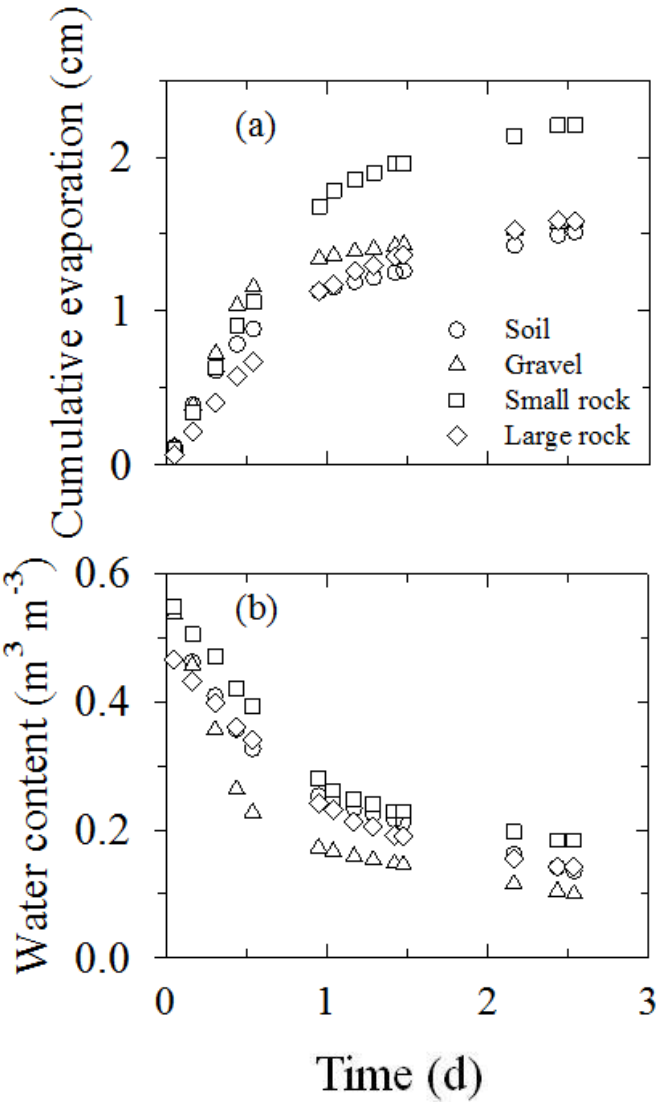

Fig. 6.5 Cumulative evaporation (a) and changes in water content (b) in 5-cm long columns with soil, soil + gravel (R_v = 0.20 m^3 m^{-3}), soil + small rock (R_v = 0.12 m^3 m^{-3}), and soil + large rock (R_v = 0.24 m^3 m^{-3}).

Optimization with the VG Model

Figure 6.6 compares measured and modeled evaporation and *h* for soil without rock and soil with three different volume fraction of rock using the optimized VG model parameters in Table 6.1. We optimized the six unknown parameters defined by Eqs. [6.6] and [6.7]: θr, θ_S, α, n, K_s, and l over a wide range (Table 6.1). The VG model yielded good results for the clay loam (Figs. 6.6a and 6.6b). However, the optimized parameter l based on results from the evaporation method was 0.001, much lower than the 0.5 recommended by Mualem (1979).

The VG model did not perform well for rocky soil (Figs. 6.6c-h). Measurements showed that addition of the gravel and small rocks maintained a high *h* and evaporation (*E*) over a longer period of time than for soil alone, and this was not predicted by the model. Maintenance of high *E* was not observed with the larger rock, even though the volume fraction of rock was similar to that of gravel. The model also did not simulate the steep decline in *h* when *E* was declined *E* (Figs. 6.6b and 6.6d). We did not find any relationship between the l and R_v (Table 6.1). This suggested that the VG model did not allow us to predict unsaturated hydraulic conductivity for rocky soils with the parameter l as a function of R_v.

Figure 6.7 shows simulations of temporal changes in θ profiles for soil with small rocks (R_v = 0.12 m^3 m^{-3}). R_v = 0.12 m^3 m^{-3}. The model did a good job of simulating θ at a depth of 7.5 cm, but overestimated θ near the soil surface, indicating that unsaturated hydraulic conductivity at low pressure heads was too high. Close to saturation, where relatively capillary flow dominates, the parameter l may represent

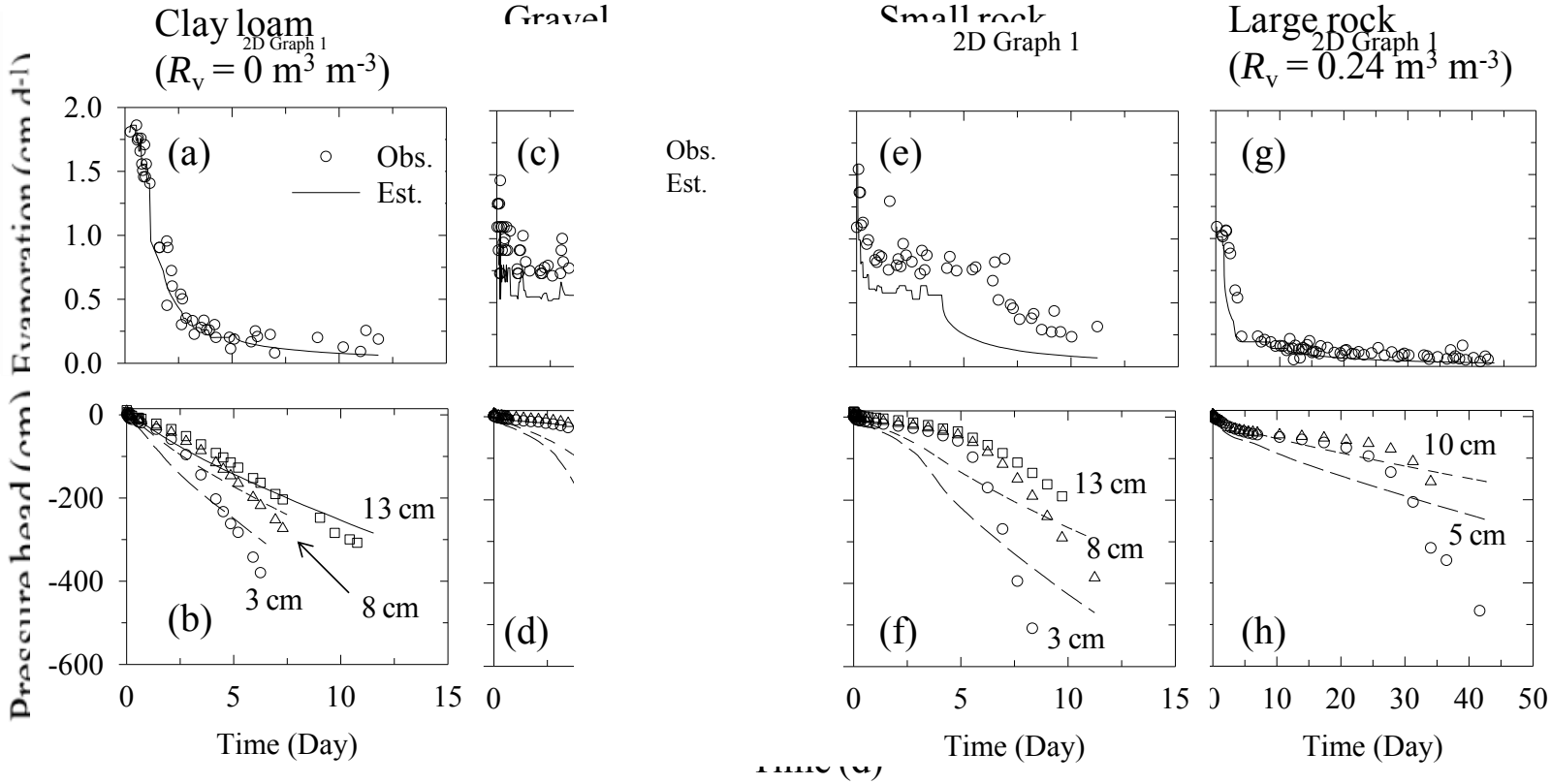

Fig. 6.6 Comparison of VG of evaporation and pressure heads with measured values for loam without rock (a and b), gravel (R_v = 0.20 m^3 m^{-3}) (c and d), 4-cm small rock (R_v = 0.12 m^3 m^{-3}) (e and f), and 7-cm large rocks (R_v = 0.24 m^3 m^{-3}) (g and h), respectively, using the parameters shown in Table 6.1.

Table 6.1 Optimized parameters and the estimation ranges (low→high values) of the VG model.

		Rocky soil types		
Parameters	Clay loam (R_v = 0 m^3 m^{-3})	Gravel (R_v = 0.20 m^3 m^{-3})	Small rock (R_v = 0.12 m^3 m^{-3})	Big rock (R_v = 0.24 m^3 m^{-3})
θ_r [m^3 m^{-3}]	0.07 (0.07→0.1)	0.055 (0.055→0.095)	0.06 (0.055→0.095)	0.07 (0.05→0.07)
θ_s [m^3 m^{-3}]	0.54 (0.45→0.57)	0.44 (0.4→0.45)	0.48 (0.42→0.48)	0.41 (0.4→0.43)
α [cm^{-1}]	0.042 (0.01→0.08)	0.04 (0.025→0.1)	0.038 (0.025→0.08)	0.07 (0.04→0.08)
n	1.30 (1.0→1.5)	1.3 (1.3→1.4)	1.29 (1.0→1.4)	1.29 (1.29→1.4)
K_s [cm d^{-1}]	36 (14→36)	14.4 (3→15)	14.4 (1.5→15)	21.6 (1.5→22)
l	0.001 (0.001→0.5)	0.00012 (0.0001→0.5)	0.00012 (0.0001→0.5)	0.00012 (0.0001→0.5)
r^2	0.967	0.768	0.784	0.798

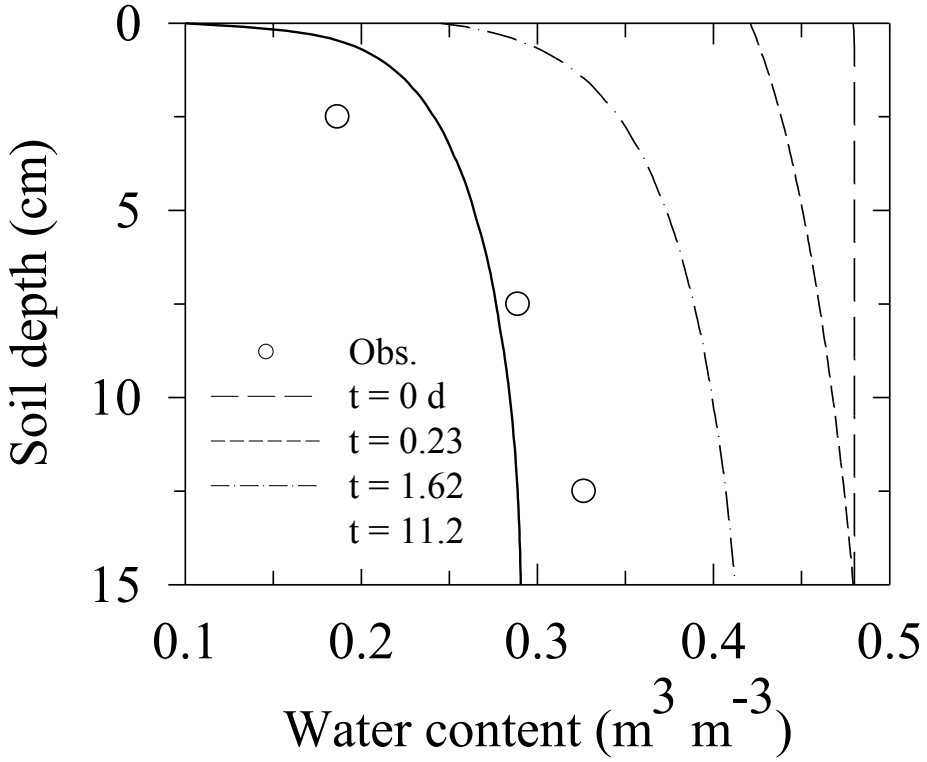

Fig. 6.7 S

c

Obs.
t = 0 d
t = 0.23
t = 1.62
t = 11.2

water flow around rock fragments. At low pressure heads where flow involves thin films of water as (Tuller and Or, 2001), however, the limited performance of the VG model may be attributed to the of the WRC, because n is very sensitive to θ_r as demonstrated by Šimůnek et al. (1998). If n is related to θ_r in rocky soil, the range over which n can be adjusted to optimize parameters will decrease with increasing R_v. In fact, our result showed that optimized n was nearly lack of consideration of the film flow around rock fragments. In addition to the film flow issue, a particularly difficult problem was the limited adjustment of parameter n, the slope constant among the different R_v (Table 6.1), so the VG model resulted in less sensitivity of unsaturated hydraulic conductivity to R_v.

Optimization with the Durner Model

When the Durner model was applied to the inverse analysis of water retention curves for gravel ($R_v = 0.20$ m^3 m^{-3}), small rock ($R_v = 0.12$ m^3 m^{-3}), and large rock ($R_v = 0.24$ m^3 m^{-3}), the fitting of evaporation showed slight improvements (Figs. 6.8a, 6.8b, and 6.8c). However, we found good fits for measured h (Figs. 6.8d, 6.8e, and 6.8f), especially for wet end of h curves. In general, h near the soil surface exhibited a higher sensitivity to the optimized parameters than from deeper locations (Šimůnek et al., 1998). Table 6.2 shows the optimized Durner model parameters. Comparisons with r^2 values with those of the VG model shown in Table 6.1 suggest that the Durner model was more appropriate than the VG model to estimate water retention curves for rocky soils.

It may seem contradictory that the simulations of evaporation using with gravels or small rocks in the soil were not better (Figs. 6.8a and 6.8b), because simulated h was

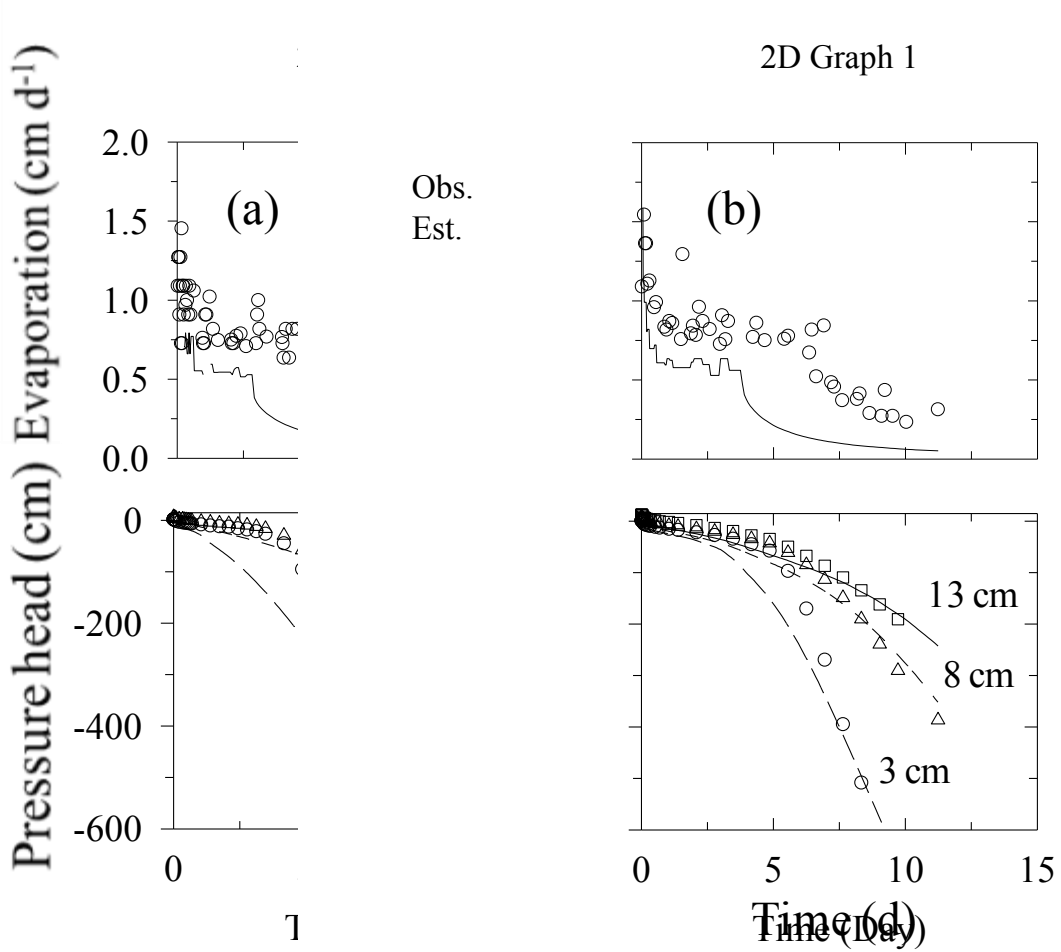

Fig.6.8 Comparison of Durner model simulation of evaporation and pressure head with measured values for soil + gravel (a), soil + small rock (b), and soil + large rock (c) using the model parameters shown in Table 6.2.

Table 6.2 Optimized parameters and the parameter ranges (low→high values) of the Durner model.

		Rocky soil types	
Parameters	Gravel (R_v = 0.20 m^3 m^{-3})	Small rock (R_v = 0.12 m^3 m^{-3})	Big rock (R_v = 0.24 m^3 m^{-3})
θ_r [m^3 m^{-3}]	0.055 (0.055→0.06)	0.06 (0.06→0.11)	0.069 (0.045→0.085)
θ_s [m^3 m^{-3}]	0.44 (0.43→0.45)	0.49 (0.45→0.49)	0.37 (0.37→0.43)
α_1 [cm^{-1}]	0.118 (0.1→0.15)	0.042 (0.01→0.07)	0.077 (0.01→0.1)
n_1	1.5 (1.4→1.5)	2.3 (1.3→2.3)	2 (1.0→2.0)
K_s [cm d^{-1}]	21.6 (1.5→22)	14.4 (3→15)	12.1 (1.5→22)
l	0.0003 (0.0001→0.0005)	0.03 (0.0001→0.5)	0.0005 (0.0001→0.5)
w_2	0.49 (0.45→0.5)	0.51 (0.4→0.9)	0.56 (0.4→0.7)
α_2 [cm^{-1}]	0.0009 (0.0009→0.002)	0.001 (0.001→0.008)	0.0005 (0.0005→0.0075)
n_2	1.4 (1.4→1.5)	1.17 (1.0→1.8)	1.21 (1.0→1.8)
r^2	0.884	0.936	0.972

in good agreement with measured h (Figs. 6.8d and 6.8e). These results imply an uncertainty about the influence of rock size and R_v on unsaturated hydraulic conductivity $K(h)$. In saturated soil, K_s should decrease with R_v (Ravina and Magier, 1984; Novák et al., 2011). In unsaturated conditions, however, the comparison between Figs. 6.6a, 6.8d, and 6.8e shows that rocky soil with R_v (< 0.2 m^3 m^{-3}) maintained a stable evaporation flux longer than the non-rocky soil. What we did to express $K(h)$ was to increase $K(h)$ with the parameter l ranging from 0.5 to 0.0001 (Table 6.2). However, it was difficult to match the high evaporation flux in the unsaturated condition. However, simulations with the larger rocks (higher R_v) matched observations quite well. This suggests a more accurate expression of $K(h)$ (Fig. 6.8c) with large rocks. It is likely that higher rock volume disrupted capillary connections with the surface, creating regions of higher water content beneath the rocks.

Estimated water retention curves for the gravel, the small rocks, and the large rocks with the Durner model are shown in Fig. 6.9. The measured retention curve for the non-rocky soil is also shown for comparison. To optimize the Durner model parameters, we assumed that the air entry value of the rocky soil would be similar to the value for the clay loam and the second curve would dominate the water retention curve for rocky soil. Our results showed that the difference between the optimized θ_s and the θ_s estimated by Eq. [6.2] were less than 0.03 m^3 m^{-3}. This suggests that the air entry values of the rocky soil were similar to the value for the clay loam. This differs from results of Fiés et al. (2002) that showed the air entry value of mixtures of soils and glass fragments (< 6 mm) increased with volume fraction of glass (> 30%) even though θ_s and θ_r decreased as

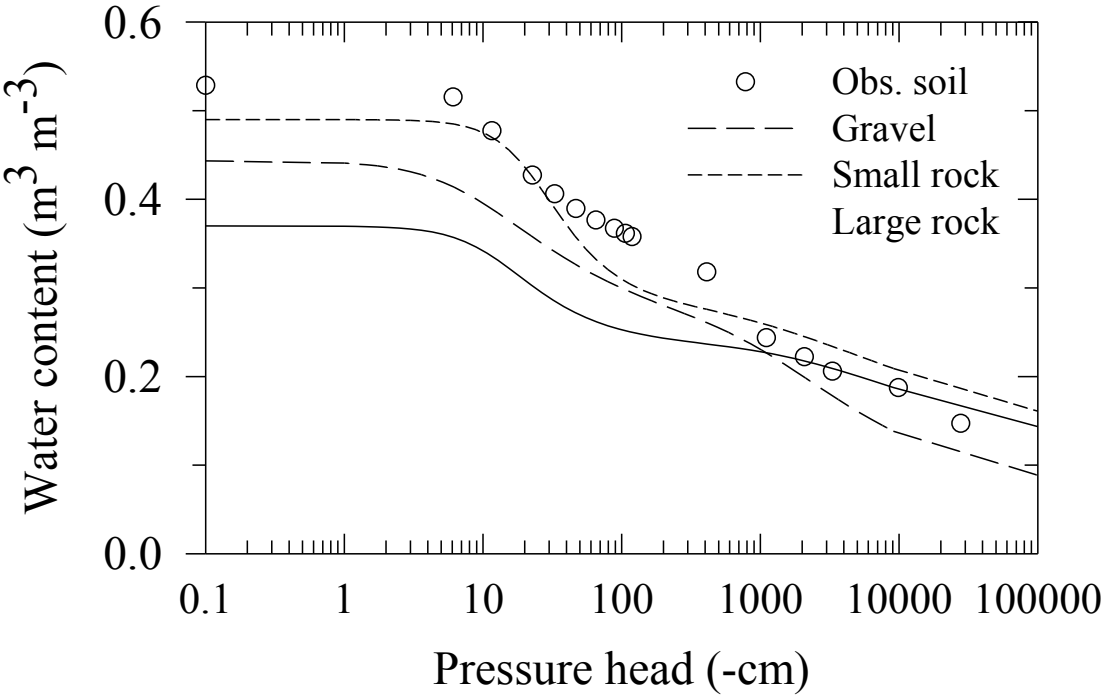

Fig. 6.9 Water retention curves for the gravel (R_v = 0.20 m^3 m^{-3}), the small rock (R_v = 0.12 m^3 m^{-3}) and the large rocks (R_v = 0.24 m^3 m^{-3}) using the Durner model.

glass volume increased. This might have occurred because of increasing air gaps between glass fragments. However, if large air gaps do not exist, as was likely the case in our study, the impact of change in the air entry value due to larger air-filled porosity may be ignored. Evaluating whether the second curve can dominate a water retention curve for rocky soil is difficult, but the initial w_2 value (≥ 0.5) led to an increase in the flexibility of the Durner model in describing retention and hydraulic data across the range of *h*. For example, if initial w_2 value was lower than 0.4, it resulted in overestimated K_s (> 30 cm d^{-1}) and θ_s (> 0.50 m^3 m^{-3}). Thus, the initial w_2 value (≥ 0.5) was helpful to obtain reasonable water retention curves for rocky soil.

Analysis of evaporation experiments showed that the retention curve for the rocky soil can be obtained with the retention curve for clay loam using our parameter estimation technique. A simulation without the water retention curve for the clay loam as a starting point for optimizing Durner parameters for the soil + gravel case ($\theta_r = 0.045$ m^3 m^{-3}, $\theta_s = 0.43$ m^3 m^{-3}, $\alpha_1 = 0.03$ cm^{-1}, $n_1 = 1.46$, $l = 0.1$, $w_2 = 0.42$, $\alpha_2 = 0.0042$ cm^{-1}, and $n_2 = 1.01$) produced an unreasonable K_s of 87 cm d^{-1}. Our estimation technique may reduce the problem of parameter optimization, but K_s of the Durner model will still be sensitive to parameters l, α_1 and α_2 (Sakai and Toride, 2007b).

Conclusions

Estimation of hydraulic properties for rocky soils was investigated using the evaporation method with soil cores containing gravel ($R_v = 0.20$ m^3 m^{-3}), small rock ($R_v = 0.12$ m^3 m^{-3}), or large rock ($R_v = 0.24$ m^3 m^{-3}). Cumulative evaporation from a clay loam soil containing small rock gradually increased when compared to that from soil

alone. These results suggest that small rocks slowed upward movement of water, thereby maintaining flow of liquid water to the surface for a longer period of time. Evaporation from soil with larger rock ($R_v = 0.24$ m^3 m^{-3}) was lower than that from soil alone.

Two simulation models, Van Genuchten (VG) and Durner, were evaluated for estimating hydraulic properties of rocky soils. Simulations were compared with the observed evaporation and h, ranging from approximately -50 cm and -600 cm. Pore connectivity parameter l, representing tortuosity was estimated. Estimated l (≤ 0.03) was lower than 0.5, the value recommended by Mualem (1975), which improved simulation performance for both models. Results showed that the Durner model was more appropriate than the VG model for describing water retention and hydraulic conductivity of rocky soils across the range of pressure heads.

CHAPTER VII

CONCLUSIONS

Conclusions of this study are:

1. Neutron probe and gamma probe measurements are effective methods of characterizing spatial variability in θ and ρ_b in rocky soils in karst terrain, provided access tubes can be sealed to prevent flow of water along the soil-tube interface. Expandable polyurethane foam is an effective sealant, but it creates non-linear neutron probe calibration curves.

2. Rock in karst savannas creates high spatial variability in water storage in the root zone, and coupled with heterogeneous distribution of trees leads to high spatial variability in root water uptake. Because spatial and temporal variability in water storage and retention are high in karst landscapes, a large number of measurements are required to quantify water dynamics in the root zone. Hydrologic and vegetation models must account for this variability, and need to include the impact of water storage within the rock matrix if they are to provide realistic simulations of evapotranspiration and water dynamics.

3. Water uptake in karst savannas comes largely from shallow roots, but uptake from sources in rock, either from soil pockets within the rock matrix or with the rock itself, can be sufficient to sustain transpiration when shallow sources of available water are depleted.

4. Distribution of rock is correlated with water content, and spatial autocorrelation between dry bulk density and water content was found in karst landscapes.

5. Small volume fractions of rock can increase evaporation from soils by slowing upward movement of water, thereby maintaining capillary connectivity to the surface for a longer period of time.

6. The Durner model is more appropriate than the van Genuchten model for estimating hydraulic properties of rocky soils.

REFERENCES

Afinowicz, J.D., Munster, C.L., and Wilcox., B.P., 2005. Modeling the effects of brush management for increasing water yield on the Edwards Plateau, Texas. Journal of the American Water Resources Association, 41: 181-193.

Allen, MF., 2007. Mycorrhizal fungi: Highways for water and nutrients in arid soils. Vadose Zone Journal, 6: 291-297.

Amoozegar, A., Martin, K.C., and Hoover, M.T., 1989. Effect of access hole properties on soil water content determination by neutron thermalization. Soil Science Society of America Journal, 53: 330-335.

Arbel, Y., Greenbaum, N., Lange, J., and Inbar, M., 2010. Infiltration processes and flow rates in developed karst vadose zone using tracers in cave drips. Earth Surface Processes and Landforms, 35: 1682-1693.

Archer, S., Boutton, T.W., and Hibbard, K.A., 2001. Trees in grasslands: Biogeochemical consequences of woody plant expansion. *In* Schulze, E-D., Heimann, M., Harrison, S.P., Holland, E.A., Lloyd, J., Prentice, I.C., and Schimel, D., (eds.) Global Biogeochemical Cycles in the Climate System, Academic Press, San Diego, p. 115-137.

Brakensiek, D.L., and Rawls, W.J., 1994. Soil containing rock fragments: effects on infiltration. Catena, 23: 99-110.

Brooks, R.H., and Corey, A.T., 1964. Hydraulic properties of porous media. Hydrological Paper 3. Colorado State University, Fort Collins, Colorado, p. 22-27.

Canton, Y., Villagarcia, L., Moro, M.J., Serrano-Ortiz, P., Were, A., Alcala, F.J., Kowalski, A.S., Sole-Benet, A., Lazaro, R., and Domingo, F., 2010. Temporal dynamics of soil water balance components in a karst range in southeastern Spain: estimation of potential recharge. Hydrological Sciences Journal-Journal Des Sciences Hydrologiques, 55: 737-753.

Christensen, E.R., 1974. Use of the gamma density gauge in combination with the neutron moisture probe. Symposium on Isotope and Radiation Techniques in Studies of Soil Physics, Irrigation and Drainage in Relation to Crop Production, Vienna, Austria, International Atomic Energy Agency, p. 27-44.

Cousin, I., Nicoullaud, B., and Coutadeur, C., 2003. Influence of rock fragments on the water retention and water percolation in a calcareous soil. Catena 53: 97-114.

Cressie, N.A.C., 1993. Statistics for Spatial Data. Wiley, New York, p. 186-209.

Cressie, N.A.C., and Read, R.C., 1989. Spatial data analysis of regional counts. Biometrical Journal, 81: 699-719.

Dasgupta, S., Mohanty, B.P., and Koehne, J.M., 2006. Impacts of juniper vegetation and karst geology on subsurface flow processes in the Edwards Plateau, Texas. Vadose Zone Journal, 5: 1076-1085.

Dugas, W.A., Hicks, R.A., and Wright, P., 1998. Effect of removal of *Juniperus ashei* on evapotranspiration and runoff in the Seco Creek watershed. Water Resources Research, 34: 1499-1506.

Dunn, A.J., and Mehuys, G.R., 1984. Relationship between gravel content of soils and saturated hydraulic conductivity in laboratory tests. *In* Nichols, J.D. (ed.), Erosion and Productivity of Soils Containing Rock Fragments. Special Publication, vol. 13. Soil Science Society of America, Madison, WI, p.55-63.

Durner, W., 1994. Hydraulic conductivity estimation for soils with heterogeneous pore structure. Water Resources Research, 30: 211-223.

Elkington, R.J., Rebel, K.T., Heilman, J.L., Litvak, M.E., Dekker, S.C., and Moore, G.W., 2012. Species-specific water use by woody plants on the Edwards Plateau, Texas. Ecohydrology, DOI: 10.1002/eco.1344.

Estrada-Medina, H., Graham, R.C., Allen, M.F., Jiménez-Osornio, J.J., and Robles-Casolco, S., 2012. The importance of limestone bedrock and dissolution karst features on tree root distribution in northern Yucatán, Mexico. Plant Soil, DOI 10.1007/s11104-012-1175-x.

Evett, S.R., 2003. Soil water measurement by neutron thermalization. *In* Stewart, B.A., and Howell, T.A., (eds.) Encyclopedia of Water Science. Marcel Dekker, Inc., New York, p. 888-893.

Evett, S.R., Tolk, J.A., and Howell, T.A., 2003. A depth control stand for improved accuracy with the neutron probe. Vadose Zone Journal, 2: 642-649.

Famiglietti, J.S., Rudnicki, J.W., and Rodell, M., 1998. Variability in surface moisture content along a hillslope transect: Rattlesnake Hill, Texas. Journal of Hydrology, 210: 259-281.

Fiés, J.C., De Louvigny, N., and Chanzy, A., 2002. The role of stones in soil water retention. European Journal of Soil Science, 53: 95-104.

Graham, R.C., Schoeneberger, P.J., Anderson, M.A., Sternberg, P.D., and Tice, K.R, 1997. Morphology, porosity, and hydraulic conductivity of weathered granitic bedrock and overlying soils. Soil Science Society of America Journal, 61: 516-522.

Greacen, E.L., Correll, R.L., Cunningham, R.B., Johns, O.C., and Nichols, K.D., 1981. Calibration. *In* Greacen, E.L., (ed.) Soil Water Assessment by the Neutron Method. CSIRO, Melbourne, Australia, p. 50-78.

Gregory, L., Wilcox, B.P., Shade, B., Munster, C.L., Owens, K., and Veni, G., 2009. Large-scale rainfall simulation over shallow caves on karst shrublands. Ecohydrology, 2: 72-80.

Grigg, A.M., Lambers, H., and Veneklaas, E.J., 2010. Changes in water relations for Acacia ancistrocarpa on natural and mine-rehabilitation sites in response to an experimental wetting pulse in the Great Sandy Desert. Plant and Soil, 326: 75-96.

Heilman, J.L., Litvak, M.E., McInnes, K.J., Kjelgaard, J.F., Kamps, R.H., and Schwinning, S., 2012. Water-storage capacity controls energy partitioning and water use in karst ecosystems on the Edwards Plateau, Texas. Ecohydrology, DOI 10.1002/eco.1327.

Heilman, J.L., McInnes, K.J., Kjelgaard, J.F., Owens, M.K., and Schwinning, S., 2009. Energy balance and water use in a subtropical karst woodland. Journal of Hydrology, 373: 426-435.

Hignett, C., and Evett, S.R., 2002. Neutron thermalization. *In* Dane, J.H., and Topp, G.C., (eds.) Methods of Soil Analysis. part 4 – Physical Methods. Soil Science Society of America, Madison, WI, p.501-521.

Hu, W., Shao, M., Wang, Q., Fan, J., and Reichardt, K., 2008. Soil water content temporal-spatial variability of the surface layer of a Loess Plateau hillslope in China. Scientia Agricola, 65: 277-289.

Hu, W., Shao, M., Wang, Q., Han, F., and Reichardt, K., 2011. Spatio-temporal variability behavior of land surface soil water content in shrub- and grass-land. Geoderma, 162: 260-272.

Jackson, R.B., Moore, L.A., Hoffmann, W.A., Pockman, W.T., and Linder, C.R., 1999. Ecosystem rooting depth determined with caves and DNA. Proceedings of the National Academy of Sciences USA, 96: 11387-11392.

Jackson, R.B., Sperry, J.S., and Dawson, T.E., 2000. Root water uptake and transport: using physiological processes in global predictions. Trends in Plant Science, 5: 482-488.

Jacques, D., Mohanty, B.P., Timmermana, A., and Feyen, J., 2001. Study of time dependency of factors affecting the spatial distribution of soil water content in a field-plot. Physics and Chemistry of the Earth B, 26: 629-634.

Jacques, D., Mouvet, C., Mohanty, B.P., Vereecken, H. and Feyen, J., 1999. Spatial variability of atrazine sorption parameters and other soil properties in a podzoluvisol. Journal of Contaminant Hydrology, 36: 31-52.

Joshi, C., Mohanty, B.P., Jacobs, J.M., and Ines, A.V.M., 2011. Spatiotemporal analyses of soil moisture from point to footprint scale in two different hydroclimatic regions. Water Resources Research, DOI:10.1029/2009WR009002.

Kachanoski, R.G., and de Jong, E., 1998. Scale dependence and the temporal persistence of spatial patterns of soil water storage. Water Resources Research, 24: 85-91.

Katsura, S., Kosugi, K., Mizutani, T., and Mizuyama, T., 2009. Hydraulic properties of variously weathered granitic bedrock in headwater catchments. Vadose Zone Journal, 8: 557-573.

Katsura, S., Kosugi, K., Yamamoto, N., and Mizuyama, T., 2006. Saturated and unsaturated hydraulic conductivities and water retention characteristics of weathered granitic bedrock. Vadose Zone Journal, 5: 35-47.

Keller, B.R., Everett, L.G., and Marks, R.J., 1990. Effects of access tube material and grout on neutron probe measurements in the vadose zone. Groundwater Monitoring & Remediation, 10: 96-100.

Knight, R., and Abad, A., 1995. Rock/water interaction in dielectric properties: Experiments with hydrophobic sandstones. Geophysics, 60: 431-436.

Kukowski, K., Schwinning, S., and Schwartz, B., 2012. Hydraulic responses to extreme drought conditions in three co-dominant tree species in shallow soil over bedrock. Oecologia, DOI: 10.1007/s00442-012-2466-x.

Lal, R., 1979. Concentration and size of gravel in relation to neutron moisture and density probe calibration. Soil Science, 127:41-50.

Lee, X., Finnigan, J., and Paw, U.K.T., 2004. Coordinate systems and flux bias error. *In* Lee X, Massman, W., and Law, B., (eds) Handbook of Micrometeorology, A Guide for Surface Flux Measurement and Analysis. Kluwer Academic Publishers, Dordrecht, Netherlands, p. 33-66.

Li, J., Smith, D.W., and Fityus, S.G., 2003. The effect of air gaps between the access tube and the soil during neutron probe measurements. Australian Journal of Soil Research, 41: 151-164.

Lyons, R.K., Owens, M.K., and Alejandro, C.J., 2006. Impact of juniper trees on local water budgets. The Cattleman, 98-106.

Ma, D., and Shao, M., 2008. Simulating infiltration into stony soils with a dual-porosity model. European Journal of Soil Science, 59: 950-959.

Ma, D., Shao, M., Zhang, J., and Wang, Q., 2010. Validation of an analytical method for determining soil hydraulic properties of stony soils using experimental data. Geoderma, 159: 262-269.

Ma, D.H., Wang, Q.J., and Shao, M.A., 2009. Analytical method for estimating soil hydraulic parameters from horizontal absorption. Soil Science Society of America Journal 73: 727-736.

Marquardt, D.W., 1963. An algorithm for least-squares estimation of nonlinear parameters. Society for Industrial and Applied Mathematics Journal on Applied Mathematics, 11: 431-441.

Massman, W.J., 2000. A simple method for estimating frequency response corrections for eddy covariance systems. Agricultural and Forest Meteorology, 104: 185-198.

Mualem, Y., 1976. A new model for predicting the hydraulic conductivity of unsaturated porous media. Water Resources Research, 12: 513-522.

McCole, A.A., and Stern, L.A., 2007. Seasonal water use patterns of *Juniperus ashei* on the Edwards Plateau, Texas, based on stable isotopes in water. Journal of Hydrology, 342: 238-248.

Mohanty, B.P., Famiglietti, J.S., and Skaggs, T.H., 2000. Evolution of soil moisture spatial structure in a mixed-vegetation pixel during the SGP97 hydrology experiment. Water Resources Research, 36: 3675-3686.

Mohanty, B.P. and Kanwer. R.S., 1994. Spatial variability of residual nitrate-nitrogen under two tillage systems in central Iowa: A composite three-dimensional resistant and exploratory approach. Water Resources Research, 30: 237-251.

Morris, P.H., and Williams, D.J., 1990. Generalized calibration of a neuclear moisture/ density depth gauge. Geotechnical Testing Journal, 13: 24-35.

Mehuys, G.R., Stolzey, L.H., and Letey, J., 1975. Temperature distributions under stones submitted to a diurnal heat wave. Soil Science, 120: 437-441.

Novák, V., Kňava, K., and Šimůnek, J., 2011. Determining the influence of stones on hydraulic conductivity of saturated soil using numerical method. Geoderma, 161: 177-181.

Olenick, K.L., Conner, J.R., Wilkins, R.N., Kreuter, U.P., and Hamilton, W.T., 2004. Economic implications of brush treatments to improve water yield. Journal of Range Management, 57: 337-345.

Owens, M.K., 2008. Juniper tree impacts on local water budgets. *In* VanAuken, O.W., (ed) Western North American Juniperus Communities. Springer, New York, p. 188-200.

Owens, M.K., Lyons, R., and Alejandro, C.L., 2006. Rainfall partitioning within semiarid juniper communities: effects of event size and canopy cover. Hydrological Processes, 20: 3179-3180.

Peters, A., and Durner, W., 2008. Simplified evaporation method for determining soil hydraulic properties. Journal of Hydrology, 356: 147-162.

Philips, J.R., 1957. The theory of infiltration: 4. sorptivity and algebraic infiltration equations. Soil Science, 84: 257-264.

Priesack, E. and Durner, W., 2006. Closed-form expression for the multi-modal unsaturated conductivity function. Vadose Zone Journal, 5: 892-898.

Pockman, W.T., McElrone, A.J., Bleby, T.M., and Jackson, R.B., 2008. The structure and function of roots of woody species on the Edwards Plateau, Texas, USA. Abstract H34A-02, Joint Assembly of American Geophysical Union, Fort Lauderdale, Florida.

Poesen, J., and Lavee, H., 1994. Rock fragments in top soils: significance and processes. Catena, 23: 1-28.

Poot, P., and Lambers, H., 2008. Shallow-soil endemics: adaptive advantage and constraints of a specialized root-system morphology. New Phytologist, 178: 371-381.

Querejeta, J.I., Estrada-Medina, H., Allen, M.F., Jimenez-Osornio, J.J., and Ruenes, R., 2006. Utilization of bedrock water by Brosimum alicastrum trees growing on shallow soil atop limestone in a dry tropical climate. Plant and Soil, 287: 187-197.

R Development Core Team, 2010. R: A language and environment for statistical computing, reference index version 2.12.1. (URL: http://www.r-project.org/).

Ravina, I. and Magier, J., 1984. Hydraulic conductivity and water retention of clay soils containing coarse fragments. Soil Science Society of America Journal, 48: 894-905.

Richardson, Z.B., 1966. Installation of soil moisture access tubes in rocky soils. Journal of Soil and Water Conservation, 21:143-145.

Sakai, M., and Toride, N., 2007a. Soil water hydraulic functions for a sandy soil and an aggregated soil. (In Japanese with English abstract) Journal of Japanese Society Soil Physics, 107: 63-77.

Sakai, M., and Toride, N., 2007b. Optimum conditions for predicting unsaturated hydraulic properties using the evaporation method. (In Japanese with English abstract) Journal of Japanese Society Soil Physics, 106: 33-46.

Schenk, H.J., and Jackson, R.B., 2002. Rooting depths, lateral root spreads and below-ground/ above-ground allometries of plants in water-limited ecosystems. Journal of Ecology, 90: 480-494.

Schume, H., Jost, G., and Katzensteiner, K., 2003. Spatio-temporal analysis of the soil water content in a mixed Norway spruce (*Picea abies* (L.) Karst.)–European beech (*Fagus sylvatica* L.) stand. Geoderma, 112: 273-287.

Schwinning, S. 2008. The water relations of two evergreen tree species in a karst savanna. Oecologia, 158: 373-383.

Schwinning, S., 2010. The ecohydrology of roots in rocks. Ecohydrology, 3: 238-245.

Schwinning, S., 2013. Do we need new rhizosphere models for rock-dominated landscapes? Plant and Soil, 362: 25-31.

Seyfried, M.S., and Wilcox, B.P., 2006. Soil water storage and rooting depth: key factors controlling recharge on rangelands. Hydrological Processes, 20: 3261-3276.

Šimůnek, J., van Genuchten, M.Th., and Snjna. M., 2005. The HYDRUS-1D software package for simulating the movement of water, heat, and multiple solutes in variably saturated media. Version 3.0. HYDRUS Software, Department of Environmental Sciences, University of California, Riverside.

Šimůnek, J., Wendroth, O., and van Genuchten, M.Th., 1998. Parameter estimation analysis of the evaporation method for determining soil hydraulic properties. Soil Science Society of America Journal, 62: 894-905.

Strock, J.S., Cassel, D.K., and Gumpertz, M.L., 2001. Spatial variability of water and bromide transport through variably saturated soil blocks. Soil Science Society of America Journal, 65: 1607-1617.

Teasdale, W.E., and Johnson, A.I., 1970. Evaluation of installation method for neutron-meter access tubes. US Geological Survey Professional Paper. 700-C. p. C237-C241.

Tennesen, M., 2008. When juniper and other woody plants invade, water may retreat. Science, 322: 1630-1631.

Tokumoto, I., Heilman, J.L., McInnes, K.J., and Kamps, R., 2011. Sealing neutron probe access-tubes in rocky soils using expandable polyurethane foam. Soil Science Society of America Journal, 75: 1922-1925.

Tokumoto, I., Heilman, J.L., McInnes, K.J., Morgan, C.L.S., and Kamps, R., 2012. Calibration and use of neutron moisture and gamma density probes in rocky soils. Soil Science Society of America Journal, 76: 2136-2142.

Tuller, M., and Or, D., 2001. Hydraulic conductivity of variably saturated porous media. Water Resources Research, 37: 1257-1276.

Twine, T.E., Kustas, W.P., Norman, J.M., Coork, D.R., House, P.R., Meyers, T.P., Prueger, J.H., Starks, P.J., and Wesely, M.L., 2000. Correcting eddy-covariance flux underestimates over a grassland. Agricultural and Forest Meteorology, 103: 279-300.

Valentin, C., 1994. Surface sealing as affected by various rock fragment covers in West Africa. Catena, 23: 87-97.

Valentin, C., and Casenave, A., 1992. Infiltration into sealed soils as influenced by gravel cover. Soil Science Society of America Journal, 56: 1667-1673.

van Genuchten, M.Th., 1980. A closed-form equation for predicting the hydraulic conductivity of unsaturated soils. Soil Science Society of America Journal, 44: 892-898.

van Genuchten, M.Th., Leij, F.J., and Yates, S.R., 1991. The RETC Code for Quantifying the Hydraulic Functions of Unsaturated Soils, Version 1.0. EPA Report 600/2-91/065, U.S. Salinity Laboratory, USDA, ARS, Riverside, California.

van Wesemael, B., Poesen, J., Kosmas, C.S., Danalatos, N.G., and Nachtergaele, J., 1996. Evaporation from cultivated soils containing rock fragments. Journal of Hydrology, 182: 65-82.

Veni, G., 2002. Revising the karst map of the United States. Journal of Cave and Karst Studies, 64: 45-50.

Webb, E.K., Pearman, G.I., and Leuning, R., 1980. Correction of flux measurements for density effects due to heat and water vapour transfer. Quarterly Journal of the Royal Meteorological Society, 106: 85-100.

White, W.B., Culver, D.C., Herman, J.S., Kane, T.C., and Mylroie, J., 1995. Karst lands. American Scientist, 83: 450-59.

Wilcox, B.P., Huang, Y., and Walker, J.W., 2008. Long-term trends in stream flow from semiarid rangelands: Uncovering drivers of change. Global Change Biology, 14: 1676-1689.

Wilcox, B.P., and Huang, Y., 2010. Woody plant encroachment paradox: Rivers rebound as degraded grasslands convert to woodlands. Geophysical Research Letters, DOI: 10.1029/2009GL041929.

Wilcox, B.P., and Thurow, T.L., 2006. Emerging issue in rangeland ecohydrology: Vegetation change and the water cycle. Rangeland Ecology & Management, 59: 220-224.

Williams D.G, and Ehleringer, J.R., 2000. Intra- and interspecific variation for summer precipitation use in pinyon-juniper woodlands. Ecological Monographs, 70: 517-537.

Wind, G.P., 1968. Capillary conductivity data estimated by a simple method. Water in the unsaturated zone. Proceeding of Wageningen Symposium, IASAH, Gentbrugge, Belgium, p. 181-191.

Wu, X.B., Redeker, E.J., and Thurow, T.L., 2001. Vegetation and water yield dynamics in an Edwards Plateau watershed. Journal of Range Management, 50: 98-105.

Young, M.H., Fleming, J.B., Wierenga, P.J., and Warrick, A.W., 1997. Rapid laboratory calibration of time domain reflectometry using upward infiltration. Soil Science Society of America Journal, 61: 707-712.

Zil'berbord, A.F., Kornienko, N.D., Vasil'ev, A.A., and Ladyzhenskii, I.L., 1979. Measuring the moisture content of the rock around an underground structure. Journal of Mining Science, 15: 299-303.

Zhao P., and Shao, M., 2011. Predication of soil water storage by spatial dependence in a deposited soil farmland. African Journal of Agricultural Research, 6: 3475-3482.